MACHINABILITY OF AISI304 STAINLESS STEEL USING ETHYLENE
GLYCOL NANO PARTICLES BASED COOLANT

YOGESWARAN A/L MUTHUSAMY

Thesis submitted in fulfillment of the requirements
for the award of the degree of
Master of Engineering in Mechanical Engineering

Faculty of Mechanical Engineering
UNIVERSITI MALAYSIA PAHANG

MARCH 2015

UNIVERSITI MALAYSIA PAHANG

DECLARATION OF THE THESIS AND COPYRIGHT

Author's full name   : YOGESWARAN MUTHUSAMY

Date of birth   : 9TH DECEMBER 1988

Title   : MACHINABILITY OF AISI304 STAINLESS STEEL USING ETHYLENE GLYCOL NANO PARTICLES BASED COOLANT

Academic Session   : 2013-2015

I declare that this thesis is classified as:

☐ **CONFIDENTIAL**   (contains confidential information under the Official Secret Act 1972)

☐ **RESTICTED**   (contains restricted information as specified by the organization where research was done)

☑ **OPEN ACCESS**   I agree that my thesis to be published as online open access (Full text)

I acknowledge that Universiti Malaysia Pahang reserve the right as follows:

1.   The Thesis is the Property of Universiti Malaysia Pahang.

2.   The Library of Universiti Malaysia Pahang has the right to make copies for the purpose of research only.

3.   The Library has the right to make copies of the thesis for academic exchange.

Certified By:

_____   _____

(Student's Signature)   (Signature of Supervisor)

__881209-01-5311__   Engr. Dr. Kumaran Kadirgama

New IC/ Passport Number   Name of the Supervisor

Date: Date:

NOTES   : *If the thesis is CONFIDENTIAL or RESTRICTED, please attach with the letter from the organization with period and reasons for confidentiality or restriction.

SUPERVISOR'S DECLARATION

We hereby declare that We have checked this thesis and in our opinion, this thesis is adequate in terms of scope and quality for the award of the degree of Master of Engineering in Mechanical.

Signature

Name of Supervisor: DR. KUMARAN KADIRGAMA

Position: LECTURER

Date:

Signature

Name of Co-Supervisor: PROF. DR. MD. MUSTAFIZUR RAHMAN

Position: PROFESSOR, FACULTY OF MECHANICAL ENGINEERING
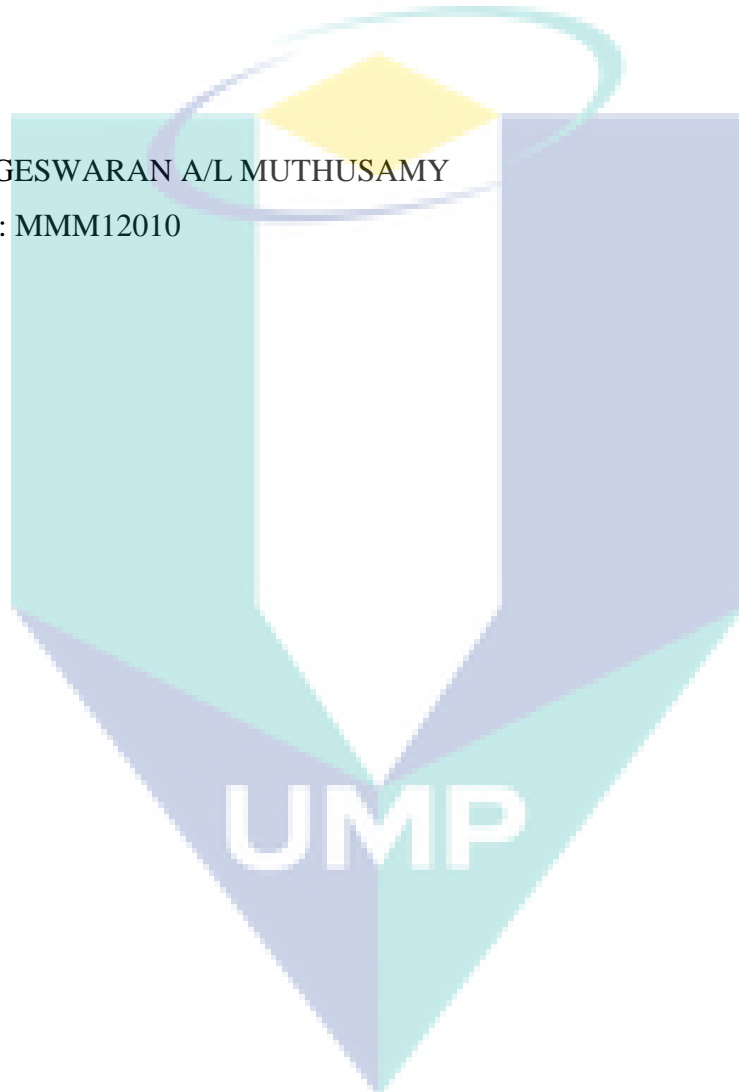
Date:

STUDENT'S DECLARATION

I hereby declare that the work in this thesis is my own except for quotations and summaries which have been duly acknowledged. The thesis has not been accepted for any degree and is not concurrently submitted for award of other degree.
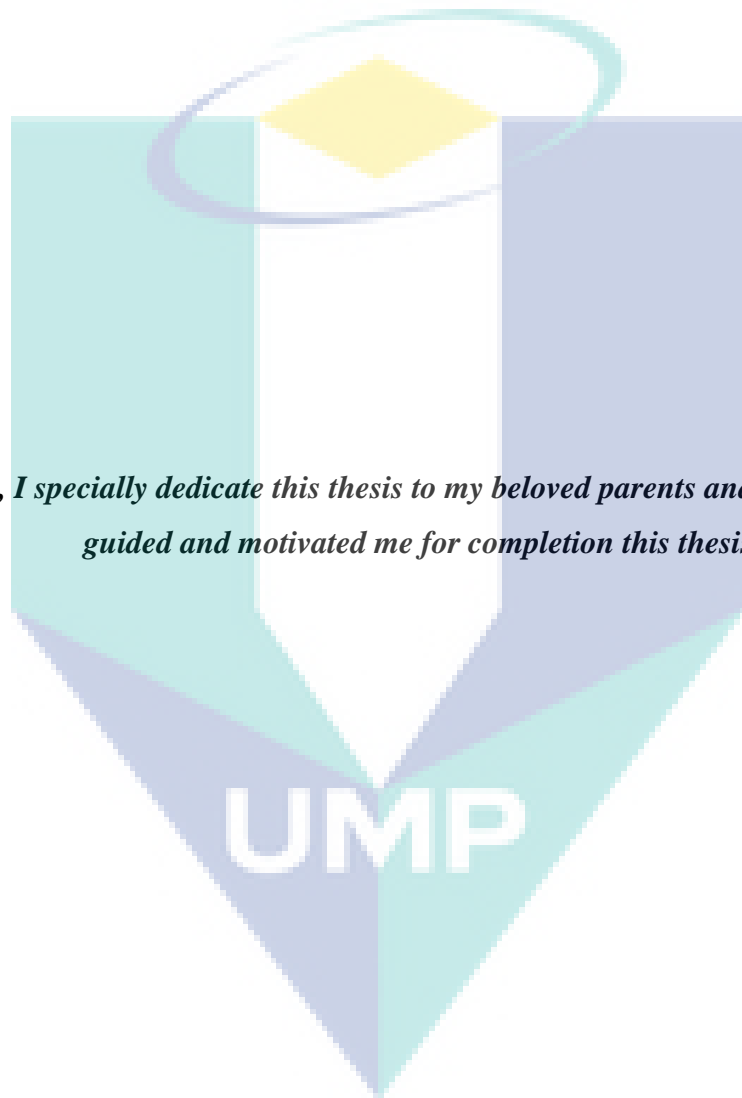
Signature
Name: YOGESWARAN A/L MUTHUSAMY
ID Number: MMM12010
Date:

Foremost, I specially dedicate this thesis to my beloved parents and those who have guided and motivated me for completion this thesis

ACKNOWLEDGEMENT

ABSTRACT

This thesis present the development of linear model order for predicting the milling parameter such as surface roughness, tool life and wear mechanism for end-milling operation of AISI304 stainless steel using TiN coated carbide insert with water soluble coolant and nano particle based coolant (TiO_2/EG). The linear model equation of surface roughness and tool life are developed using response surface methodology (RSM). The cutting variables are cutting speed, feed rate, and axial depth. The developed linear model equations for the surface roughness tool life show that the most significant input parameter is the feed rate, followed by axial depth and cutting speed. The end-milling operation by using nano particle based coolant (TiO_2/EG) obtains lower surface roughness and high tool life compared with end-milling operation by using water soluble coolant. In general, the tool failure for milling with water soluble coolant was flank wear, crater wear, crack, chipping and fracture at cutting distance of 720 mm. The milling process with nano particle based coolant (TiO_2/EG) obtains a chipping and fracture and cutting distance of 1200 mm. According to ISO 8688-2-1989 (E) the wear criteria for milling with water soluble coolant reached at average of cutting distance of 800 mm but the cutting distance for milling with nano particle based coolant (TiO_2/EG) reached the ISO 8688-2-1989 (E) the wear criteria at cutting distance of 1300 mm. The SEM and EDX spectrum shows there are nano layer of Ti nano particle from the nanofluid embedded and fills the holes in the insert and for a layer which act as a thermal bridge for the cutting insert. Attrition and oxidation at the cutting edge were the main tool wear mechanism present during end-milling operation nano particle based coolant (TiO_2/EG). An oxide layer has been formed during the oxidation wear which shield the cutting tool from the impact during the milling process.

ABSTRAK

Tesis ini ialah mengenai pembinaan model linear untuk meramal parameter pengisaran seperti penyudahan bahagian terkeras, jangka hayat mata alat pemotong dan mekanisme haus yang dialami oleh mata alat tersebut untuk pengisaran hujung keluli AISI 304 menggunakan sisip karbida bersalut TiN dan bendalir penyejuk berasaskan zarah nano TiO_2/EG. Persamaan model linear untuk meramal kekasaran permukaan dan jangka hayat mata alat ini dibina menggunakan kaedah RSM. Kelajuan pemotongan, suapan dan kedalaman pemotongan merupakan pembolehubah dalam eksperimen ini. Persamaan model linear menunjukkan keputusan bahawa kekasaran permukaan dan jangka hayat mata alat sangat terkesan oleh kelajuan pemotongan, diikuti oleh kedalaman pemotongan dan suapan. Pemesinan dengan menggunakan bendalir penyejuk berasaskan zarah nano TiO_2/EG memberi hasil kekasaran permukaan yang rendah dan jangka hayat mata alat yang lebih tinggi berbanding dengan pemesinan menggunakan bendalir penyejuk larut air. Secara umumnya, kegagalan alat pemotongan apabila memesin menggunakan bendalir penyejuk larut air adalah kehausan di bahagian tepi, retak dan pecah pada jarak pemotongan 720 mm manakala pemesinan dengan mengunakan bendalir penyejuk berasaskan zarah bersaiz nano TiO_2/EG cuma memberi kesan pecah pada jarak pemotongan 1200 mm. Berdasarkan standard ISO 8688-2-1989 (E) kriteria kehausan mata alat untuk pemesinan mengunakan bendalir penyejuk larut air, alat mejadi haus pada jarak pemesinan 800 mm manakala untuk pemesinan dengan bendalir penyejuk berasaskan zarah nano TiO_2/EG pada jarak pemesinan 1300 mm. SEM dan EDX mununjukkan bahawa lapisan nano yang wujud daripada zarah Ti telah menjadi jambatan termal untuk alat pemotongan. Pergeseran dan pengoksidaan di pinggir merupakan mekanisma kehausan yang utama semasa operasi pemesinan dengan mengunakan bendalir penyejuk berasaskan zarah bersaiz nano TiO_2/EG. Satu lapisan telah wujud dan mejadi penghalang kepada alat pemotong daripada haus.

TABLE OF CONTENTS

CHAPTER 4   RESULTS AND DISCUSSION

CHAPTER 5   CONCLUSION AND RECOMMENDATION

LIST OF TABLES

LIST OF FIGURES

LIST OF SYMBOLS

R_a	Roughness Average
R_z	Roughness Depth
k	Thermal Conductivity of Nanofluid
k_0	Thermal Conductivity of based liquid
L	Sampling Length
Y	Ordinate of the Profile Curve
K	Kelvin
γ	tool rake angle
l_c	tool-chip contact distance
l_s	shear plane length
a_c	undeformed chip thickness
a_o	deformed chip thickness
ϕ	shear angle
α	clearance angle
V	Volts
ω	weight percentage
φ	volume percentage
F_m	Feed Rate in mm/min
TL	Total Length to reach Flank Wear Criterion 0.3mm

LIST OF ABBREVIATION

TiO_2	Titanium Oxide
SiO_2	Silicon Oxide
ZnO	Zinc Oxide
TiN	Titanium Nitrite
AISI	American Iron and Steel Institute
BUE	Build- Up- Edge
CVD	Chemical Vapor Deposition
RSM	Response Surface Method
SEM	Scanning Electron Microscope
EG	Ethylene Glycol
TEM	Transmission Electron Micsroscope
Al_2O_3	Aluminium Oxide
CrN	Chromium Nitride
Cr_2O_3	Chromium(iii) oxide
DOE	Design of Experiment
CCD	Central Composite Design
BBD	Box-Behnken Design
CBED	Convergent Beam Electron Diffraction
EDX	Energy Dispersive X-ray

CHAPTER 1

GENERAL INTRODUCTION

1.1   INTRODUCTION

Coolant is very crucial in all machining process because it can reduce the thermal deformation of the work-piece and produce a fine surface. However, many manufacturing industries are facing a real challenge in the cooling system in the machining process. There are still thermal damages occur on the work-piece surfaces which affect the manufacturing cost of the industry. This is due to the high cutting temperature during the milling process. Many researchers have conducted various researches on alternating the machining coolant. Most of the investigation of alternating the machining coolant is mainly focused on minimum quantity lubricant technique and there are very few research and publication about using nanofluid as a milling machine coolant (Yazid et al., 2011). On the other hand, it is reported that the dispersed nanoparticle additives (TiO_2, ZnO, SiC, etc) in the based liquid exhibits higher load carrying capacity, anti-wear and friction reduction properties (Murshed et al., 2008) Therefore, these features can make the nanofluid very attractive in usage of machining coolant.

The concept of nanocoolant or nanofluid is referred to dispersions of nanopaticle into the based liquid which is water or ethylene glycol. Choi et al., 2008 reported that nanofluids are the next generation heat transfer fluid due to their higher thermal conductivity than those of based liquid. From the viewpoints of heat transfer rate, nanofluid are considered as alternatives to conventional coolant for machining. Therefore, ethylene glycol based TiO_2 nanocoolant could produce a better surface finish than the conventional coolant. Besides that, the cutting temperature could also be reduced in both work-piece and cutting tools due to its high heat transfer rate. Therefore, the tool life and the surface integrity is considered to be much improved compared with normal commercial coolant.

AISI 304 austenite stainless steels are commonly used in manufacturing industries to manufacture automotive company. Furthermore, aircraft industries are also depending on austenite steel to fabricate part in aerospace engines. AISI 304 austenite stainless steels are grades of chromium-nickel steels. It is very great corrosion resistant and having an outstanding mechanical property which is not exists in other alloy. Besides that, this alloy also categorized as non-magnetic and it can only be hardened by natural cold working process. However, this alloy is classified as poor machinability material (Novak et al., 1977).

AISI 304 austenite stainless steels are an alloy with high fracture toughness, high tensile strength high ductility, low heat conductivity and high work hardening rates. These undesirable properties contributed to a number of difficulties such as poor surface integrity and short tool life (Shao et al., 2007). Besides that, machining austenite stainless steel comes across with built-up-edge (BUE) on the cutting flank face. BUE will contribute a rises in tool wear and reduce the surface integrity of workpiece. Moreover, having a low thermal conductivity which is 50% lower than normal carbon steel, increases the rates of tool wear and damages on the workpiece due to high absorption of heat in cutting tool and workpiece (Hossien and Yahya, 2005). One way to reduce the low thermal conductivity effect on tool life is to conduct the milling operation with essential cutting fluid.

1.2   PROBLEM STATEMENT

End mill is the most common machine used in the manufacturing industries nowadays. The manufacturing industries are facing a lot of problems in producing the final product. The most common problem occurs is due to the unsuitable coolant. Hence, it will contribute to poor surface roughness on the work-piece. Furthermore, stainless steel endowed with some special properties such as low thermal conductivity and high ductility which classified as a poor machinability that produce a lot of difficulty during cutting. Moreover, machining of stainless steel usually having some difficulties such as build up edge (BUE). These will straight away contribute to high tool wear rate and reduce the surface integrity of the workpiece (Hossien and Yahya,

2005). Therefore, choosing the proper cutting parameter and cooling lubricant is very crucial in the milling process of hard material such as stainless steel.

1.3   OBJECTIVE

The objectives of research are as follows;

1. To determine the effect of nano particle bese coolant (TiO$_2$/EG) on the milling surface quality and tool life of Stainless Steel AISI 304.
2. To establish predicted models between cutting parameter and responce of surface roughness and tool life during milling operation of AISI 304 stainless steel using water soluble coolant and nanofluid.
3. To investigate the tool wear and wear mechanism during milling operation of AISI 304 stainless steel using water soluble coolant and nano particle based coolant.

1.4   SCOPE OF STUDY

To achieve the research objectives, end milling type was used to cut the work piece. The material that was used as work piece to conduct the research experiment is AISI 304 austenite stainless steel. The mill holder diameter that was used to conduct the experiment is 16mm. Besides that, the insert type that was used to cut the work piece is coated carbide tool. The inserts coating specification is CVD with single layer 1mm TiN coated. Furthermore, the nano particles that have been chosen for to produce the coolant is TiO$_2$ and the concentration of the nano coolant will be 0.5, 1.0 and 1.5 volume percentage. The milling parameter has been chosen according to the insert catalog which the cutting speed range is 1500 rpm to 2500 rpm, feed rate between 0.02 mm/tooth to 0.04 mm/tooth and the axial depth of cut between 0.1 mm to 0.3 mm. the radial depth of cut has not been included is this study. Rather than that, the cutting temperature measurement also not included in the scope of this study.

1.5   THESIS OUTLINE

This thesis contains five chapters which is every chapter have its own purpose. After viewing the entire chapter in this thesis hopefully viewer can understand the whole system design for this project.

Chapter 1 contains of the introduction, problem statement, objectives, the scopes of study and the outline of this thesis.

Chapter 2 contains all the theory of milling operation, tool life, tool wear, surface roughness, and milling temperature are discussed. Besides that, the behavior and properties of nanoparticle are also discussed. The application of some statistical modelling are discussed in the end this chapter.

In chapter 3 the experimental procedure and development of statistical modelling created with response surface method (RSM) are presented. This chapter also explain about the detail of the research. It also includes the information about the progress of the experiment and the specification of the apparatus used throughout the research.

Chapter 4 discusses the result and the analysis for this research. The results between experimental with ethylene glycol based TiO_2 nanocoolant and experimental with normal conventional coolant are compared and analyzed. The model obtained from RSM are also compared and analyzed in this chapter.

Chapter 5 present the conclusion and suggestion for further work of the research.

CHAPTER 2

LITERATURE REVIEW

2.1 INTRODUCTION

The main purpose of this chapter is to deliver the information about milling process, cutting parameter, nanofluid and so on. Information from this chapter will provide a huge point from other researcher's results and findings. This information can be linked with the finding of this research that has been discussed in chapter 5.

2.2 THEORY OF METAL CUTTING

The study of metal cutting process has been carried out for over last hundred year. However, most of the study has been focused on down-to-earth reduction machining cost with an unsatisfactory accuracy and surface quality. But, the actual modern fundamental of metal cutting study has been carried out in 1945 by Merchant when he revealed the vision of metal cutting phenomena. However, Merchant failed to develop the predictive skills. Therefore, the objective of metal cutting research became unclear. However, the actual fundamental of metal cutting experiment was started in 1960s (Astakhov, 1998). In this decade, the metal cutting practice has been advanced by own way of trial and error method. However, it has been very complex due to lack of valid data produced.

2.3 MECHANIC OF METAL CUTTING

There are two different views of mechanic of metal cutting which is a new surface is formed by plastic deformation on the tip of cutting tool and the amount of energy required for cutting due to plasticity and friction forces (Atkins, 2006). But, the energy required for formation of new surface is considered unimportant. The energy formed during the metal removal is converted to thermal energy which is released from the work of plastic deformation and friction force. The mechanical thermal in the tool-

chip interface is extremely important for study the metal removal process. The thermal-mechanical energy in the tool–chip interface is vitally important for the design of metal cutting processes. This thermal-mechanical energy is mostly determined by the stress of plastic deformation and friction force which is classified as primary and secondary shear zone. The sliding velocity on the tool-chip interface combined with stress of plastic deformation and friction force generate a very high temperature until reaching the melting point of the workpiece material (Hoppe, 2004). This temperature is sufficient enough for plastic deformation take place on the surface of the workpiece. The area where the metal deforms is called primary shear zone as shown in Figure 2.1 where, γ is the tool rake angle, l_c is the tool-chip contact distance, l_s is the shear plane length, a_c is undeformed chip thickness, a_o is deformed chip thickness, ϕ is shear angle and α is the clearance angle (Yahya et al., 2005). As the temperature at this point reach yield point, a chip break away from the workpiece material and slips away the primary shear plane. On the other hand, secondary shear zone happens along the face of cutting tool. Once the chip slip away along the up direction of the cutting tool, friction force raises the temperature in this zone. Previous studies reported that the temperature on the secondary zone can reach up to 1200 ^{o}C when machining tool steel. During machining process, the cutting edge moves through the workpiece and deforming the workpiece material to shear a chip, a third shear zone formed under the leading edge (Hill, 1954). A material springback is the outcome of this zone.
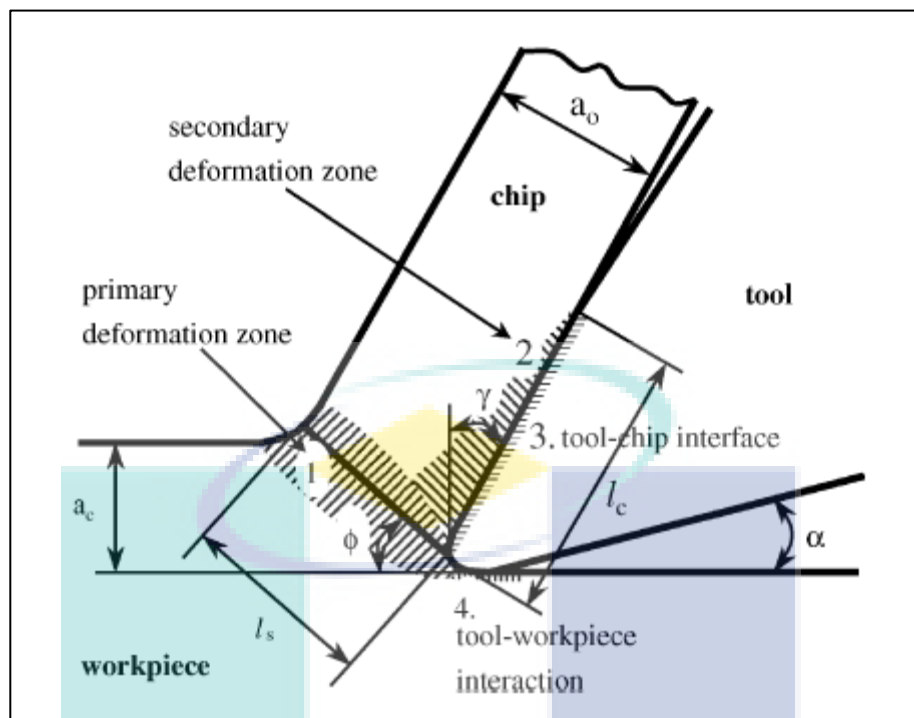
Figure 2.1: The primary and secondary shear zone during machining

Source: Neugebauer et al. (2011)

2.4   FORMATION OF BUILD-UP-EDGE

The build-up-edge (BUE) can occur during the low cutting speed. This is formed by the particle of the workpiece material which is stick to the rack face and cutting face as shown in Figure 2.2. These particles have been highly deformed and subject to strain-hardened. Previous study has been concluded that BUE is much harder than the workpiece material (Doege and Behrens, 2007). Previously an investigation has been done to found the possibilities of BUE occur during machining (Hoffmeister and Wessels, 1992). This investigation concluded that BUE only occur due to the reasons below as stated below:

   a. Strain hardening has been occurring on workpiece material.
   b. A stable and stationary chip formation.
   c. A low temperature during the chip formation which do not allow for recrystallization.

d. There is a stationary zone in the material flow on the cutting edge.

BUE affect the geometry of the cutting edge. During machining, it can drag along the workpiece material and causing an adhesive wear on cutting tool. It can also affect the newly formed surface integrity. Therefore BUE is commonly unwanted during the machining process. However, previous experimental study stated that BUE does not occur at high cutting speed because there is no strain hardening if the recrystallization temperature is much greater during the deformation process (Klose and Werkstofftechnologie, 1993).
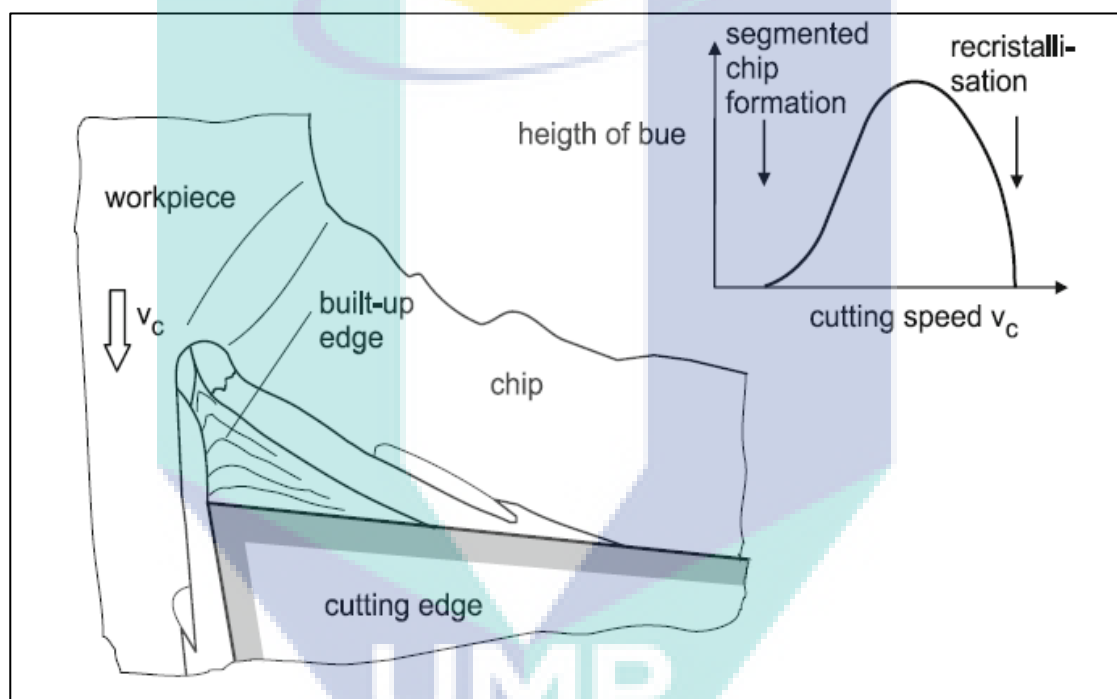
Figure 2.2: Formation of build-up-edge

Source: Klose and Werkstofftechnologie (1993)

2.5   TOOL LIFE AND WEAR MECHANISM

Tool wear can be categorized into several of types as follows:

a. Adhesive wear accompanied by shear plan deformation.

b. Abrasive wear caused by hard particles cutting action.

c. Diffusion wears due to relatively high temperature.

d. Fracture wear produced by fatigue.

Tool wear is a gradual process occurs with combination of prime wear mode. It is extremely dependent on cutting conditions, workpiece material, cutting tool type and the tool geometry. However, using insert as a cutting tool always can detect some kind of wear on it. It is highly depending on the cutting parameter used and different type of wear can be observed and the tool life of the insert will be varying too. To determine the failure criteria of an insert, normally it is set to be 0.35 mm as worn tool (Coromant, 1994). It does not depend on the type of wear that makes the insert to be worn. The most common wear types on insert reviewed in this section.

The most common wear of insert is flank wear. It is an abrasive wear and also can be predict. The edge of the insert is changing its structure and the quality of workpiece surface is not satisfactory. The greater the flank wear, the higher the cutting force needed for the cutting process since the insert becomes blunt at the edge of the inserts. Figure 2.3 shows the sample of flank wear developed on cutting insert. The measurement of flank wear is done from the unworn edge to the worn edge as shown in Figure 2.4. The W measured in Figure 2.4 is a failure criteria of flank wear which is 0.3 mm (Coromant, 1994).
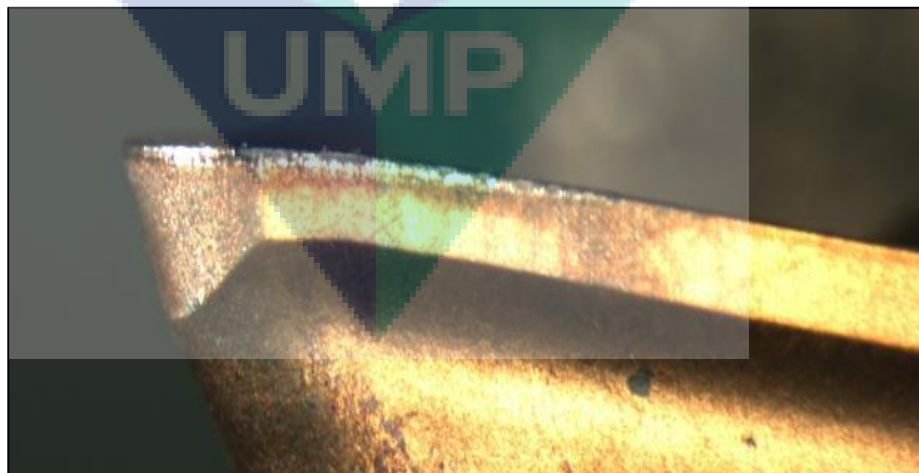
Figure 2.3: Progression of flank wear.

Source: Bjurka (2011)
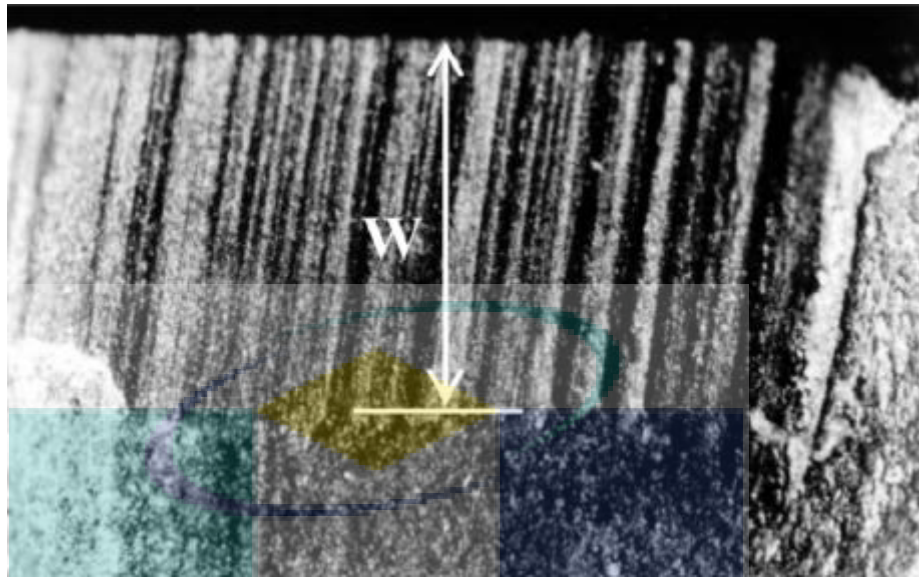
Figure 2.4: Measurement of flank wear.

Source: Palmai (2011)

Crater wear is another type of wear which commonly observed in machining. The cause of this wear is due to an abrasive wear on the chip surface of the insert. Furthermore, crater wear also cause by the chemical diffusion between chips and the cutting insert. This is due to relatively high temperature on the cutting zone. Therefore, cavity appears on this zone where the highest temperature point in the cutting zone in combination with chip as well. The feed rate of the machining determine how far into the insert the crater begin. At high feed rate, the crater start far from the edge of the insert. The distance from the edge of the insert is measured to find the crater wear (Coromant, 2007). Figure 2.5 shows the common crater wear.
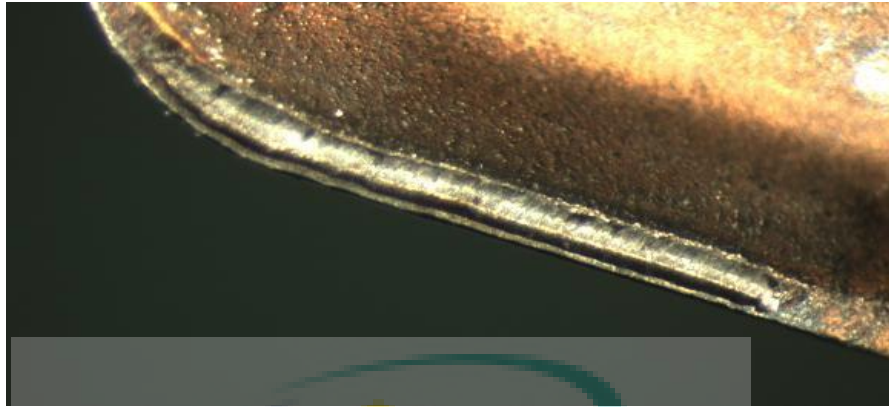
Figure 2.5: Progression of crater wear

Source: Coromant (1994)

Notch wear is another wear which is ussually occur during machining at high depth of cut. Besides that, it is also occurs during maching a harder material that will cause deformation hardening on the surface. The hard workpiece surface will then tear the insert. Figure 2.6 shows the notch wear which is due to machining hard material (Coromant, 2007 and Kasim et al., 2013).

Figure 2.6: Progression of notch wear

Source: Kasim et al. (2013)

Chipping is a type of wear which the fracture occurs on edge due to existing of comb cracks. The chipping wear is totally randomized based on the composition of the workpiece material. Therefore, it is very hard to determine whether the insert is worn or not. Normally the chipping criteria also been fixed as 0.35 mm to find the wear insert (Coromant, 2007 and Dadona et al., 2011). Figure 2.7 shows the example of chipping wear.
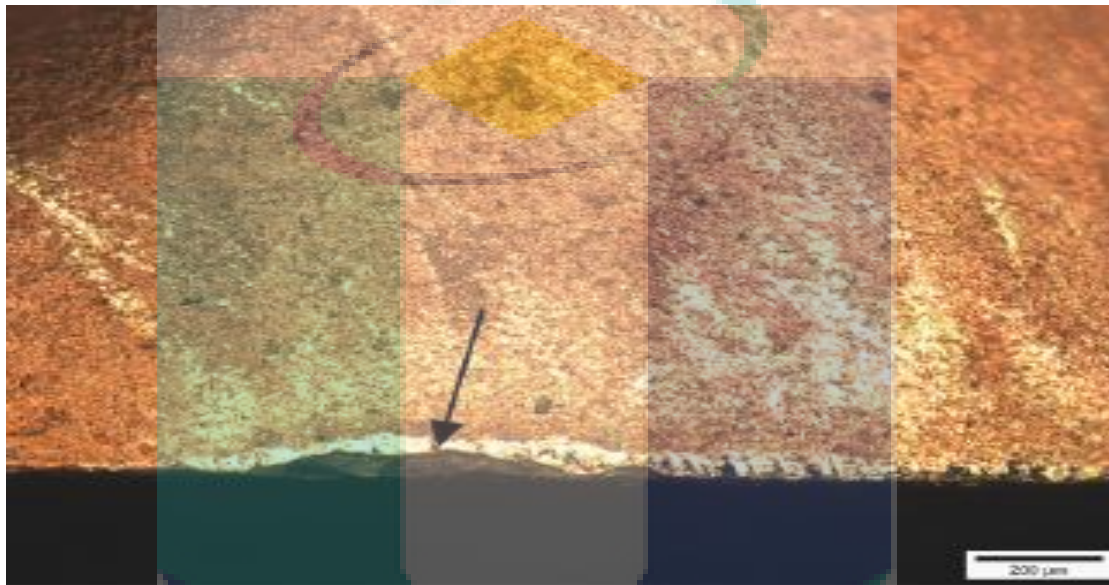
Figure 2.7: Chipping

Source: Dadona et al. (2011)

Comb crack is usually formed on the tip of the cutting edge, on a height that equals half of the axial depth of cut. This is because the yielding temperature is the greatest here (Eriksson and Johansson, 2008) (Ulutan and Ozel, 2011). After the crack has been occurred, a different crack will tend to form on the half of the height from the initial comb crack. The coating of the insert will be ground down after the comb crack occurred. Generally, the crack will turn into cavity. Previously, a research has been concluded that comb crack can lead to the formation of BUE. The development of comb crack is influced by the sudden temperature variation. Therefore, using a proper coolant can reduce the possibilities of comb crack during machining (Coromant, 2007). Figure 2.8 shows the comb crack on the edge of cutting insert.
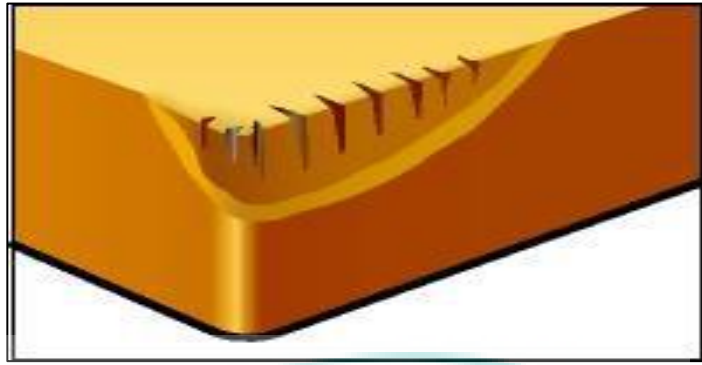
Figure 2.8: Comb crack

Source: Bjurka (2011)

2.6   SURFACE ROUGHNESS

Surface finish and surface roughness are widely used term in industry. It is used to measure the smoothness of the machined surface (Lou et al., 1999). Surface finish could be stated in many dissimilar parameters. A large number of recently developed surface roughness parameter are due to the variety of machining operation. The most common parameter for surface roughness are described as follows:

- Roughness average (R_a): This parameter is known as arithmetic mean roughness value. R_a is the universal recognized and most commonly used throughout international as surface roughness parameter.

$$R_{a =} \ \frac{1}{L} \int_0^L |Y(x)| dx \tag{2.1}$$

Where, R_a is the arithmetic average deviation from the mean line, L is the sampling length and Y is the ordinate of the profile curve. It is the arithmetic average deviation from the mean of the roughness profile from the mean line.

Previously a research has been conducted to find the surface roughness on end-milling process for stainless steel with different cutting parameter. Mostly, the surface roughness increases with increases in cutting speed. But, this theory is only for the cutting speed reach 104 m/min. Beyond this cutting speed the surface roughness seen to be decreases even the cutting speed increases. Besides that surface roughness also

increases gradually with increases in feed rates. It has been concluded that the finest surface roughness can be produced at highest cutting speed and lowest feed rate.

A number of approaches for inspecting and characterizing the surfaces have been developed. Inspection equipment based on both contact and non-contact principles is available. Contact–type instruments, generally employing styluses, are commonly used. Non-contact instruments are usually based on optical interferometry or electron beam principle. A large relief angle may reduce friction between the tool and workpiece, but excess relief angle reduces the support under the cutting edge, thereby causing failure under heavy-duty operation, and may result in inferior surface roughness on machined parts (Astakhov, 1999).

Previous research conducted by Baradie (1993) and Bandyopadhyay (1990) have shown that the surface quality can be improved at high cutting speed. According to Gorlenko (1981) and Thomas (1981), surface finish can be characterized by various parameters. Numerous roughness height parameters such as average roughness (Ra), smoothening depth (Rp), root mean square (Rq), and maximum peak-to-valley height (Rt) can be closely correlated. The present study uses average roughness (Ra) for the characterization of surface roughness, due to the fact that it is widely adopted in the industry for specifying the surface roughness. Mital and Mehta (1988) have conducted a survey of the previously developed surface roughness prediction models and factors influencing the surface roughness. They have found that most of the surface roughness prediction models have been developed for steels.

2.7   COOLANT

Coolant or cutting fluid is a liquid which is used to produce cooling and lubricant between the cutting tool and the work piece. Cutting fluid also reducing the contact processes in the chip formation zone. Cooling and lubrication is very important in cutting process. According to Boothroyd and Knight (2006) the lubricant action is very important and low cutting speed and the cooling is important at higher cutting speed due the high increases in heat in cutting zone.

Historically, water was used as a cooling medium in various machining operation (Astakhov, 2006). However, water is an excellent cooling medium due to its high thermal conductivity but it corrodes the part and poor lubrication. Nowdays, oils and synthetic fluids are used as coolant in machining. There are four types of cutting fluid used nowadays which consist of straight or neat oils, soluble oil, synthetic fluids and semi-synthetic fluids. Around 80% of cutting fluids in industries are using water based oil and synthetic fluids as a coolant in machining (Boothroyd and Knight, 2006).

There are several advantages of using coolant in machining. First, using a proper coolant will increase the tool life. As reported by Boothroyd and Knight (2006) improvement in the machining coolant causes some reduction in temperature. The tool wears extremely sensitive to the small changes of temperature in the region where the tool in contact with the work piece. Besides that, coolant also will reduce the thermal distortion caused by temperature gradient generated within the work piece during machining. There are some books stated that using coolant will easier to handle the finished work piece (Boothroyd and Knight, 2006). However, Edward and Paul (2000) stated that by using a suitable cutting fluid will improve the surface quality and also useful for clear the chips from cutting area.

Large machining centers often have a coolant station that is very complex. The coolant station provides coolant through the tools in order to increase the amount of fluid for cutting operation. Coolant stations are usually made up of a series of filters to remove impurities and chips that have been carried in the coolant and pumps. Some coolant stations provide pressures of more than 1000 psi to the cutting operation. The relatively high pressure value allows good removal of chips, significant cooling, and better surface finish (Matsumoto et al., 1999)

2.8   NANOFLUID

Nanofluid is fluid which suspended with nanoparticle. The nanoparticle will suspend with the conventional fluids such as water, ethylene glycol (EG) and engine oil. Nanofluid are thought to be next the generation heat transfer fluids due to its existing properties (Yu et al., 2009). Nanofluid have attracted great interest of various industries

such as micro electric, automotive, manufacturing and so on. According to Murshed et al. (2005) the advantages of nanofluids are performing better stability than micro-sized and mili size particle. Additionally, nanofluids obtain higher thermal conductivity than the based liquid. More than twenty laboratories worldwide have published the data regarding the thermal conductivity of nanofluids. All the results shows that the thermal conductivity of nanofluids exhibits higher thermal properties even the concentration of liquid is less than 5% in volume percentage. The viscosity of the nanofluids is another important property for heat transfer application. As reported by Murshed et al. (2005) the pH value and the viscosity of the nanofluids are considered as factors that affect the stability of the nanofluid at room temperature.

In a previous researh by Giovanni and Claudio (2011) they specified that the TiO$_2$ nano particle was prepared by supplier (Nanostructured & Amorphous Material Inc. USA). The TiO$_2$ particle structure is ructile with purity higher than 99.9% with particle diameter size around 30-50nm. Nanofluid will prepared by a two-step technique. Two step techniques are nano-particle powder will subsequently disperse in the base liquid. Giovanni and Claudio (2011) also stated that there will be no surfactants to be added to reduce the particle agglomeration. To ensure good dispersion of nanofluids and reduce the agglomeration, mechanical treatments need to be done to the nanofluid. The mechanical treatment will be mechanical stirring for one hour and following with sonication at 25 kHz for 48 hours.

Yu et al. (2009) carried out their investigation on properties of ethylene gylcol based ZnO nanofluid. The average size of ZnO nanoparticle is 10-20nm with a density of 5.6 g/cm^3. The ZnO nanoparticle powder with different volume concentration was dispersed in ethylene glycol. The volume fraction of nanoparticle was calculated by using the density provide by the supplier and the total volume of nanofluid prepared. The ethylene gylcol based ZnO nanofluid mixture were stirred and sonicated for 3 hours to ensure nanoparticle fully dispersed in the based liquid. In this research, Malvern Nanosizer was used to measure the dispersion of nano particle in the based liquid which is ethylene glycol. Besides that, the thermal conductivity of the nanofluid was measured by using the transient hot-wire technique.

Xuan and Li (1999) carried out properties study on ethylene glycol based TiO_2 nanofluid and ethylene glycol based ZnO nanofluid. Table 2.1 shows the stability result of these two types of nanofluid.

Table 2.1: Preparing specification of two type of nanofluid

Source: Xuan and Li (1999)

Preparation	Nanoparticle	
	TiO$_2$	ZnO
Mechanical stiring time	48 hour	48 hour
Nanoparticle size	100 nm	100 nm
Volume Percentage	1.0 %	1.0 %
Stablelization time	2week in stationary state (no sedimentation found)	30 hours in stationary state

2.8.1 Micrographic analysis

Transmission electron microscope (TEM) was used to monitor the dispersion, clustering and morphology of the nanoparticle in the base liquid. As stated by Murshed et al, the size of nanoparticle in the base liquid is higher than the actual size specified by the supplier. This is due to large nano particle density, higher number of particle, inter-particle attraction and agglomeration between the nano particle and base water. Figure 2.9 and Figure 2.10 shows clustering and agglomeration of TiO_2 nanofluids after the dispertion.
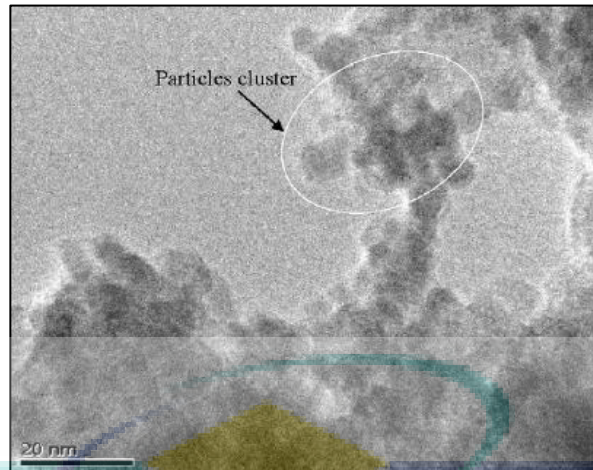
Figure 2.9: TEM photograph of TiO$_2$ nanofluid with particle size 15nm in diameter.

Source: Murshed et al. (2005)
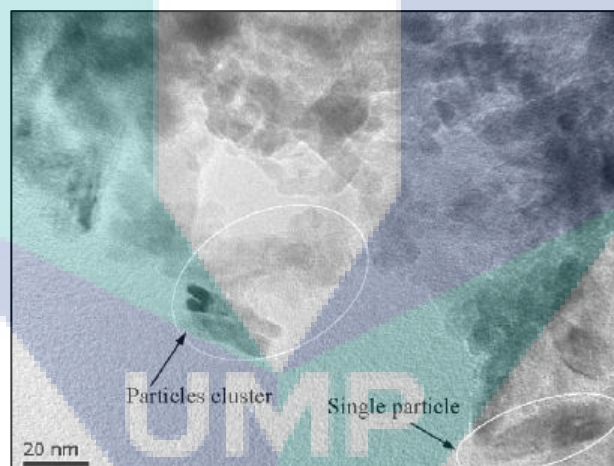
Figure 2.10: TEM photograph of TiO$_2$ nanofluid with particle size 10nm in diameter.

Source: Murshed et al. (2005)

Yu et al. (2009) stated that thermal conductivity of nanofluid is independent of the time. This had been proven by the experimental data in Figure 2.11 which shows the ratio of thermal conductivity, $(k-k_0)/k_o$ as a function of time. k and k_o represent the thermal conductivity of nanofluid and based liquid respectively.
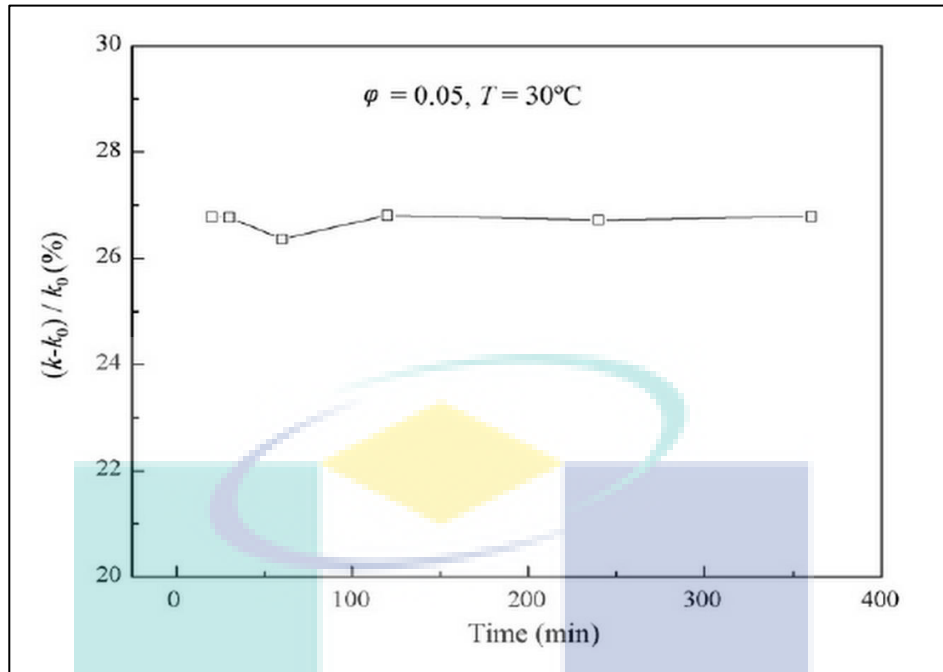
Figure 2.11: Thermal conductivity of nanofluid against time

Source: Yu et al. (2009)

The result shows that, the thermal conductivity of ethlylene glycol based ZnO nanofluids is independent of time from 20 to 360 mininutes (Yu et al., 2009). However, Liu et al. (2009) says that the thermal conductivity is decreasing with time. This literature stated that the thermal conductivity of nanofluids obtained straight after the preparation was not the true value. This is because of sedimentation of nanoparticle in nanofluids will reduce the volume concentration. Therefore the stability of nanofluids is an important factor which determines the properties.

Yu et al. (2009) has shown the effect of temperature on the thermal conductivity of nanofluids. The thermal conductivity has been measured for different temperature at a range of 10 to 60°C. Figure 2.12 shows the result of thermal conductivity of nanofluids for different temperature at range 10 to 60°C.
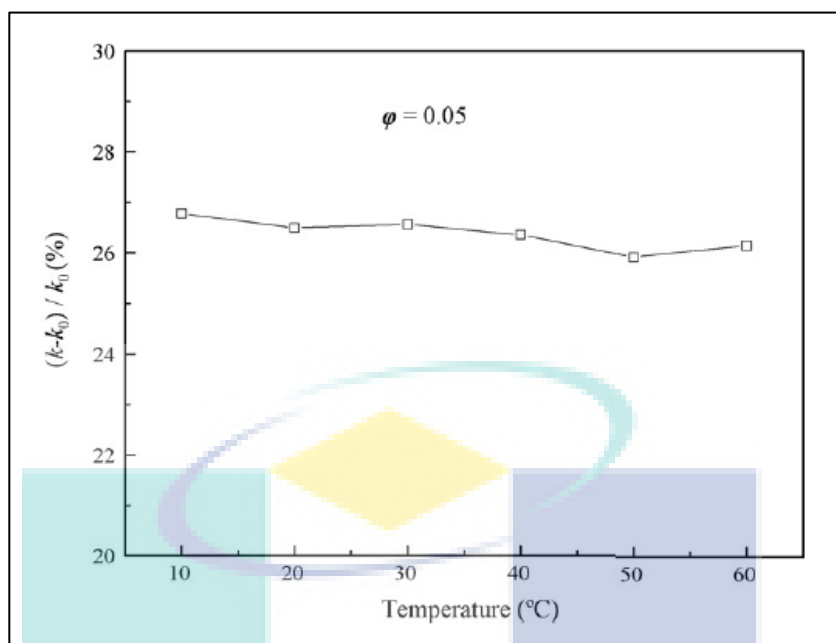
Figure 2.12: Ratio of thermal conductivity versus temperature

Source: Timofeeva et al. (2007)

From the Figure 2.12, the thermal conductivity of nanofluid increases with the increases of temperature, since the enhanced ratio is almost constant and the thermal conductivity of nanofluids tract the thermal conductivity of base liquid which was similar to the conclusion of Timofeeva et al. (2007). However, the temperature has a very small effect on the thermal conductivity of nanaofluid because of the high viscosity of the base liquid and large aggregates of the nanoparticles.

The previous study by Giovanni and Claudio (2011), shows that the thermal conductivity of nanofluids is sensitive to the particle volume fraction and temperature and weak sensitivity to clustering size. This means that the the size of particle has very little influence on the properties of nanofluids.

Giovanni et al, (2010) has proved that thermal conductivity has less sensitivity to cluster average size. For example, at temperature $40^{o}C$ for TiO_2/EG nanofluid at 4% volume percentage the thermal conductivity is 23% higher than the based liquid.

The thermal conductivity ratio graph as shown in Figure 2.13 for TiO_2 shows that the TiO_2 nanofluids are much more sensitive to temperature. But, the thermal conductivity of TiO_2 nanofluids is lower than water at a temperature below $10^{o}C$.

Giovanni and Claudio (2011) stated that this is due to experimental uncertainty of the measurement.
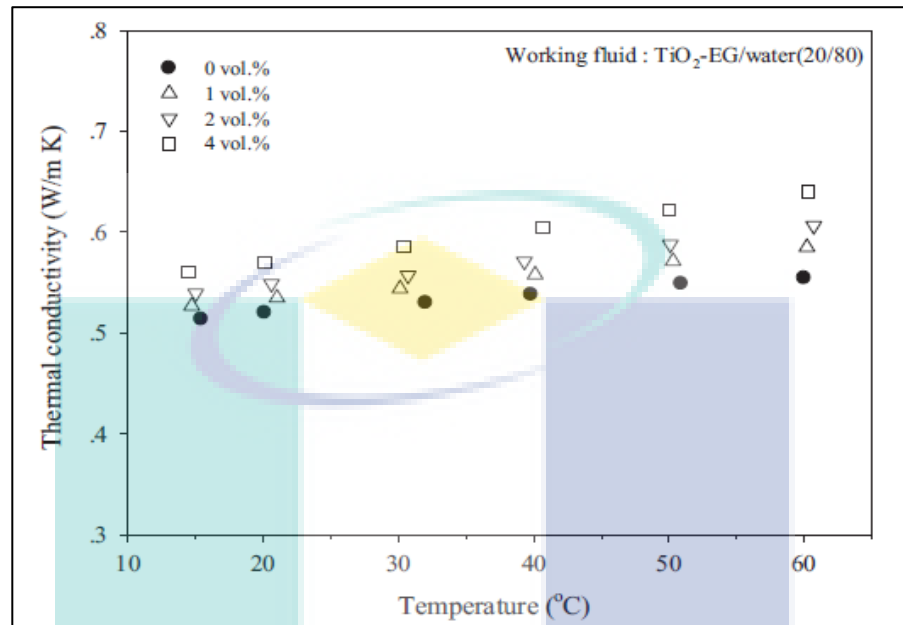
Figure 2.13: Thermal conductivity versus teperature for TiO$_2$/EG nanofluids at different volume percentage.

Source: Yiamsawad et al. (2012)

2.9   AISI 304 STAINLESS STEEL

AISI 304 stainless steel are mainly used in air craft fitting, aerospace components and some components in chemical environment. Besides that, it is also being used for welded construction in aerospace structural components. Most of this application needs certain machining process with different machines. All the machining process of AISI 304 stainless steel come across with huge number of difficulties such as poor surface finish due to high temperature in the cutting zone (Hossein and Yahya, 2005). The properties of AISI 304 stainless steel that contribute to the defect in the machining can be summarized as follows:

   a. Low thermal conductivity contributes to massive heat at the cutting zone which will effects the surface integrity (Hossein and Yahya, 2005).

b. High deformation hardening of AISI 304 stainless steel will cause wear on the flank of the cutting tool (Hossein and Yahya, 2005).

c. It is also classified as alloy with higher tendency of build-up-edge (BUE) which affects the life span of the cutting tool and the surface roughness (Shao et al., 2007).

d. It is also classified as high hardness and wear resistant which contribute to poor surface roughness during machining (Safian et al., 2009)

Furthermore, during the machining of this alloy, a strong bong has been form between the workpiece and the cutting tool and when the chip is formed, it may bring with it a fragment of the tool and cause a flank wear. This is mainly for cemented carbide tool (Shao et al., 2007). Basically, machining AISI 304 stainless will encounter a lot of problem and this is very common in industry. Therefore according to Xavior (2012) machining with optimum cutting parameter will reduce the defects on the machining surface. The best cutting speed and feed rate parameter were determined according to flack wear, BUE, chip form and also surface roughness (Yazid et al., 2011).

2.10 CUTTING TOOL MATERIAL FOR AISI 304 AUSTENITE STAINLESS STEEL

Since AISI austenite stainless steel has been classified as a "difficult-to-cut" material, the cutting tool material used to cut this material must be good in strength, thermal properties, wear resistant and also adequacy of chemical stability at high temperature. According to Benardos and Vosniakos (2002) modern cutting tool are coated with ceramic and thus providing lower attraction to tool and lower thermal conductivity of the tool which rise the chip temperature and enabled flow of the chip (Yazid et al., 2011). Various alloys have been added to the coating element to advance the properties of the cutting tool. Titanium nitride (TiN) is one of the protective hard coating materials for carbide cutting tool (Hossein and Yahya, 2005). But, according to Oskouei and Ibrahim (2012) chromium nitride (CrN) is consider superior than TiN in term of corrosion and wear resistant, friction behavior and toughness. However, TiN and CrN are limited up to 500 $^\circ$C and 600 $^\circ$C temperatures respectively. Besides that,

(Ti,Al)N and (Al,Cr)N coating showed a great improvement thermal resistant up to 900 $^{\circ}$C which can withstand huge amount cutting temperature. This is due to the formation of steady oxidation layer of Al_2O_3, Cr_2O_3 and TiO_2 layers. On the other hand, (Ti, Al)N coating had enhanced abrasive wear resistant but (Al, Cr)N coating are more recommended has thermally stable.

According to Sim, 1972 cutting tool materials used for AISI 304 stainless steel shall be good in wear resistance, strength, toughness, hot hardness, thermal shock properties and adequacy of chemical stability at elevated temperatures. High-speed steels and cemented carbide cutting tools are widely used for machining stainless steel and these tools materials are the only choice for the machining of exotic superalloys for several decades. High speed steels are usually employed for intermittent cutting operations such as milling, drilling, tapping and broaching. Cemented carbides are mainly used for continuous cutting operations such as turning, boring and facing. Currently, some new ceramic tool materials such as Al_2O_3–TiC mixed ceramics, Si3N4 ceramics and the latest SiC whisker-reinforced Al_2O_3 ceramics (containing 25% SiC whiskers) have been increasingly used for machining stainless steel (Richards and Aspinwall, 1989). The use of single-layer (TiN) coated carbide tools, produced by the physical vapor deposition (PVD) technique have also shown remarkable improvement in the machining of nickel-based alloys (Ezugwu and Wang, 1996). Cubic boron nitride (CBN) cutting tools appear to give better overall performance than cemented carbides when machining nickel-based alloys although the principal application areas for CBN are in the machining of ferrous materials (Shintani et al.,1992). The cost of CBN tools does which is expensive.

2.11   RESPONSE SURFACE METHOD

Response surface method (RSM) is a collection of mathematical and statistical techniques for empirical model building. In a design of experiments, the objective is to optimize a response (output variable) which is influenced by several independent variables (input variables). An experiment is a series of tests, called runs, in which changes are made in the input variables in order to identify the reasons for changes in the output response. RSM is firstly developed to model experimental responses and then

migrated into the modeling of numerical experiments. The difference is in the type of error generated by the response. In physical experiments, inaccuracy can be due to measurement errors whereas in computer experiments, numerical errors are due to incomplete convergence of iterative processes, round-off error or the discrete representation of continuous physical phenomena. In RSM, the errors are assumed to be random (Douglas, 1997). The Response surface method (RSM) is a methodology of constructing approximations of the system behavior using results of the response analyses calculated at a series of points in the variable space. Optimization of RSM can be solved in the following three stages:

- Design of experiment.
- Building the model.
- Solution of minimization problem according to the criterion selected.

RSM is a combination of experimental and regression analysis and statistical inferences. The concept of a response surface involves a dependent variable *y* called the response variable and several independent variables *x1*, *x2*, . . .,*xk* (Khuri and Cornal, 1996). If all of these variables are assumed to be measurable, the response surface can be expressed as:

$$y = f(x1; x2; \ldots; xk) \tag{2.2}$$

Usually a low order polynomial (first-order and second-order) is employed in some regions of the independent variables. The first-order model:

$$y = \beta_0 + \sum_{i=1}^{k} \beta_i x_i + \varepsilon \tag{2.3}$$

and the second–order model:

$$\sum_{i=1}^{k} \beta_i x_i + \sum_{i=1}^{k} \beta_{ij} x^2_i + \sum_i \sum_j \beta_{ij} x_i x_j + \varepsilon \text{ for } i<j \tag{2.4}$$

They are generally utilised in RSM problems. The β parameters of the polynomials are estimated.The RSM is practical, economical and relatively easy to use and it has been employed by many researchers for modeling machining processes (Baradie, 1996).

Mead and Pike (1975) and Hill and Hunter (1966) have reviewed the earliest works on RSM. In order to institute an adequate functional relationship between the surface roughness and the cutting parameters (speed, depth of cut and feeds), a large number of tests are needed, requiring a separate set of tests for each combination of cutting tools and workpiece materials. Fuh and Wu (1995) have proposed prediction models based on the Takushi method and RSM. By using factors such as cutting speed, feed and depth of cut, Alauddin et al. (1995) have developed surface roughness models and determined the cutting conditions for AISI 304 stainless steel and Inconel 718. They have found that the variations of both tool angles have important effects on surface roughness. In order to model and analyse the effect of each variable in minimizing the number of cutting tests, surface roughness models based on RSM and experimental design have been determined in this investigation. Mishra (1985) has derived a relationship to study the residual stresses based on a moving heat source under various simulated cutting conditions, but the predicted trend is not in good agreement with the results of actual machining. RSM has been utilized to determine the residual stresses under different cutting conditions and materials. Whilst the properties of the materials are not identical except for tensile strength, some materials machined by a tool with a chamfer have been subjected to microstructure change due to temperature effect (Wu and Matsumoto, 1990).

2.12 CONCLUDING REMARK

1. There are two different view of mechanic of metal cutting which a new surface are formed by plastic deformation on the tip of cutting tool and the amount of energy required to cutting due to plasticity and friction forces.

2. The build-up-edge (BUE) can occur during the low cutting speed and does not occur at high cutting speed because there is no strain hardening if the recrystallization temperature is much greater during the deformation process.

3. The most common type of tool wear for milling AISI 304 stainless steel is flank wear, crater wear, notch wear, chipping and comb crack. The failure criteria of flank wear is 0.3 mm.

4. The surface roughness increases when the cutting speed and feed rate increases and the surface roughness decreases when the axial depth of cut increases.

5. All the results shows that the thermal conductivity of nanofluids exhibits higher thermal properties even the concentration of liquid is less than 5% in volume percentage.

6. ZnO/EG nanofluid have low stabilization time than TiO_2/EG nanofluid which is stable for more than 2 weeks.

7. TiO_2 nanofluids are much more sensitive to temperature than ZnO nanofluid. The thermal conductivity of nanodfluid increases with increases in temperature.

8. Machining process of AISI 304 stainless steel come across with huge number of difficulties such as poor surface finish due to high temperature in the cutting zone.

9. RSM was developed to model experimental responses and then migrated into the modelling of numerical experiments. The difference is in the type of error generated by the response. In physical experiments, inaccuracy can be due to measurement errors whereas, in computer experiments numerical errors are due to incomplete convergence of iterative processes, round-off errors or the discrete representation of continuous physical phenomena.

10. The RSM is practical, economical and relatively easy to use and was employed by many researchers for modeling machining processes.

CHAPTER 3

METHODOLOGY

3.1   INTRODUCTION

The purpose of this chapter is to provide the information regarding the design of experiment, equipment used throughout the experiment, cutting tool material, workpiece material that has been used in this research. The experiment has been carried out in two stages which is preliminary run and real experiment. The aim of preliminary run is to find excellent range of cutting parameter. The real experiment will carry out by using the detailed base on the preliminary run.

3.2   EXPERIMENTAL DESIGN AND SELECTION OF CUTTING DATA

Based on the literature review, the process of discover a proper combination of cutting parameter is very high cost and time consuming. The results from preliminary test with different combination of cutting parameter which consist of cutting speed, feed rate, and depth of cut, it is decided to use design of experiment (DOE) to find the optimum range of cutting parameter of the cutting tool selected. Besides that, response surface method (RSM) is used to found the optimum cutting parameter for AISI 304 stainless steel.

3.3   DESIGN OF EXPERIMENT

For the purpose of design and analysis the experimental results the following guiding principle has been followed:

   a. Recognition and statement of the problem
   b. Selection of factors, ranges and level.
   c. Selection of response variable
   d. Selection of experiment design
   e. Run the experiment

    f. Analysis of data by using statistical model

    g. Conclusion and recommendation

Each of the guidance above has been explained in detail as follows:

3.3.1   Recognition and statement of the problem

The purpose of this study is to analysis and optimizes the cutting parameter such as cutting speed, feed rate and depth of cut on tool wear, tool life and surface roughness.

3.3.2   Selection of factors, ranges and level

The factor that has been selected from the preliminary experiment is cutting speed, feed rates and axial depth of cut. These are the factor that are used to analysis and optimized the result against the tool life, tool wear and surface roughness. Three level of cutting condition has been selected which consist of high, medium and low. The range of the cutting parameter has been selected based on the preliminary experiment to avoid quick damages on tool and workpiece.

3.3.3   Selection of response variable

Based on the preliminary test, the response variable are tool life, tool wear, and surface roughness. The variable has been identified whether it have to maximized or minimized.

3.3.4   Selection of experiment design

Response surface method (RSM) is used to design the experiment. The combination of factor which consists of cutting parameter has been generated by using RSM. Besides that RSM can generate the optimal parameter value based on the mathematical and statistical technique. The benefit of RSM as follow:

    a. Clearly shows the relation between the factor and response in term of mathematical and statistical.

    b. Find factor settings in which process specifications are satisfied.

c. Find factor settings that optimize the process response.

d. Identify new operating conditions that produce demonstrated quality improvement over the quality achieved by current condition.

There are two type of DOE's which is central composite design (CCD) and box-behnken design (BBD). Throughout this study, BBD was chosen as the design of experiment. BBD produce a quadratic relationship between the experimental factor and response. The key reason for choosing BBD is to estimate the response in term of first-order and second-order. Besides that, BBD is much cheaper in term of cost compared to CCD. Figure 3.1 shows the example of BBD for three different variables where X_1 = cutting speed, X_2 = feed rate and X_3 = axial depth of cut.
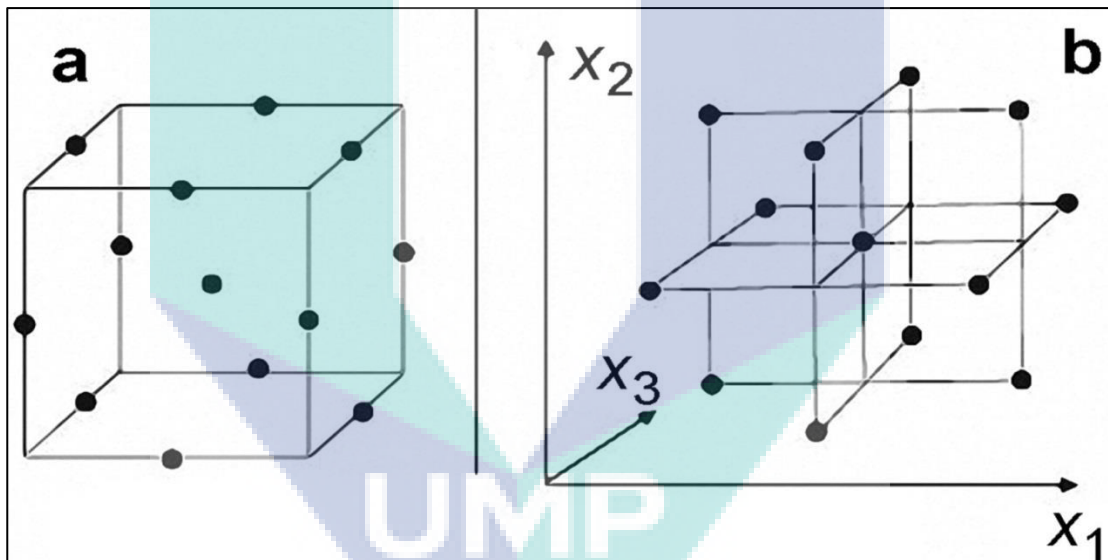
Figure 3.1: Example of BBD for three different variable

Source: Chakraborty et al. (2008)

3.4   CUTTING TOOL MATERIAL

The milling insert are made by Ceratizit on the basis of the ISO catalogue number of XDKT 11T308SR-F50. This milling insert is a coated carbide grade with TiN coating CVD. TiN is considered as very ductile because it's relatively very hard. The thickness TiN used for coating is 3 μm. TiN coating will increases the wear resistant and reduces the friction during machining process. This coating will form a metallurgical bond the cutting tool that will not peel easily during the machining process. The shape of the insert used in this study is X-shaped insert which is slotted into a 32 mm diameter tool holder. This insert is specified to use under flooded machining. Throughout this study, only one insert per experiment mounted to the tool holder to perform the milling experiment. The cutting tool implement in this experiment are shown in Figure 3.2. The specification of the insert shown in figure 3.3 where where $d = 4.9$ mm, $l_1 = 1.2$ mm, $l = 7.8$ mm, $\alpha = 15^{\circ}$, $d_1 = 2.5$ mm and $s = 3.18$ mm.
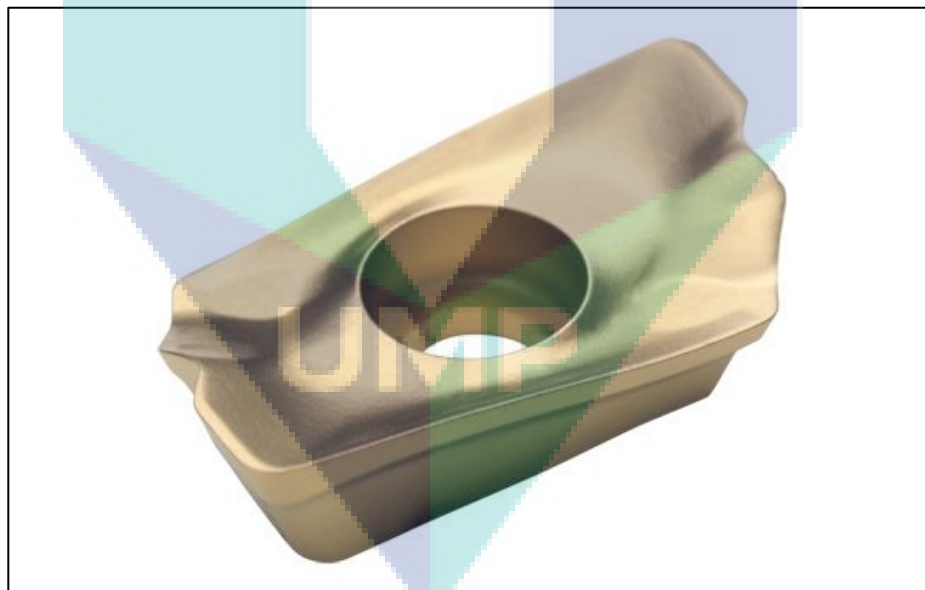
Figure 3.2: Cutting tool used in these experiment

Source: (https://www.toolingcenter-india.com)
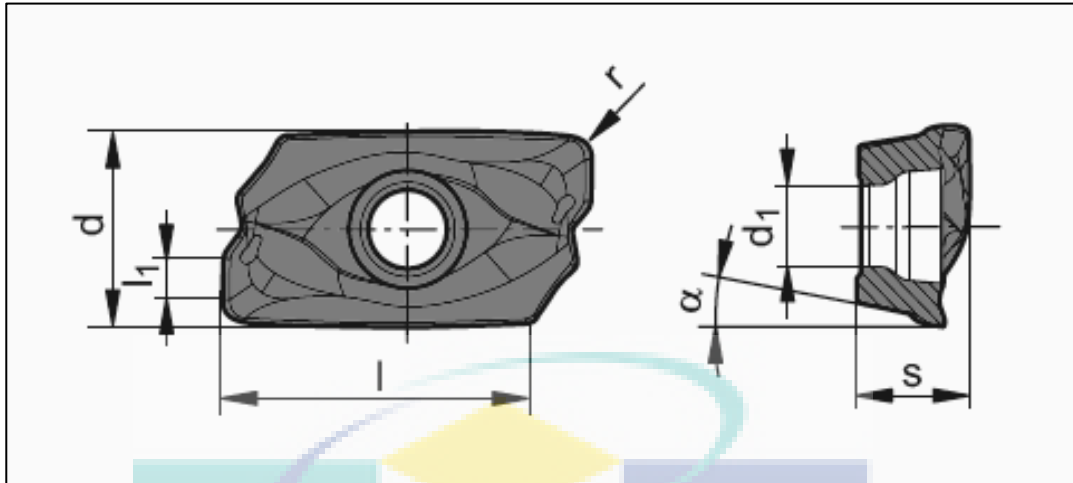
Figure 3.3: Geometry of the insert

Source: (https://www.toolingcenter-india.com)

3.5   CUTTING SPEED

The term of cutting speed is referring to the linear speed on the cutting zone. The measured unit for this speed is rpm. As stated before, three level of cutting speed is selected which is high, medium and low. However, the selected range of the cutting speed is based on the cutting tool supplier to estimate the flank wear criteria for AISI 304 stainless steel. The three level of cutting speed are as follow:

a.   1500 rpm

b.   2000 rpm

c.   2500 rpm

3.6   FEED RATE

Tool feed rate is defined as the relative motion of the cutting tool during the cutting process. The feed rate is measured in millimeter per tooth (mm/tooth). Three level of feed rate is selected which is low, medium and high. The rate of the feed rate is in between the feeds suggested by the workpiece supplier. The three level of feed rate are as follow:

a. 0.02 mm/tooth

b. 0.03 mm/tooth

c. 0.04 mm/tooth

3.7   AXIAL DEPTH OF CUT

The axial depth of cut is the distance of the tool along its axis in the workpiece as it makes a cut. The axial depth of cut in this study is focused on this finishing end-mill process. Previous study stated that finish cut for milling process is below than 0.4 mm of cut. Above this axial depth the roughness is considered ruthless and never considered as finishing process for austenite stainless steel (Zhou et al., 2010). Besides that, since austenite stainless steel is considered very hard material with hardness around Rockwell B 70 it is suggested to use low axial depth of cut during milling to avoid huge wear on cutting tool. Therefore three axial depth of cut which is selected for this study are as below:

a. 0.01 mm

b. 0.02 mm

c. 0.03 mm

3.8   DESIGN OF EXPERIMENT

There are two type of experiment design has been created to conduct the end-milling process on AISI 304 stainless steel. The first set of experiment design was created for end-milling process by using water soluble coolant and the second set of experiment coolant was created for end-milling process by using ethylene glycol based TiO_2 nanocoolant. However, the milling parameter used for each set of experiment set is similar as shown in Table 3.1. The range of cutting speed value was selected of 1500 rpm and 2500 rpm. The range of feed rate value was selected between 0.02 mm/tooth to 0.04 mm/tooth and the range of axial depth of cut value was selected between 0.1 mm to 0.3 mm

Table 3.1: The value selected for each parameter

Parameter/ Coding level	-1	0	+1
Cutting speed (rpm)	1500	2000	2500
Feed rate (mm/tooth)	0.02	0.03	0.04
Axial depth (mm)	0.1	0.2	0.3

The first set of end-mill experiment was conducted with water soluble coolant. Therefore the concentration of the coolant was not count for this experiment. By using Minitab 15, the experiment design was created with aid of Box-behnken design. The total end-milling test for this experiment was 15 with varying cutting speed, feed rate and axial depth of cut. Table 3.2 show the selected value for each parameter.

Table 3.2: Selected value for each parameter for end-mill experiment using water soluble coolant

Experiment	Cutting Speed, rpm	Feed Rate, mm/tooth	Depth of Cut, mm
1	2000	0.03	0.2
2	2500	0.03	0.3
3	2000	0.02	0.1
4	2500	0.04	0.2
5	2000	0.03	0.2
6	2000	0.02	0.3
7	2500	0.03	0.1
8	1500	0.04	0.2
9	2000	0.03	0.2
10	1500	0.02	0.2
11	2500	0.02	0.2
12	1500	0.03	0.1
13	1500	0.03	0.3

14	2000	0.04	0.3
15	2000	0.04	0.1

The second set of end-mil experiment was conducted with ethylene glycol based TiO_2 nanocoolant. In this experiment another parameter has been included which is concentration of the coolant. Three concentration of coolant has been selected after analyzing the properties study of the nano fluid which is 0.5, 1.0 and 1.5 volume percentage. Therefore, the total end-milling test which generated by statistical software for this experiment was 27 as shown in Table 3.3.

Table 3.3: Selected value for each parameter for end-mill experiment using ethylene glycol based TiO_2 nanocoolant.

Experiment	Cutting Speed, rpm	Feed Rate, mm/tooth	Depth of Cut, mm	Concerntration, V%
1	2000	0.04	0.2	0.5
2	2000	0.03	0.1	1.5
3	2000	0.03	0.1	0.5
4	2000	0.03	0.3	0.5
5	2500	0.04	0.2	1
6	2000	0.04	0.1	1
7	2000	0.03	0.2	1
8	1500	0.03	0.3	1
9	2000	0.04	0.2	1.5
10	1500	0.03	0.2	0.5
11	1500	0.03	0.1	1
12	2000	0.02	0.2	1.5
13	2000	0.02	0.3	1
14	2000	0.03	0.2	1
15	1500	0.02	0.2	1
16	2000	0.04	0.3	1
17	2500	0.03	0.3	1
18	2000	0.02	0.2	0.5

19	2000	0.03	0.3	1.5
20	1500	0.04	0.2	1
21	2000	0.02	0.1	1
22	1500	0.03	0.2	1.5
23	2500	0.03	0.2	0.5
24	2500	0.03	0.2	1.5
25	2500	0.03	0.1	1
26	2500	0.02	0.2	1
27	2000	0.03	0.2	1

3.9   TOOL LIFE MEASUREMENT

The measurement of tool life is measured by the total distance of cuts by the milling inserts to reach the maximum flack wear criteria which is 0.3 mm. ISO 8688-2:1989 (E) stated that a recommended uniform wear criteria is 0.3 mm and the maximum wear criteria is 0.5 mm when end-mill austenite stainless steel (ISO 8688-2:1989 End mill testing. However, there is no specific ISO standard for end-mill AISI 304 stainless steel by using CVD TiN coated carbide inserts. The end-milling test will be conducted until anyone of the below criteria is archieved:

    a.   Flank wear reached 0.3 mm

    b.   Maximum wear criteria reached 0.5 mm

    c.   Major fracture or catastrophic failure

3.10   PHYSICAL EQUIPMENT AND MATERIAL

3.10.1 Workpiece material

AISI 304 stainless steel block supplied by Haynes International were used for the experiment as shown in Figure 3.4. The size of the block is 180×100×25 mm. The hardness of this block is around Rockwell B 70. The chemical and physical properties of the workpiece material are shown in Table 3.4 and Table 3.5.
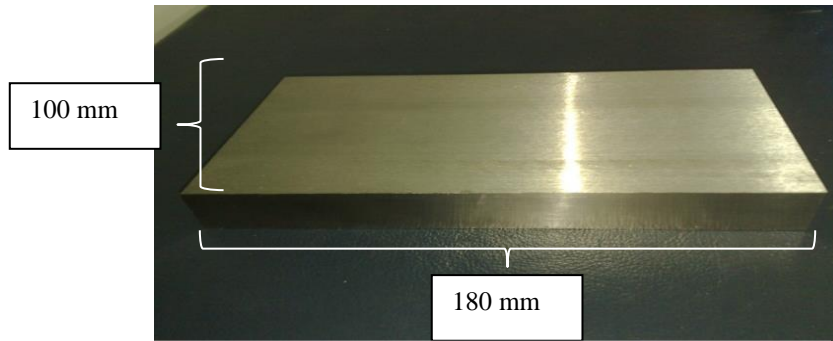
Figure 3.4: Workpiece marterial

Table 3.4: Chemical composition of workpiece material.

Source: Hossien and Yahya (2005)

Element	C	Si	Mn	Cr	Mo	P	S	Ni
Wt %	0.02	0.32	1.31	16.4	2.03	0.30	0.20	12.17

Table 3.5: Physical properties of workpiece material.

Source: Shah and Gawande (2012)

Properties	Value
Density (kg/m^3)	8000
Elastic Modulus (GPa)	193
Mean Coefficient of Thermal Expansion (μm/m/^{o}C)	17.8
Thermal Conductivity at 100°C	16.2
Thermal Conductivity at 500°C	21.5
Specific Heat (J/kg.K)	500

3.10.2 CNC MACHINING CENTER

The CNC machine which was used for the end-milling experiment is HAAS CNC Minimill machine. This machine was driven by a 5.6 kW electrical motor. This is a vertical machine center with size of 406×305×245 mm and maximum spindle speed of 6000 rpm. Figure 3.5 shows the CNC machine that was used to perform the end-mill experiment. Table 3.6 shows the specification of HAAS CNC Minimill center.

Figure 3.5: HAAS CNC Minimill that was used for this study

Table 3.6: Specification of HAAS CNC Minimill

Specification	Value
X-axis	406 mm
Y-axis	305 mm
Z-axis	254 mm
Spindle nose to table (maximum)	356 mm
Spindle nose to table (minimum)	102 mm

Table working area	730 mm
T-slot width	16 mm
Spindle speed range	10 to 6000 rpm
Maximum torque	1200 rpm
Spindle taper	Cat no. 40
Maximum cutting feed	12.7 m/mim
Maximum tool diameter	89 mm
Tool capacity	10
Maximum tool weight	5.4 kg
Air required	113 L/min
Coolant capacity	91 L

3.10.3 Scanning electron microscope

Scanning electron microscope (SEM) model Zeiss EVO 50 is equipped with EDAX X-ray was used for measuring the tool wear and to determine all the defects on the cutting tool after end-milling test. The composition and the chemical properties of the workpiece and cutting tool are tested by using the SEM with contribute a important detail for this research. Figure 3.6 sows the SEM that was used in this present study. The specification of the SEM is as follow:

a. The range of the acceleration voltage is from 0.2 to 30 kV.
b. Magnification range is from 5 to 1,000,000 times.
c. Resolution up to 3072×2304 pixel.
d. X-ray analysis is 8.5 mm AWD and 35° take off angle.

Figure 3.6: Scanning Electron Microscope (SEM) model Zeiss EVO 50

3.10.4 Surface roughness tester

A low weigh portable surface roughness tester model Mahr Pethometer S2 as shown in Figure 3.7 is used to measure the surface roughness of the workpiece after the machining done. The arithmetic average surface roughnes (R_a) mean roughness depth (R_z) was measured by using this instrument. Table 3.7 shows the specification of Pethometer S2.

Figure 3.7: Pethometer S3

Table 3.7: Specification of Pethometer S2

Specification	Detail
Roughness parameter	Ra, Rq; Rz, Rt, Rp, Rv, RSm, Rdq
Standard	DIN EN IOS/JIS/ASME 46.B
Measurement	by means of a stylus instrument
Tracing length	1/2/4/8/12/16 mm
Software	S2Prog Windows program
Unit	Mm or inch (selectable)
Display	graphics LCD module with
Dimension	approx. $150 \times 320 \times 250$ mm

3.10.5 Transmission electron microscope

Transmission electron microscope (TEM) model Philips CM-200 as shown Figure 3.8 was used to determine the size of nano particle and the agglomeration of nano particle in the based liquid with is ethylene glycol. It is equipped with a light element EDS X-ray detector and can detect the sample areas at the 10 to 20 nm scale. It is also capable of 0.27 nm resolution and has wide gap pole-piece to allow large tilt angles of specimen. The specification of the TEM as follow:

a. The acceleration is 200 kV with LaB6 cathode
b. It has 2.7 A resolution (twin lens) with about 70° sample tilt.
c. It has double-tilt, heating and cyro stages for specialized experiments
d. A fine probe and Convergent Beam Electron Diffraction (CBED)
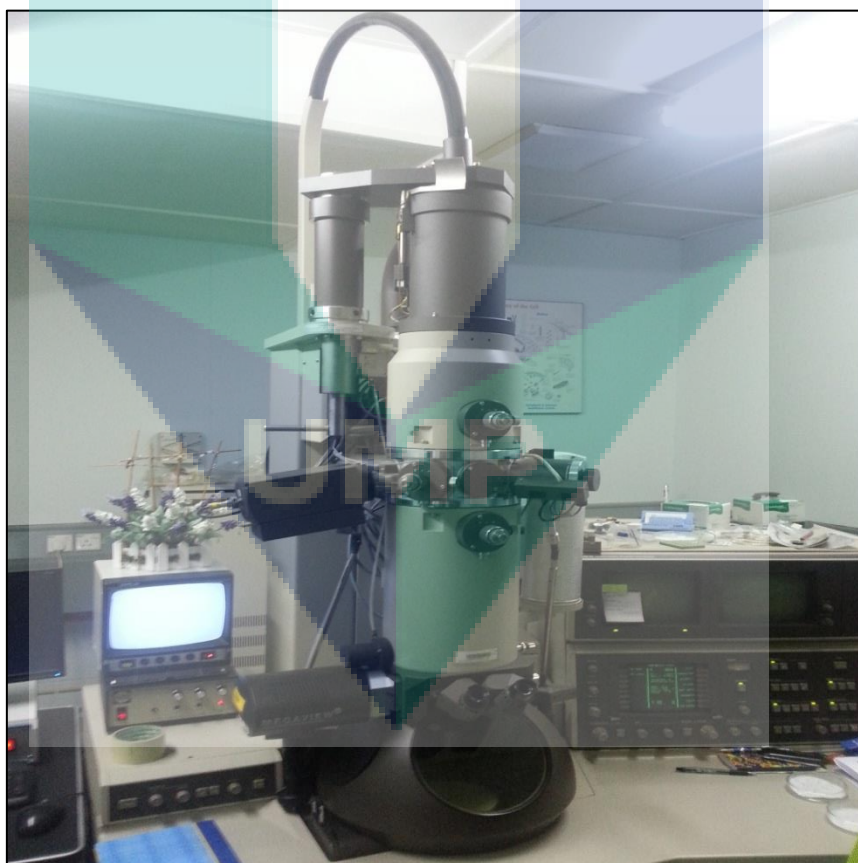
Figure 3.8: Transmission electron microscope (TEM) model Philip CM 200

3.11   METHOD OF DATA COLLECTION

The end-milling process was carried out by using the CNC machine as described in section 3.10.2 with water soluble coolant and ethylene glycol based TiO_2 nanofluid separately. Only one edge of the cutting tool was used for the testing in order to study the performance of the cutting tool. After each pass of end-milling process, the insert is removed the tool holder in order to measure the tool wear and surface roughness accordingly. Each pass of cutting is 180 mm. The surface roughness, flank wear and tool wear is measured after each pass of end-milling process. The machining process and the measured of the flack wear will repeated until the flack wear reach the ISO wear criteria which is 0.3 mm. The wear growth on the cutting tool will be measured and recorded. Along with this, the surface roughness also been measured by using Pethometer S2 as describe in section 3.10.4. The progressive of the surface roughness will be measured and recorded until the wear reaches the ISO wear criteria.

3.12   NANOFLUID PREPARATION

3.12.1 Selection of nanoparticles

Previous study reported that nanoparticles have a good convection heat transfer rate compared to its based liquid (Duangthongsuk and Wongwises, 2010) (Vajjha et al., 2010). The bonding between the pure metallic particles with oxide will tend to increase the stabilization in based liquid. Titanium oxide (TiO_2) and zinc oxide (ZnO) are among the nanoparticles which having a superlative heat transfer rate and stabilization (Zhou et al., 2010). Therefore, TiO_2 and ZnO nanoparticle was purchased from US Research Nanomaterials. Inc. These nanoparticles having a purity of 99.9 % and having a average particle size less than 50 nm. These two nanoparticle will be diluted according to the volume percentage for the further properties study. The properties study among these two nanoparticle will support to choose the preeminent nanoparticle which will selected to use as nanocoolant for the end-milling process.

3.12.2 Selection of volume percentage

In previous reviews, shows that the thermal conductivity of nanofluids is sensitive to the particle volume fraction and temperature and weak sensitivity to clustering size. This means that the size of nano particle have little effect on properties of nanofluid compare to volume concentration Giovanni and Claudio (2011). Yu et al. (2009) stated that the thermal conductivity is greater at higher volume concentration above 0.5 volume percentage (Yu et al., 2009). Hence, the nanofluids were prepared using dilution method at volume weigh percentage. Therefore, the weight percentage, ω need to be converted to volume percentage, φ by using Eq. (3.1). The volume of based liquid (60% ethylene glycol and 40% distill water), ΔV for preferred concentration, φ_2 can be found by using Eq. (3.2) with original condition of V_1 and φ_1.

$$\varphi = \frac{\omega \rho_w}{\left(1 - \frac{\omega}{100}\right)\rho_p + \frac{\omega}{100}\rho_w} \qquad \text{where } \omega = \left[\frac{m_p}{m_p + m_w}\right] \times 100 \qquad (3.1)$$

$$\Delta V = (V_2 - V_1) = V_1\left(\frac{\varphi_1}{\varphi_2} - 1\right) \qquad (3.2)$$

Next, the calculated base liquid (60% ethylene glycol and 40% water) quantity was used to dilute the 99.9% purity of nanofluid from supplier. The diluted nanofluid will be mechanical stirred for 3 hour by using digital motorized stirrer with 1200 rpm to ensure the nanoparticle fully dispersed into the based liquid as shown in Figure 3.9. However, previous study reported that the ultrasound treatment to the nanofluids produce better dispersion efficiency compared to mechanical stirring (Giovanni and Claudio, 2011).
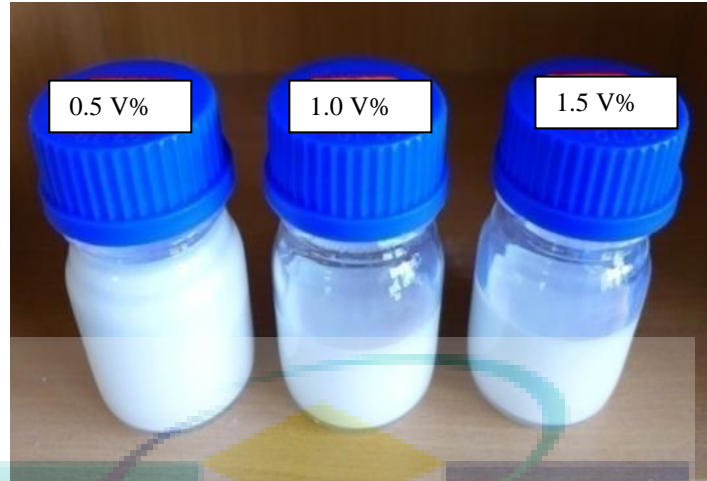
Figure 3.9: Observation process process

3.12.3 Thermal conductivity measurement of nanofluid

Thermal conductivity of the nanofluid is the important factor in this study. The thermal conductivity of the nanofluid is measured with thermal property analyzer which uses the transient line heat source to detect the thermal properties of the liquid. The thermal analyzer model is KD2 Pro as shown in Figure 3.10. The range of the measurement for this equipment is 0.2 W/m.K to 2.0 W/m.K. KS-1 sensors is used to measure the thermal conductivity of liquids. The measurement of thermal conductivity is validated by measure the thermal conductivity of distill water and glycerin. At room temperatures the thermal conductivity of distill water and glycerin was 0.610 and 0.280 W/mK, respectively. This result is agreed with the literature which thermal conductivity of distill water and glycerin is 0.613 W/mK and 0.285 W/mK, respectively, within ± 5% accuracy. The measurement of the thermal conductivity will recorded at 1 sec interval for 90 sec total 90 sec cycle. After the 90 sec cycle, the thermal conductivity value will calculated by the controller. The value of the thermal conductivity was validated by theatrical equation. As stated by Sharma et al. (2012), regression equation to predict the thermal conductivity has deviation of less than 11%.

$$K_{nf} = K_w \left[0.8938 \left(1 + \frac{\varphi}{100} \right)^{1.37} \left(1 + \frac{T_{nf}}{70} \right)^{0.277} \left(1 + \frac{d_p}{150} \right)^{-0.0336} \left(\frac{\alpha_p}{\alpha_w} \right)^{0.01737} \right]$$

(3.3)
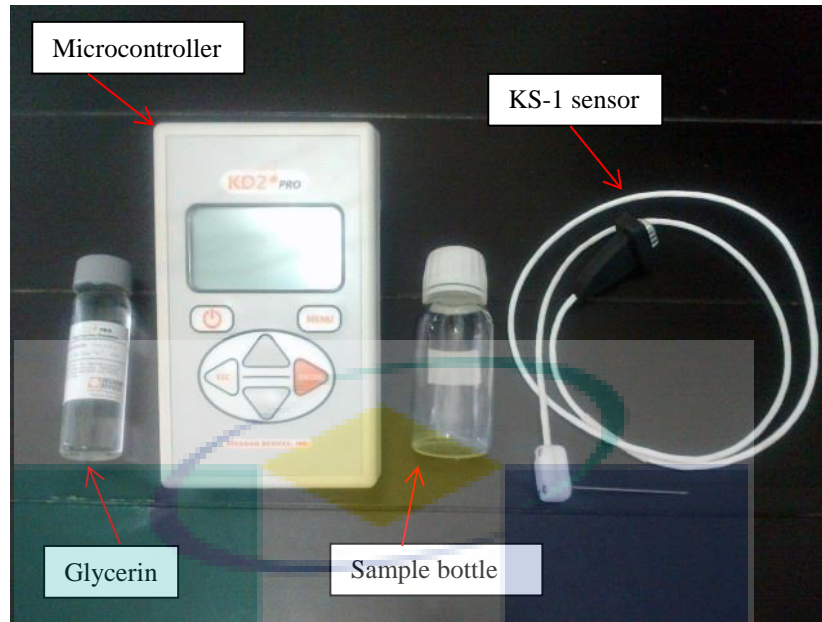
Figure 3.10: KD2 Pro used to measure the thermal conductivity of nanofluid

3.12.4 Viscosity measurement of nanofluid

The viscosity of the nanofluid is measured by using viscometer as shown in Figure 3.11. Before measuring the viscosity of nanofluid, the viscometer is validated with measurement of distill water at room temperature. The measured viscosity of nanofluid is validated by using Eq. (3.4). As detailed by Sharma et al. (2012), the regression equation can be used to predict the viscosity of nanofluid. The average deviation, standard deviation and maximum deviation for this equation is 3.18%, 3.8% and 13% receptively when compared with experimental data.

$$\frac{\mu_{nf}}{\mu_w} = C_1 \left[\left(1 + \frac{\varphi}{100}\right)^{11.3} \left(1 + \frac{T_{nf}}{70}\right)^{-0.038} \left(1 + \frac{d_p}{170}\right)^{-0.061} \right] \tag{3.4}$$

3.12.5 Preparation the grid for TEM

The TEM grid size is 3.05 mm diameter ring with thickness of 100 µm. the grid material is made of copper. The sample is placed into the inner diameter of the ring which is about 2.5 mm. First, the forceps are cleaned with 99.9% ethanol to remove any unwanted particle stick on the forceps which will distract the result. Forceps is used to grasp the carbon grid ring. Next, one drop of nanofluid sample solution dropped on the grid. Then, the drop will be dried with normal air for 15 min. After dried the grid brought to TEM as shown in Figure 3.8 for detail image.

3.13 WORKPIECE PREPARATION

First, the AISI 304 stainless steel block were cleaned up with sandpaper 240 grit to removes the dust or any undesirable dust particle on surface of the workpiece. Then, the top layer of the workpiece was removed by face milling to make sure the surface of the workpiece is stable.

3.14 PREPARING THE CUTTING TOOL

Before the experiment, each cutting insert was observed for any defects. Then, the cutting tool will be screw together with the holder. Only one side on the holder will be attached with the insert to in order to study the performance of the cutting tool.

3.15 PREPARING THE CNC MACHINE

Before run the milling experiment, the machine need to prepared. The table of the machined need to be clean up by using cloth to ensure there is no chip which will distract the stability of the workpiece. Then, place the vise on the table and put the t-slot nuts and bolts in position but it need to be loose. Before tighten up the nuts, the vise need to be square to make sure the workpiece clamped according to the dimension.

3.16   MILLING THE WORKPIECE

First, the workpiece block were clamped on the vise which on the table on the machine. CNC programming was used to cut along the surface of the workpiece which is considered 1 pass. The program was stop after 180 mm of cut which is considered 1 pass to measure the flack wear and the surface roughness on the workpiece. After each pass of cut, the workpiece surface will flat by using face milling before proceed with the next pass.

3.17   MEASURING THE SURFACE ROUGHNESS

Surface roughness values were measured by using Pethometer S2 as described in section 3.10.4. A total of 3 measured were taken to determine the average surface roughness of the end-mill surface. The surface roughness readings were taken in the center and both edge of the end-mill surface as shown in Figure 3.11. The 3 reading which is Ra_1, Ra2 and Ra_3 to determine the average surface roughness.
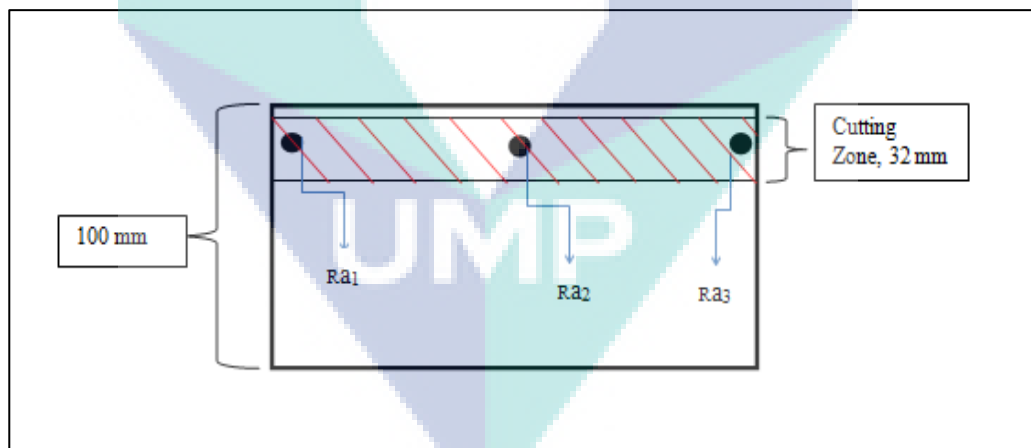
Figure 3.11: Surface roughness reading point on the milling zone

3.18   MEASURING THE FLANK WEAR

The measurement of the flank wear is done parallel together with surface roughness measurement. The flank wear measurement is the width from the original cutting edge to the limit of wear land. The measurement of flank wear is measured after each pass of end-mill process. As recommended by ISO 8688-2-1989 (E) the wear criteria for end-milling steel are 0.3 mm. The measured flank wear is recorded after each pass until the wear reaches the wear criteria. After recording the flank wear, the insert will tighten up again with tool holder to continue with next pass.
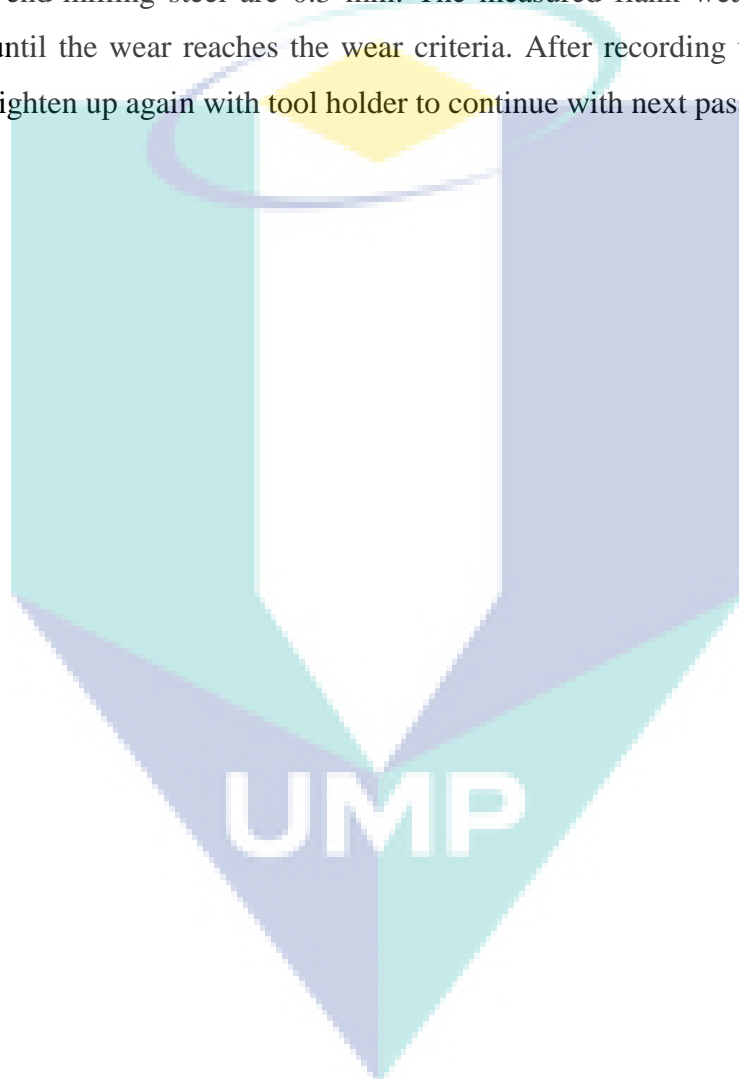
CHAPTER 4

RESULTS AND DISCUSSION

4.1 INTRODUCTION

The main purpose of this chapter is to discuss the milling responses (surface roughness, tool life and tool wear) when the milling process is conducted with different cutting conditions and coolant (water soluble coolant and ethylene glycol based TiO_2 nanofluid). The thermal properties of the nanofluids were analyzed and evaluated to select the suitable nanofluid used as milling coolant. Mathematical models have been developed by using response surface method to find the relationship between the variables and responses. The optimum cutting condition has been developed and analyzed by using surface optimizer. The type of the wear and wear mechanisms also been discussed in this chapter. The experimental result has been validated from previous research to support the results.

4.2 CHARACTERIZING OF NANOFLUIDS

4.2.1 Evaluation of nanofluids

The prepared ethylene glycol based TiO_2 nanofluid and ethylene glycol based ZnO nanofluid were evaluated and characterized based on the nanoparticle size, shape, pH value and the sedimentation time. The nanofluids were prepared at various selected concentrations which are 0.5 vol%, 1.0 vol% and 1.5 vol%. Table 4.1 shows the characteristic of each nanofluid. Figure 4.1 and Figure 4.2 shows the micrographic image from TEM in which the average nanoparticle size, shape and the agglomeration of the nanoparticle in the based liquid can be observed. It was noticeably that the shape of the TiO_2 nanoparticle is rectangular rod with average size of 30 to 50 nm as shown in Figure 4.1 (a). Figure 4.1 (b) shows the clustering average size of the TiO_2 nanoparticle

in the based liquid approximately 210 nm. This result is supported by Giovanni and Claudio (2011) where the nanofluid prepared by mechanical stirring process will produce the clustering average size of 220 nm while after sonification process the average cluster size will reduce to 155 nm for ethylene glycol based TiO_2 nanofluid. Figure 4.2 (b) shows that the average size of ZnO nanoparticle is 15 to 30 nm with spherical shape. The average size of ZnO nanoparticle is much lower than TiO_2 nanoparticle but the clustering size of ZnO is very high compared to TiO_2 nanoparticle which is approximately 710 nm. This confirms that the agglomeration in ZnO nanoparticle is much greater than TiO_2 nanoparticle in the based liquid. This is the reason for lower sedimentation time for ZnO nanofluid which is within 5 hour however TiO_2 nanofluid sedimentation only noticeable after 3 weeks. The weak stability of ZnO nanofluid can be related with the particle agglomeration and clustering size. According to Ding et al. (2007) agglomeration occur during the preparation of nanofluid due to high surface contact between the particles. This particles form a strong van der Waals force which was very hard to break it into primary nanoparticle. On the other hand, Murshed et al. stated that the surfactants will make sure the particle fully dispersed in the base liquid by electrostatic repulsive force among the nanoparticle and hydrobic surface force due to physical adsorption of surfactant in the liquid. Therefore, ZnO nanofluids required surfactants to reduce the agglomeration between the particles. TiO_2 nanofluid showed a stable suspension in ethylene glycol and able to sustain more than three weeks by just prepared with mechanical stirring process without surfactants. The stability of nanofluid is important for constant enhancement in heat transfer and prevents fouling in the coolant tank. Hence, ethylene glycol based TiO_2 nanofluid is selected as the replacement coolant for milling process rather than ethylene glycol based ZnO nanofluid.

Table 4.1: Characteristic of nanofluid

Nanoparticle type	Based Liquid	Shape	pH value	Average size (nm)	Sedimentation time
TiO_2	EG	Rectangular Rod	8.2-8.5	30-50	More than 3 week
ZnO	EG	Spherical	9.8	< 30	Within 5 hour
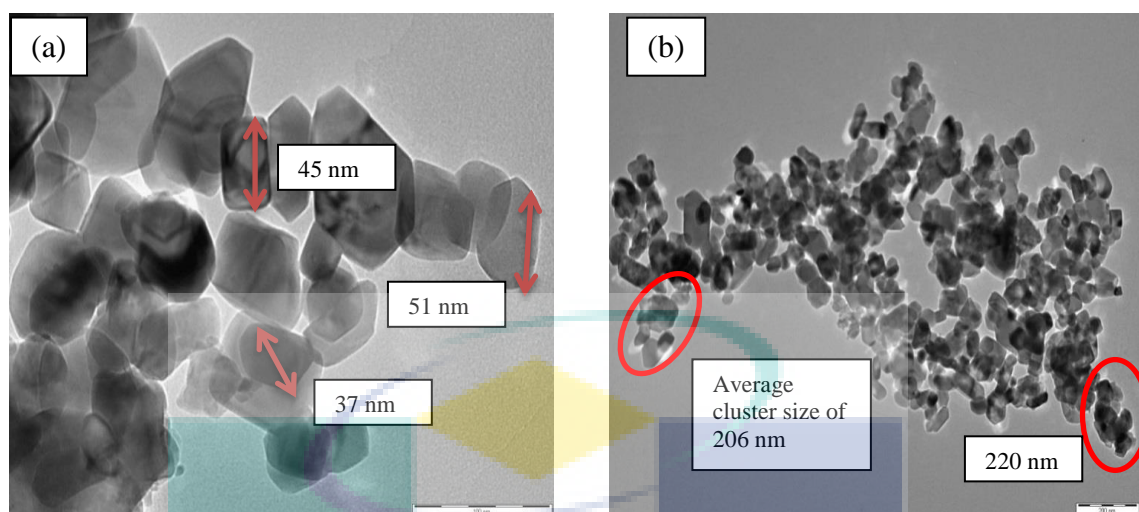
Figure 4.1: TEM micrographic image for TIO$_2$ nanofluid (a) size and shape (b) agglomeration
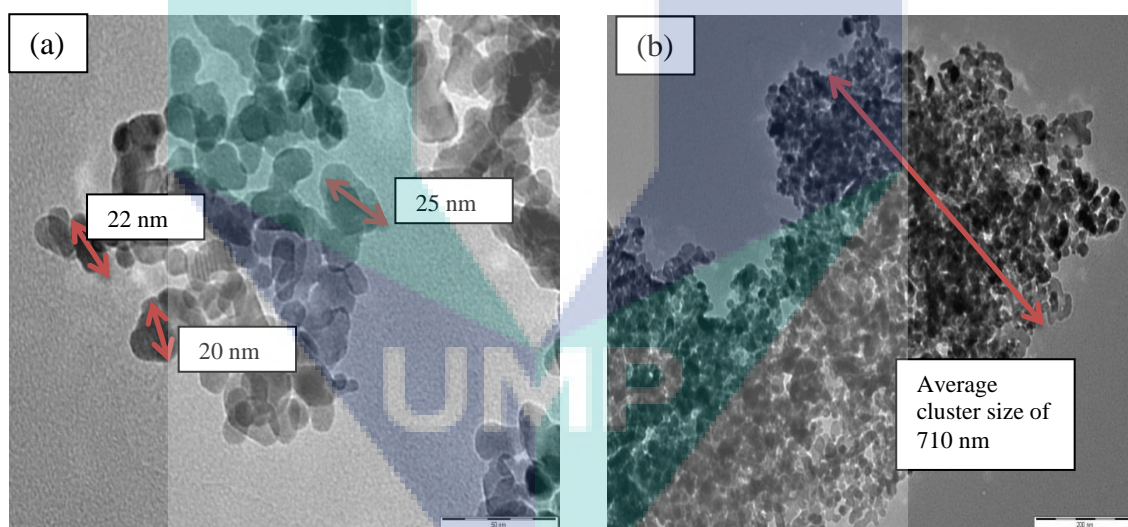
Figure 4.2: TEM micrographic image for ZnO nanofluid (a) size and shape (b) agglomeration

4.2.2 Thermal conductivity of nanofluid

The thermal conductivity of ethylene glycol based TiO$_2$ nanaofluid in volume concentration which is 0.5 vol %, 1.0 vol % and 1.5 vol % were measured at the range of 10 °C to 60 °C. The experimental result of thermal conductivity was validated with

the value with Eq. (3.3) and the data from literature review as shown in Figure 4.3-4.5. Figure 4.3 until Figure 4.5 shows that the thermal conductivity of ethylene glycol based TiO$_2$ nanofluid was in good agreement with previous study by Yiamsawad et al. (2012). The result shows that the thermal conductivity increased with an increase in temperature. This is because the nanoparticles are rapidly mobilized at high temperature. The stochastic motion of nanoparticle could be the explanation of thermal conductivity enhancement at high temperature (Das et al., 2003).
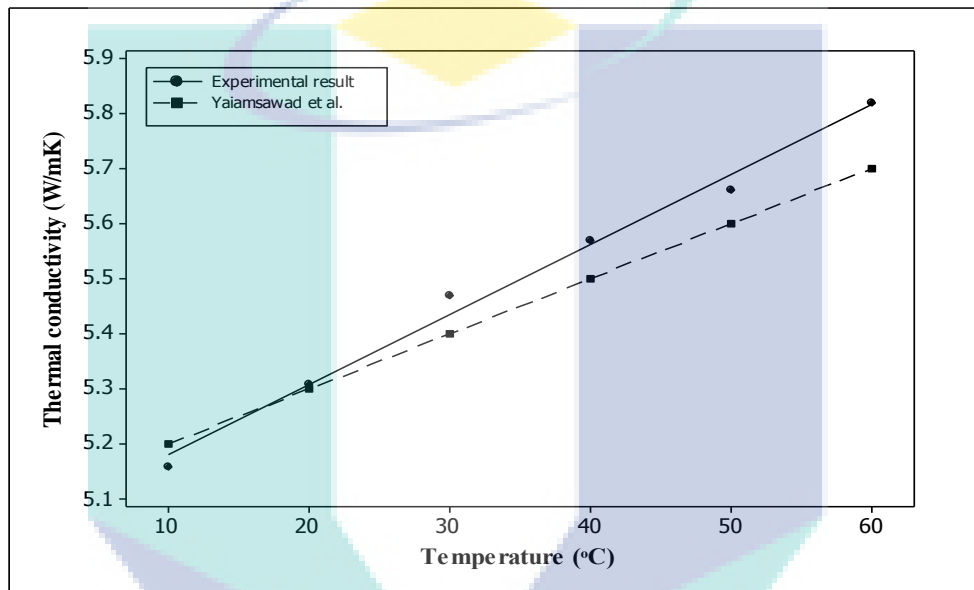
Figure 4.3: Thermal conductivity at 0.5 vol %
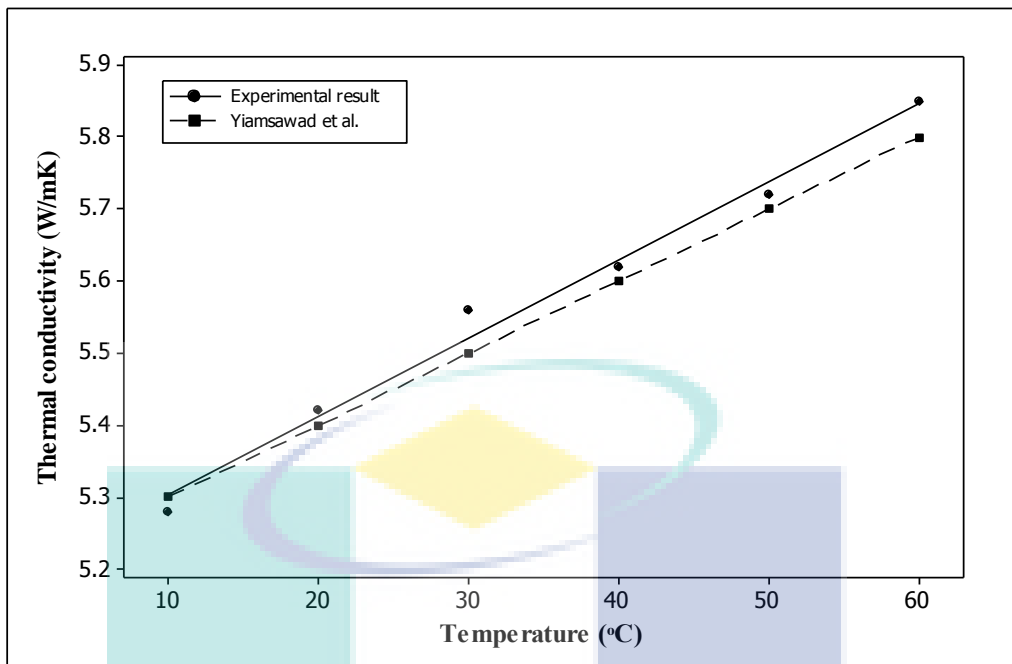
Figure 4.4: Thermal conductivity at 1.0 vol %
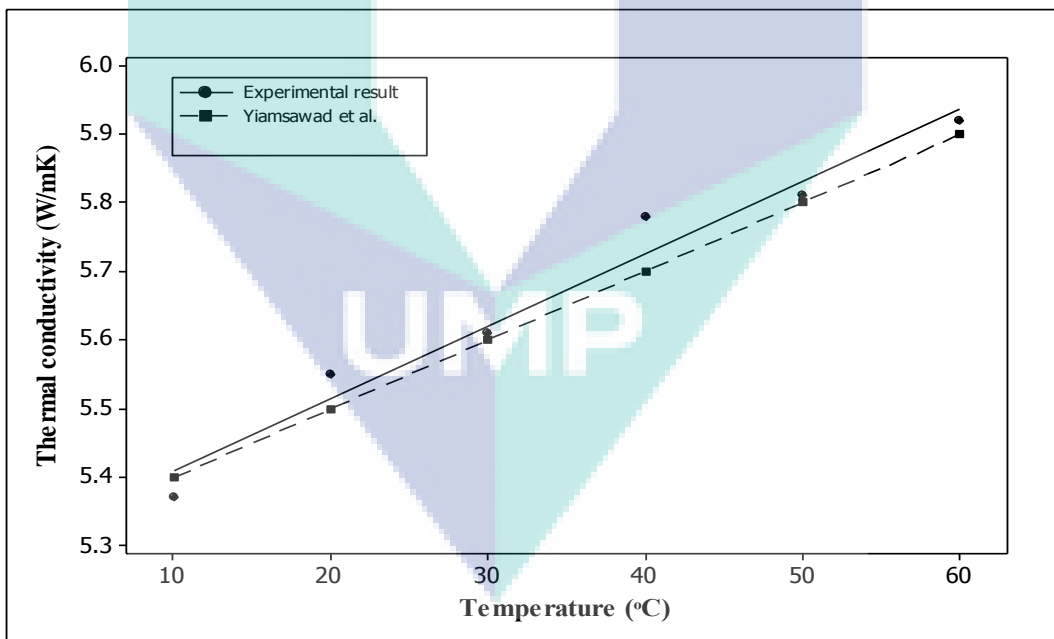
Figure 4.5: Thermal conductivity at 1.5 vol %

4.3   RESPONSES MODEL

The linear model shows the relationship between the milling response and the independent variable can be represented as following expression:

$$y' = a(cutting\ speed) + b(Feed\ rate) + c(Depth\ of\ cut) + D \tag{4.1}$$

Where *a*, *b*, *c and D* are the constants. Eq. (4.1) can be expressed in the following form:

$$y'' = \beta_0 x_0 + \beta_1 x_1 + \beta_2 x_2 + \beta_3 x_3 \tag{4.2}$$

Where y = milling response, $x_0 = 1$(dummy variable), $x_1 =$ cutting speed, $x_2 =$ feed rate, $x_3 =$ depth of cut. β_0, β_1, β_2 and β_3 are the model parameter.

4.4   DEVELOPMENT OF LINEAR SURFACE ROUGHNESS MODEL WITH WATER SOLUBLE COOLANT AND ETHYLENE GLYCOL BASED TiO$_2$ NANOFLUID.

After the first pass of milling experiment which is 180 mm of cutting, the surface roughness reading is used to generate the full quadratic model Eq. (4.2). In order to calculate this parameter, the response surface method is used with aid of Minitab Software. The linear equation is used to predict the surface roughness of milling experiment conducted with water soluble coolant and ethylene glycol based TiO$_2$ nanofluid is expressed as:

$$Surface\ Roughness = -9.0 \times 10^{-5} x_1 + 1.65 x_2 + 0.205 x_3 + 0.344 \tag{4.3}$$
Water soluble coolant

$$Surface\ Roughness = -3.725 \times 10^{-5} x_1 + 0.45 x_2 - 0.1412 x_3 + 0.2 \tag{4.4}$$
Ethylene glycol based TiO$_2$ nanofluid
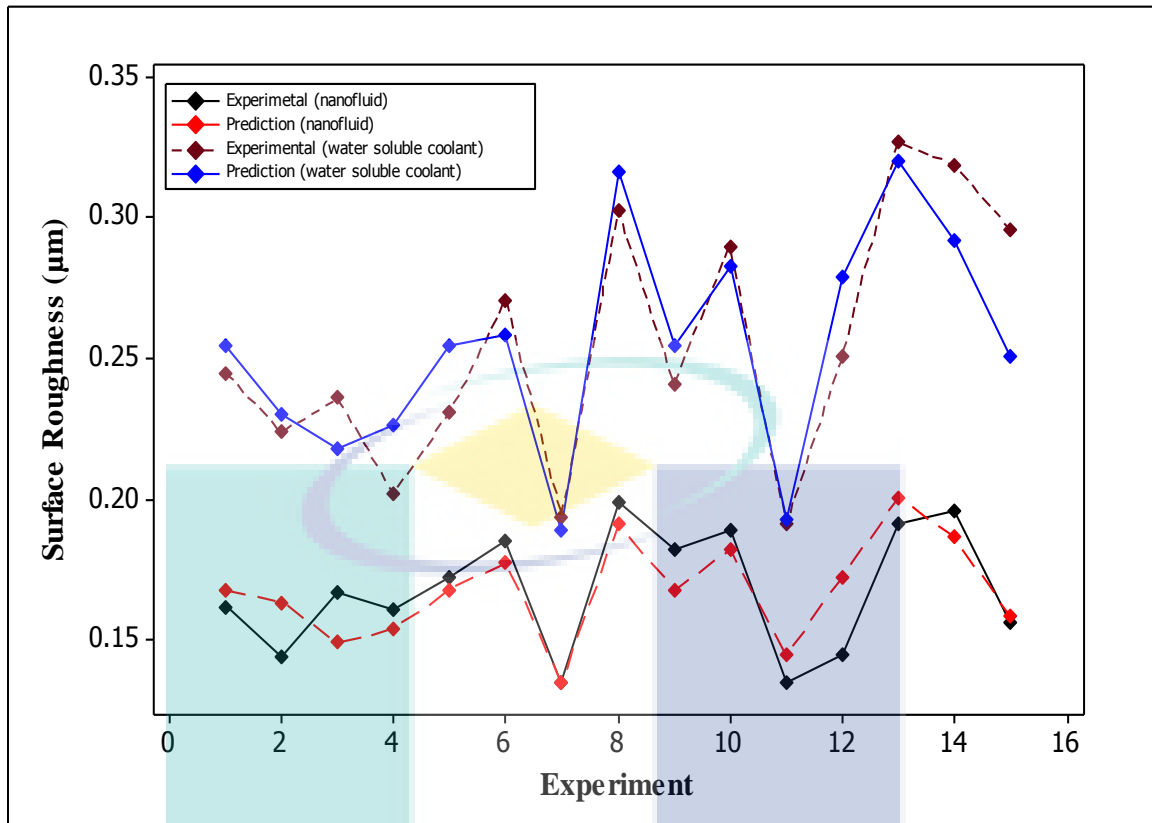
Figure 4.6: Experimental result and predicted result for full quadratic model of surface roughness

From Eqn 4.3 and Eqn 4.4, it can be noticed that the average surface roughness is affected by the feed rate, followed by axial depth of cut and cutting speed for end milling process with water soluble coolant and ethylene glycol based TiO_2 nanofluid. The similar trend has been reported by Kadirgama (2011). Besides that, increases in cutting speed will reduce the average surface roughness. According to Selvaraj et al. (2014), the decreases in average surface roughness when increase in cutting speed is due to reduction in built-up-edge (BUE) formation tendency. At lower cutting speed the tendency of BUE is much higher on the edge of tool and it would affect the surface integrity. On the other hand, feed rate has the highest impact on the surface roughness. The increases in feed rate will increases the average surface roughness. This is because of the increases in friction force between the workpiece and cutting tool interface. This friction force will increases the temperature in the cutting zone. Therefore, the shear strength of the material reduces and it behaves in ductile form. The sticky in nature of steel material is the cause for the increased surface roughness (Thakur, 2009). Besides

that, Cakir et al. (2009), stated that the increase in cutting force resulting from the increase in feed rate. Larger cutting force cause high vibration and provide worse surface finish. Furthermore, it also noticed that the average surface roughness is increases when the axial depth of cut increases. This phenomenon is due to increases in cutting force when the depth of cut increases. This cutting force will contribute to high vibration and natural frequency. Reducing the axial depth of cut will reduce the cutting force and together with effect of vibration and natural frequency and giving better surface finish (Sturesson et al., 1997). Hence, a fine surface finish can be obtain at high cutting speed, low feed rate and low axial depth of cut (Choudhurya and Baradie, 1999). This can be seen at experiment 7 in Figure 4.6 for both milling with water soluble coolant and nanofluid produce better surface roughness. Selvaraj et al. (2014) found that the combination of cutting speed 2500 rpm and feed rate of 0.04 mm/tooth would give the lowest surface roughness for hard steel milling hardened steel material. Baek et al. (1997) and Oktem et al. (2005) created a surface roughness model which concluded that the influence of cutting speed and feed rate on the surface roughness is much greater than the influence of axial depth of cut. Meanwhile, in Figure 4.7, with combination of high cutting speed and high feed rate produce roughness around 0.204 µm for water soluble coolant experiment and around 0.16 µm for nanofluid experiment. On the other hand, in Figure 4.8 with combination of low cutting speed and low feed rate produce roughness around 0.256 µm for water soluble coolant experiment and around 0.156 µm for nanofluid experiment. This indicates the influence of cutting speed is much greater for water soluble coolant experiment. But, for the nanofluid experiment it shows that the influence of feed rate is much higher. This phenomena is due to high heat generated in cutting zone is due to high cutting speed rather than feed rate and axial depth of cut (Ueda et al., 2001). The ability of nanofluid to transfer heat has become the fact to reduce the heat generated by the high cutting speed in cutting zone. Thus, the influence of cutting speed has been reduce in nanofluid experiment compare to water soluble experiment.

Besides that, end-milling experiment conducted with ethylene glycol based TiO_2 nanofluid produced better surface roughness compare with end-milling experiment conducted with water soluble coolant. The range of surface roughness for nanofluid experiment is from 0.135 µm to 0.196 µm. Meanwhile the milling experiment

conducted with water soluble coolant produce roughness range from 0.191 µm to 0.327 µm. This phenomena can be explained with theory of nanofluid behavior which is consider as heat transfer fluid due to their enhanced heat transfer performance compared to ordinary fluids (Murshed et al., 2005). In the case of machining, nanofluid acts as a heat transfer medium in the cutting zone. Therefore, the heat generated in cutting zone has been dissipated by the nanofliud since the ability of the nanofluid to carry away the heat. Hence, there is less burning occurring in the cutting zone which will affect the surface quality of the workpiece. This statement is supported by Murshed et al. (2008), saying the Brownian motion between the nanoparticle in based liquid cause a stronger transport of heat compare to sole heat conduction which increase the effective of thermal conductivity. Figure 4.6 shows that each and every combination of cutting parameter producing better surface roughness for experiment conducting with nanofluid compared with experiment conducted with water soluble coolant. Besides that, Figure 4.9 shows that the average surface roughness affected by the volume fraction of the ethylene glycol based TiO_2 nanofluid. The finest surface roughness occurs at 1.0 %V for all 3 different cutting speeds. Clustering and aggregation is one of the reasons for different feature of nanofluid in different volume concentration. Gharagozloo and Goodson, (2010) stated that the extraordinary enchantment of nanofluid in thermal conductivity and stability occur and 1.0 %V and it reduced when the volume fraction increased due to particle clustering. The clustering of particle in the based liquid reduces the Brownian motion of the nanoparticle and decreases the thermal conductivity. Hence, the roughness is absolutely great at 1.0 %V at all different cutting parameter.
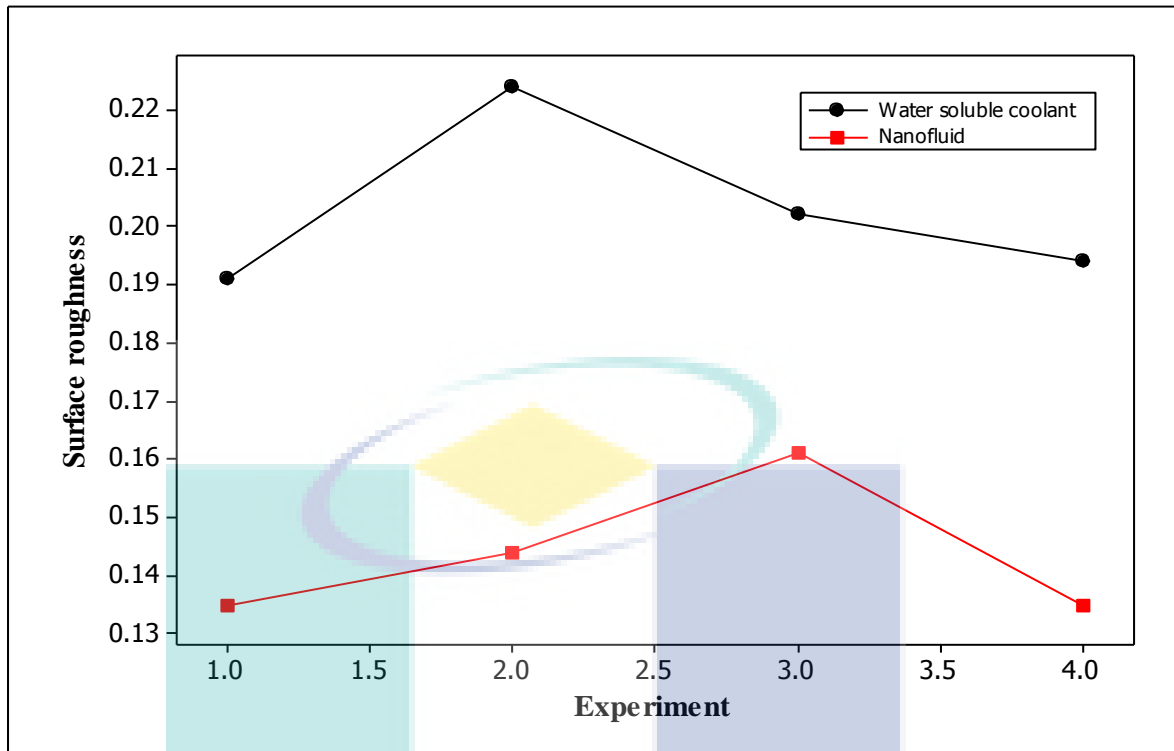
Experiment 1, cutting speed = 2500 rpm, Feed rate = 0.02 mm/tooth, depth of cut = 0.2 mm

Experiment 2, cutting speed = 2500 rpm, Feed rate = 0.03 mm/tooth, depth of cut = 0.3 mm

Experiment 3, cutting speed = 2500 rpm, Feed rate = 0.04 mm/tooth, depth of cut = 0.2 mm

Experiment 4, cutting speed = 2500 rpm, Feed rate = 0.03 mm/tooth, depth of cut = 0.1 mm

Figure 4.7: Selection of 4 experiments from 15 experiments with combination of high cutting speed, feed rate and depth of cut.
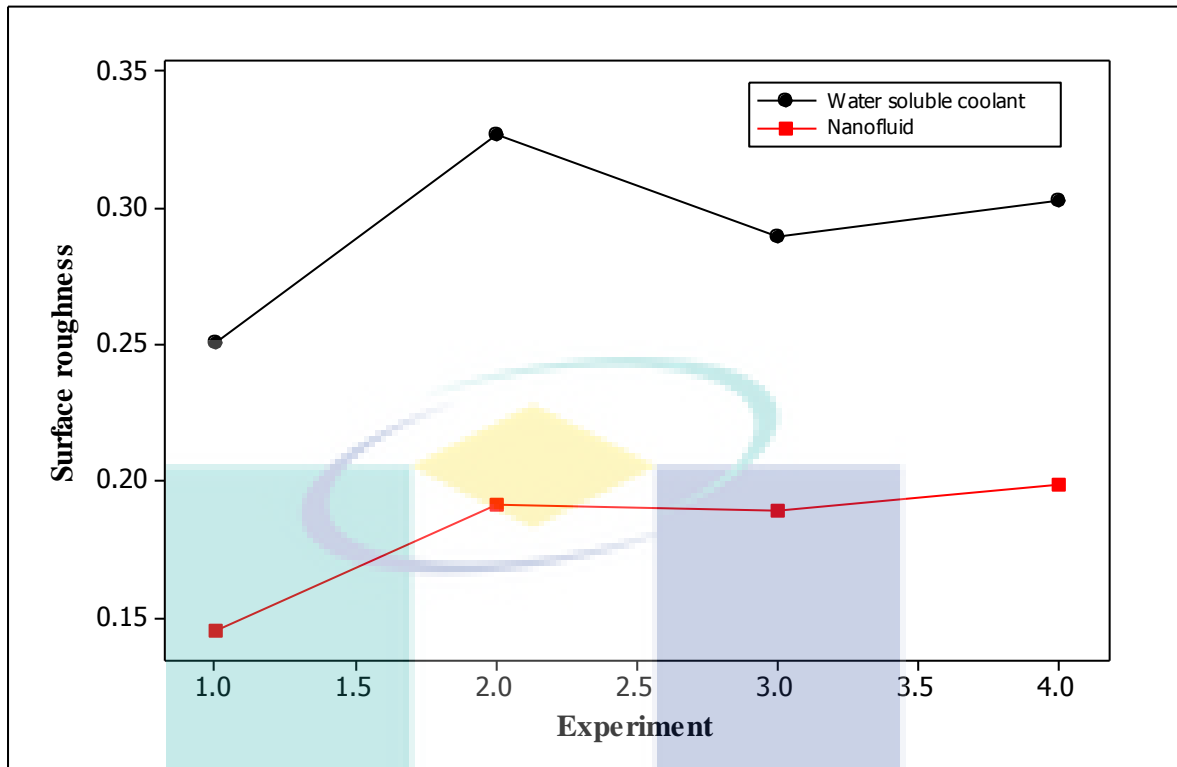
Experiment 1, cutting speed = 1500 rpm, Feed rate = 0.03 mm/tooth, depth of cut = 0.1 mm

Experiment 2, cutting speed = 1500 rpm, Feed rate = 0.03 mm/tooth, depth of cut = 0.3 mm

Experiment 3, cutting speed = 1500 rpm, Feed rate = 0.02 mm/tooth, depth of cut = 0.2 mm

Experiment 4, cutting speed = 1500 rpm, Feed rate = 0.04 mm/tooth, depth of cut = 0.2 mm

Figure 4.8: Selection of 4 experiments from 15 experiments with combination of low cutting speed, feed rate and depth of cut.
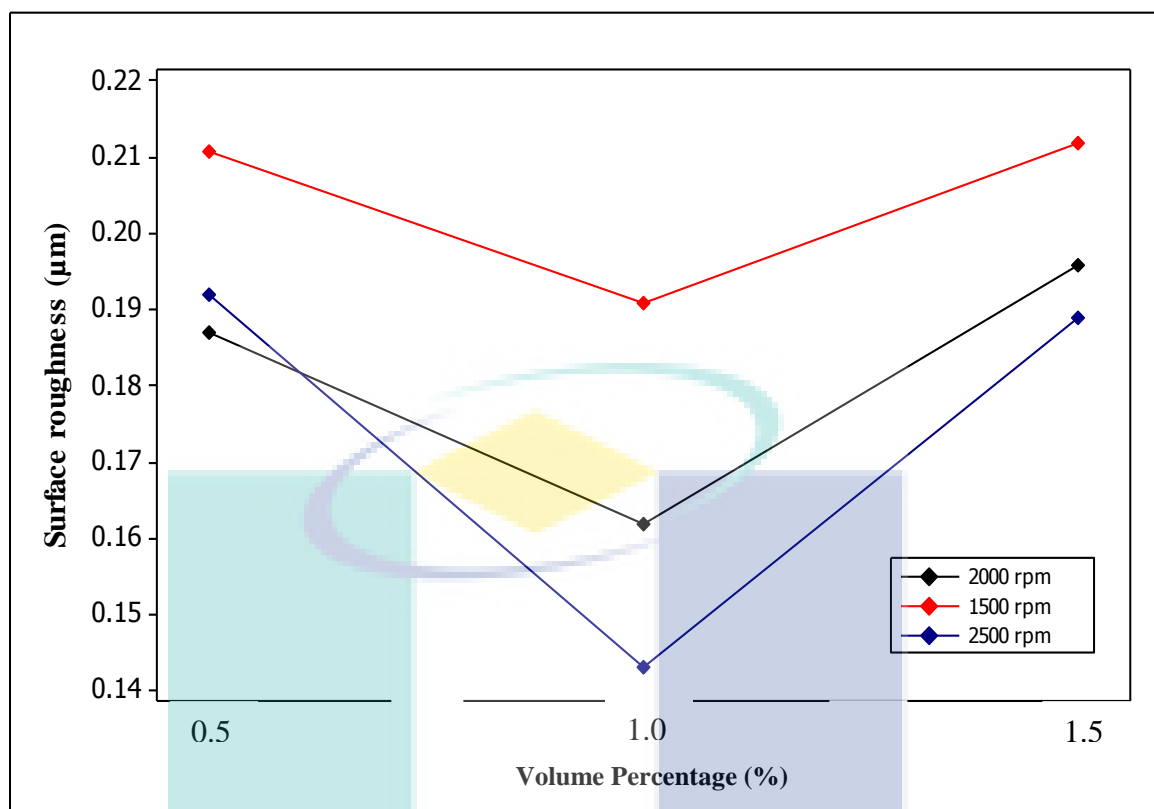
Figure 4.9: Selection of 3 experiments from 15 experiments with different volume fraction of ethylene glycol based TiO_2 nanofluid with different cutting speed.

Figure 4.6 shows the average surface roughness value obtained from experimentation and the value predicted by the linear model. It shows that the predicted values are in good agreement with the experimental value for both water soluble coolant experiment and nanofluid experiment. This indicates that the predicted linear model is useful to predict value of surface roughness. The adequacy of linear model is verified using the analysis of variance (ANOVA) at a level of confident of 95 %. As shown in Table 4.2 and Table 4.3, the probability (P-value) is not significant with lack of fit (>0.05) for both experiment. Meanwhile, F-static for the model is 12.26 for water soluble coolant experiment and 2.22 for nanofluid experiment. This implies that the Lack of Fit is not significant relative to pure error. This indicates that the linear model could fit and adequate (Kadirgama and Hossien, 2005). With the aid of the linear model equation, the contour of the average surface roughness has been plotted for water soluble coolant experiment and nanofluid experiment. Figure 4.10 and Figure 4.11 shows the surface roughness contours at different axial depth of cut. It is obvious that the finest surface

roughness occur at high cutting speed, low feed rate and low axial depth of cut for both set of experiment.

Table 4.2: Variance analysis for first order model with water soluble coolant

Source	Degree of freedom	F-static	P- value
Regression	3	13.65	0.001
Linear	3	13.65	0.001
Residual error	11		
Lack-of-fit	9	12.26	0.075
Pure error	2		
Total	14		

Table 4.3: Variance analysis for first order model with nanofluid

Source	Degree of freedom	F-static	P- value
Regression	3	7.57	0.005
Linear	3	7.57	0.005
Residual error	11		
Lack-of-fit	9	2.22	0.349
Pure error	2		
Total	14		
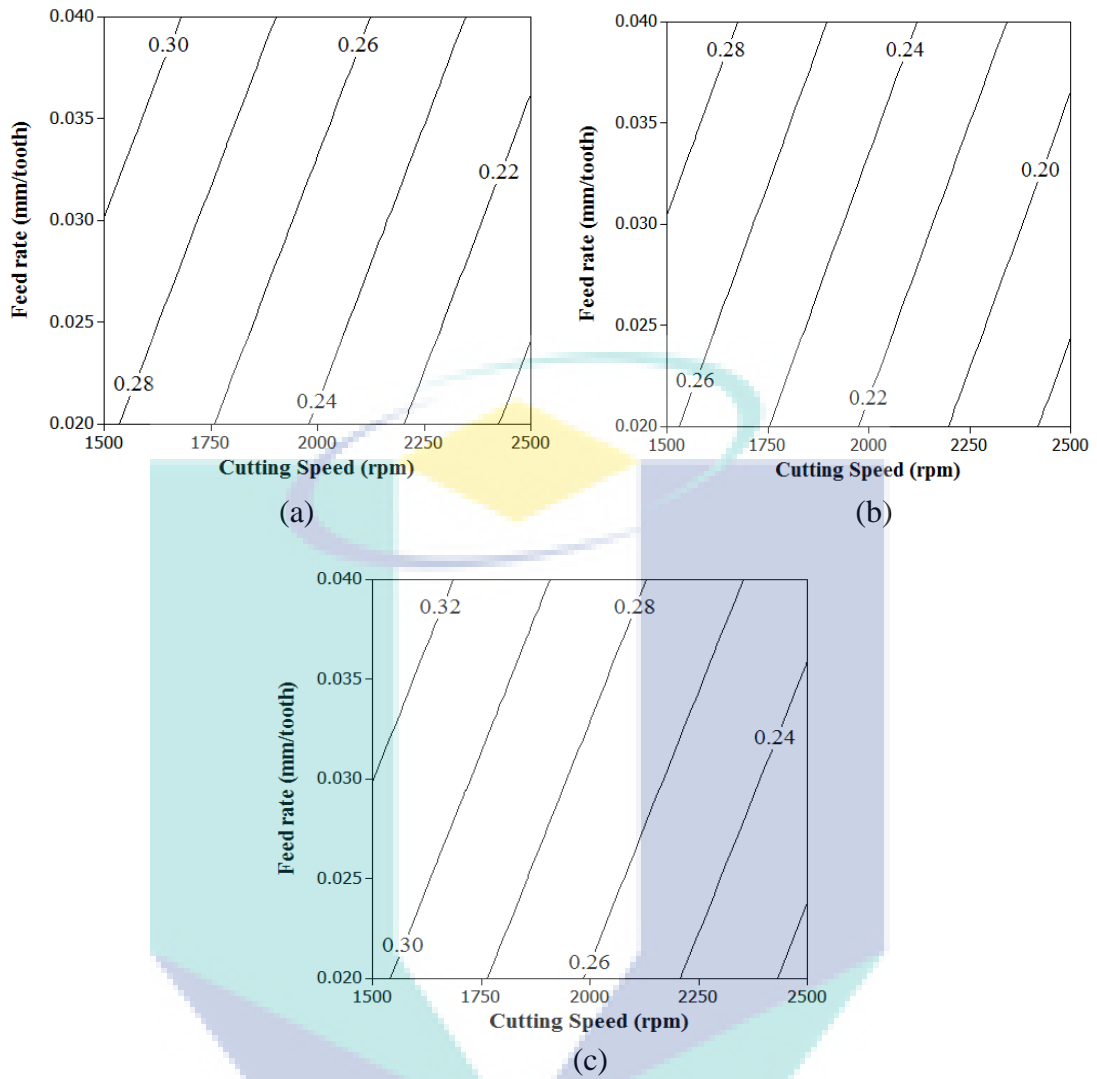
Figure 4.10: Surface roughness contour in cutting speed-feed rate plane for axial depth
(a) 0.1 mm, (b) 0.2 mm, 0.3 mm with water soluble coolant
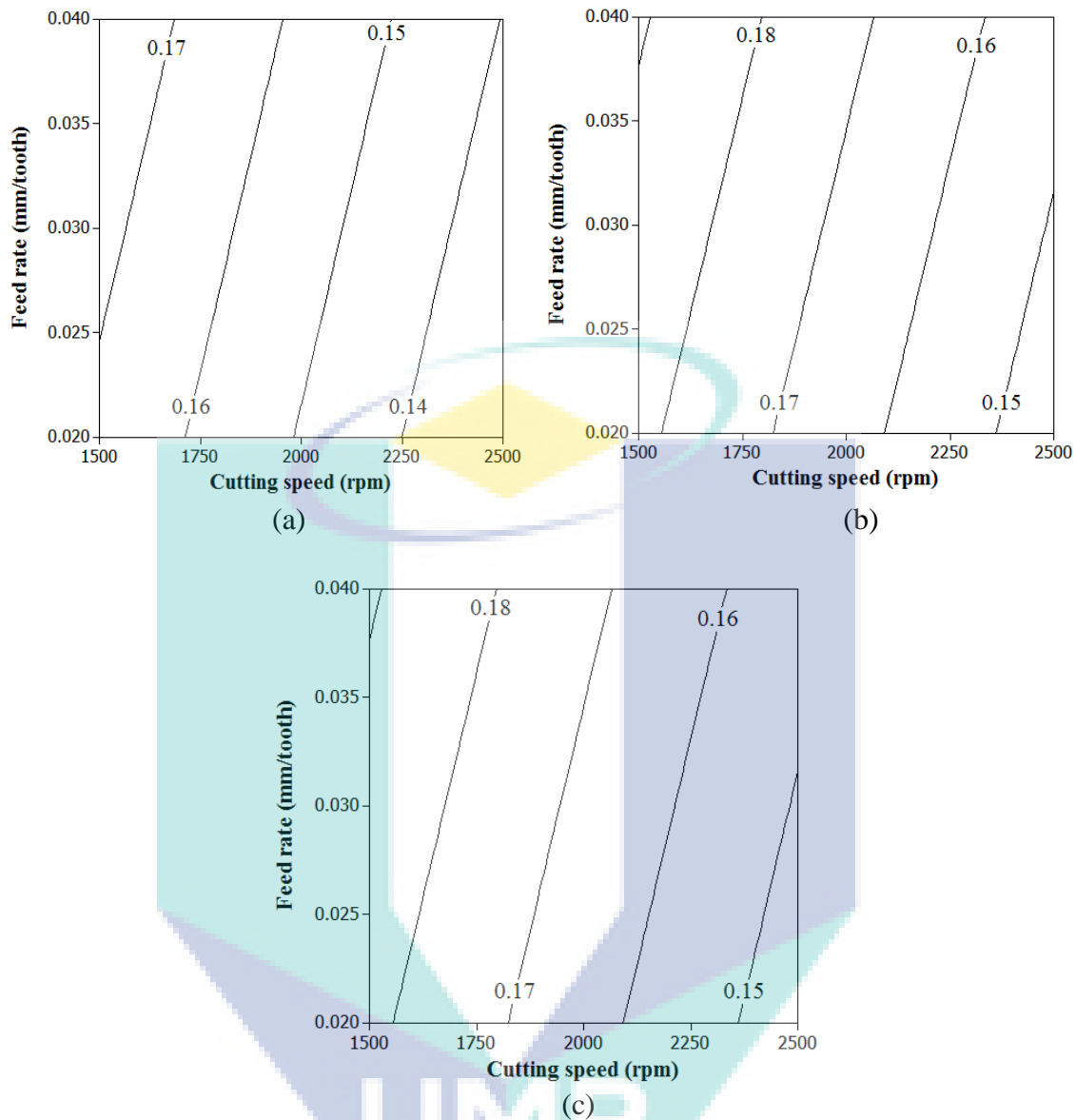
Figure 4.11: Surface roughness contour in cutting speed-feed rate plane for axial depth

(a) 0.1 mm, (b) 0.2 mm, 0.3 mm with nanofluid

4.5   OPTIMIZATION OF SURFACE ROUGHNESS VALUE

In order to optimize the surface roughness value, the response optimizer is used with aid of Minitab Software. The optimum value of surface roughness corresponds to linear model design for water soluble coolant milling experiment is 0.173 μm with cutting speed = 2500 rpm, feed rate = 0.02 mm/tooth and axial depth of cut = 0.1 mm. Meanwhile, the optimum vale of surface roughness corresponds to linear model design for nanofluid milling experiment is 0.131 μm with cutting speed = 2500 rpm, feed rate = 0.02 mm/tooth and axial depth of cut = 0.1 mm.

4.6   DEVELOPMENT OF LINEAR TOOL LIFE MODEL WITH WATER SOBLE COOLANT AND ETYLENE GLYCOL BASED TIO₂ NANOFLUID

Field and Kahles, 1971 stated that tool life can be found from the expression below:

$$Tool\ life = \frac{TL}{F_m} \tag{4.5}$$

where F_m is the feed rate in mm/min and TL is the total length to reach flank wear criterion 0.3 mm.

The linear equation used to predict the tool life for milling with water soluble coolant and nanofluid can be expressed as:

$$Tool\ life = -0.0096x_1 - 650.25x_2 - 0.205x_3 + 55.94 \tag{4.6}$$

Wter soluble coolant

$$Tool\ life = -0.0166x_1 - 1181x_2 - 4.488x_3 + 55.94 \tag{4.7}$$

Nnaofluid
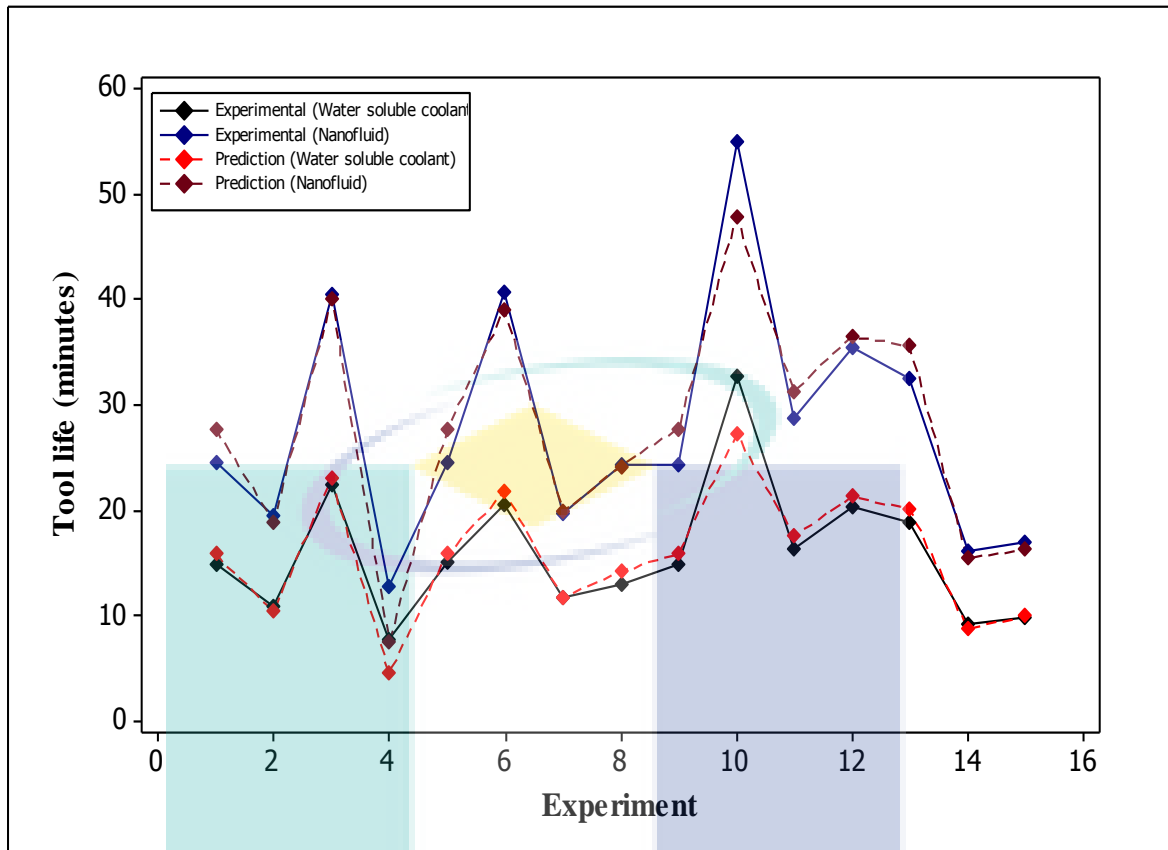
Figure 4.12: Experimental result and predicted result for linear tool life model.

Equation 4.6 and Equation 4.7 shows that the tool life increases with the decrease of cutting speed, feed rate and axial depth of cut. It is clear that feed is the most dominant parameter which effect the tool life followed by axial depth of cut and cutting speed. Therefore, the combination of low cutting speed, low feed rate and low axial depth of cut can improve the tool life for end-milling process. The similar result was found by Alauddin et al. (1997) where stated that an increase in the cutting speed, feed rate and axial depth of cut decrease the tool life. According Syzmon and Pawel, (2012) tool life decrease monotonously with the increasing of cutting speed. On the other hand, Koshy et al. (2002) obtain the similar result produced by the linear model which stated that cutting speed had only minimal influence on tool life for hardened steel workpiece. One we can notice from Figure 4.13, there is a dramatically decrement in tool life when the feed rate increased. This shows that feed rate is the most dominant parameter which contributes to the tool failure. This is cause by the increment on temperature in primary and secondary shear zone. Hence, high temperature often results in tool wear such as plastic deformation. Those factors weaken the cutting tool material and contribute to the

wear progression on the edge of the tool (Haron, 2001). Besides that, increases in cutting speed cause an increment in tool life for both experiments. Dearnley and Grearson (1986) found that at high cutting speeds has shorter contact area between chip-tool interfaces. This will cause a concentration of high temperature at the edge of cutting tool. The high temperature generated will cause the cutting tool to lose their strength and plastic deformation will be formed. These will also contribute and increase in the thermal gradient which tent to increases the tool wear as thermal crack generation rate increases (Bhatia et al., 1979). It can also be noticed that there is a significant increment in tool life when the axial depth of cut reduced. From Figure 4.13 and Figure 4.14 it is noticed that the increment of axial depth of cut have very little influence on tool life for both experiment. This result supoeted by Astakhov (2006) where stated that and increment in the axial depth of cut should not change the tool life rate dramatically. This previous research stated that once the axial depth of cut increases the specific contact stresses at the tool-chip interface and the average temperature remain unchanged. Hence, the high axial depth of cut will not alternate the tool life rate if the milling process is carried out at optimum feed rate and cutting speed. However, the some research stated that an increase in axial depth of cut will shorten the tool life to some extent by accelerating the abrasive adhesive and diffusional type of tool wear (Juneja, 2003).

Besides that, Figure 4.12 show that all the end-milling experiment with nanofluid produces highest tool life compare with water soluble coolant. From Figure 4.14, the highest tool life was archived with condition of cutting speed 1500 rpm, 0.02 mm/tooth and axial depth of cut 0.2 mm where the cutting time is 32.67 minutes for water soluble coolant and 54.9 minutes for nanofluid. This specifies that using ethylene glycol based TiO_2 nanofluid as coolant increase the tool life by 22.23 minutes. One can be pointed here is using ethylene glycol based TiO_2 nanofluid as a coolant for milling process has reduce the tool wear drastically. This can be attributed to the excellent performance of nanofluid as heat transport medium in tool-chip interface. A concentration of high temperature at the edge of the flank resulted in higher wear rate. However, using nanofluid as cutting fluid will reduce the temperature penetrate into cutting tool due to the high heat transfer rate of nanofluid. The relatively higher surface area of nanoparticles enhanced the heat transfer capabilities since the heat transfer takes place

on the surface of the particle (Murshed et al., 2010). On the other hand, Figure 4.15 depicts the comparison of tool life in function of volume percentage of nanofluid. The larger tool life performs at 1.0 vol% for all the different cutting speed. The milling experiment with 1.5 vol% nanofluid exhibits shortest tool life due to huge clustering size of nanoparticle in the based liquid. Increases in clustering size will increases the weight of the nanoparticle in the based liquid thus chances of sedimentation are also high and the nanofluid less stable. Murshed et al. (2008) stated that gravity of nanoparticle is insignificant when the clustering size is small. The massive clustering of nanoparticle in the based liquid will disrupt the Brownian motion of the nanoparticle and reduce the heat transfer rate. Thus, the tool life is very short at 1.5 vol% at all cutting parameter.

Experiment 1, cutting speed = 2500 rpm, Feed rate = 0.02 mm/tooth, depth of cut = 0.2 mm

Experiment 2, cutting speed = 2500 rpm, Feed rate = 0.03 mm/tooth, depth of cut = 0.3 mm

Experiment 3, cutting speed = 2500 rpm, Feed rate = 0.04 mm/tooth, depth of cut = 0.2 mm

Experiment 4, cutting speed = 2500 rpm, Feed rate = 0.03 mm/tooth, depth of cut = 0.1 mm
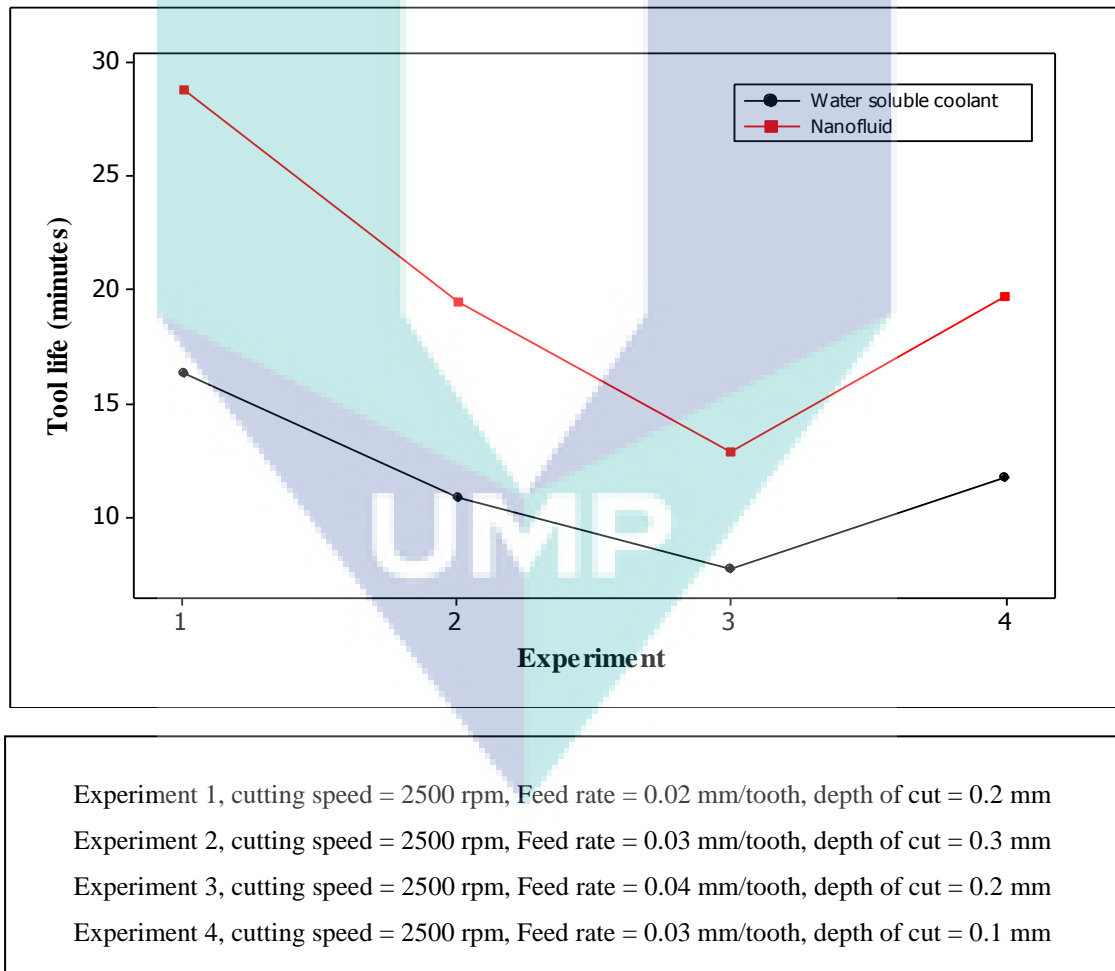
Figure 4.13: Selection of 4 experiments from 15 experiments with combination of high cutting speed, feed rate and depth of cut.
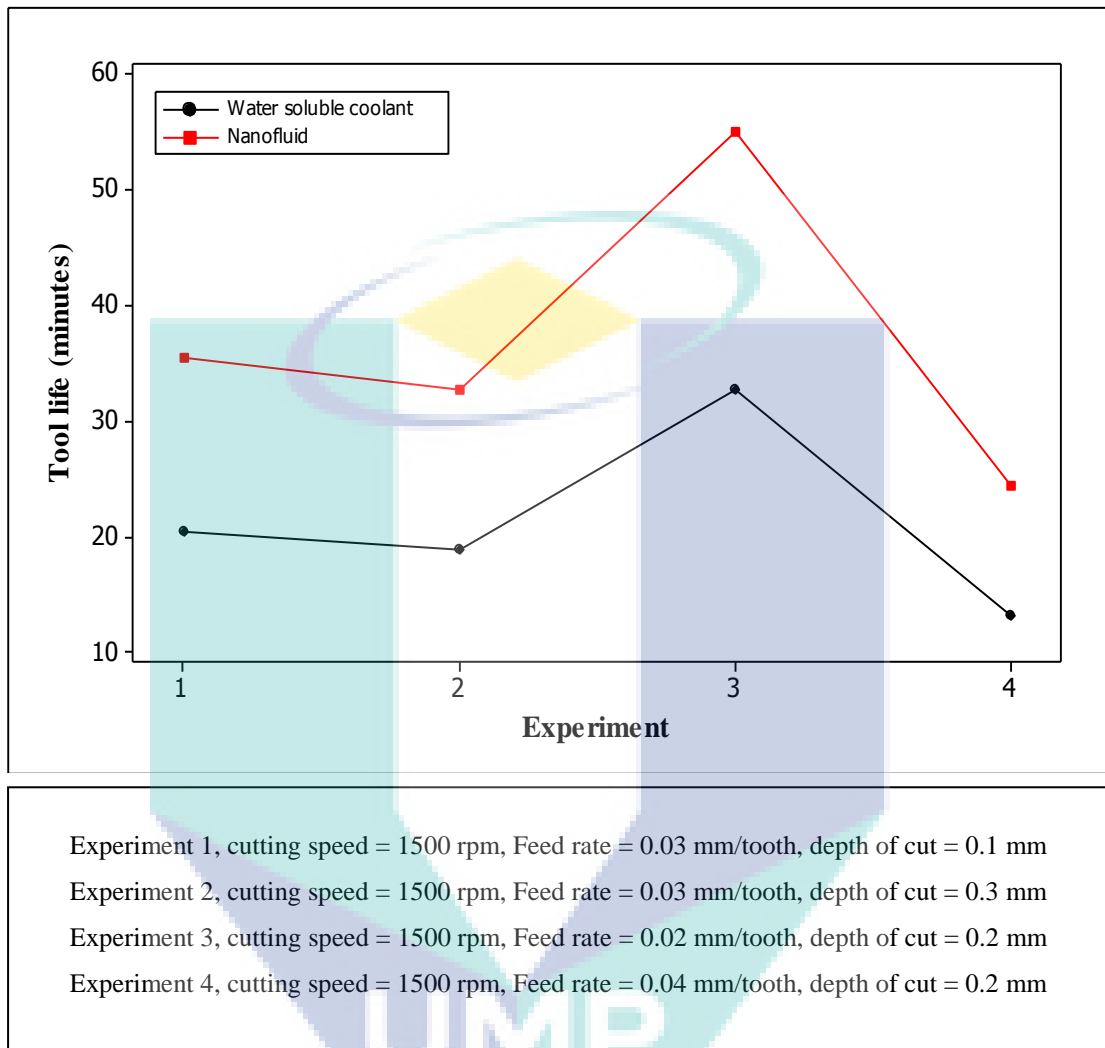
Figure 4.14: Selection of 4 experiments from 15 experiments with combination of low cutting speed, feed rate and depth of cut.
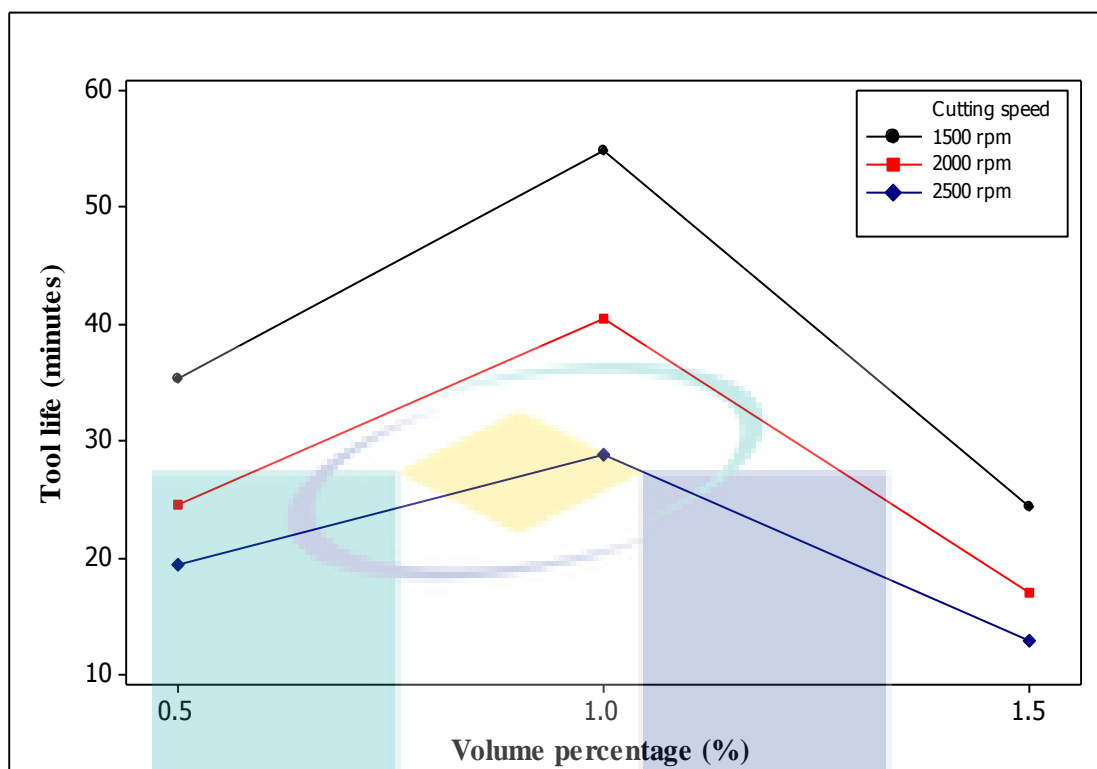
Figure 4.15: Selection of 3 experiments from 15 experiments with different volume fraction of ethylene glycol based TiO$_2$ nanofluid with different cutting speed.

Figure 4.12 shows the tool life of the cutting tool obtained from experimentation and the value predicted by the linear model. It is obviously shows that the predicted values are in good agreement with the experimental vale for both water soluble coolant experiment and nanofluid experiment. The adequacy of the linear model is verified using ANOVA at level of confident 95 %. As shown in Table 4.4 and Table 4.5 the P-value of linear model for tool life were 0.084 and 0.154 for water soluble coolant and nanofluid experiment respectively. Hence, the P-value is not significant with the lack-of-fit since the value is more than 0.05.

The linear model, Equation and Equation 4.7 is used to plot the contours of tool life at different value of axial depth of cut. Figure 4.16 and shows the tool life contours at three different combination of axial depth of cut with water soluble coolant experiment and Figure 4.17 shows similar contours with nanofluid experiment. It is clearly noticeable that the increasing the cutting speed and feed rate will reduce the tool life.

Table 4.4: Variance analysis for first order model with water soluble coolant

Source	Degree of freedom	F-static	P- value
Regression	3	25.99	0.001
Linear	3	25.99	0.001
Residual error	11		
Lack-of-fit	9	42.87	0.084
Pure error	2		
Total	14		

Table 4.5: Variance analysis for first order model with nanofluid

Source	Degree of freedom	F-static	P- value
Regression	3	19.45	0.002
Linear	3	19.45	0.002
Residual error	11		
Lack-of-fit	9	33.73	0.154
Pure error	2		
Total	14		
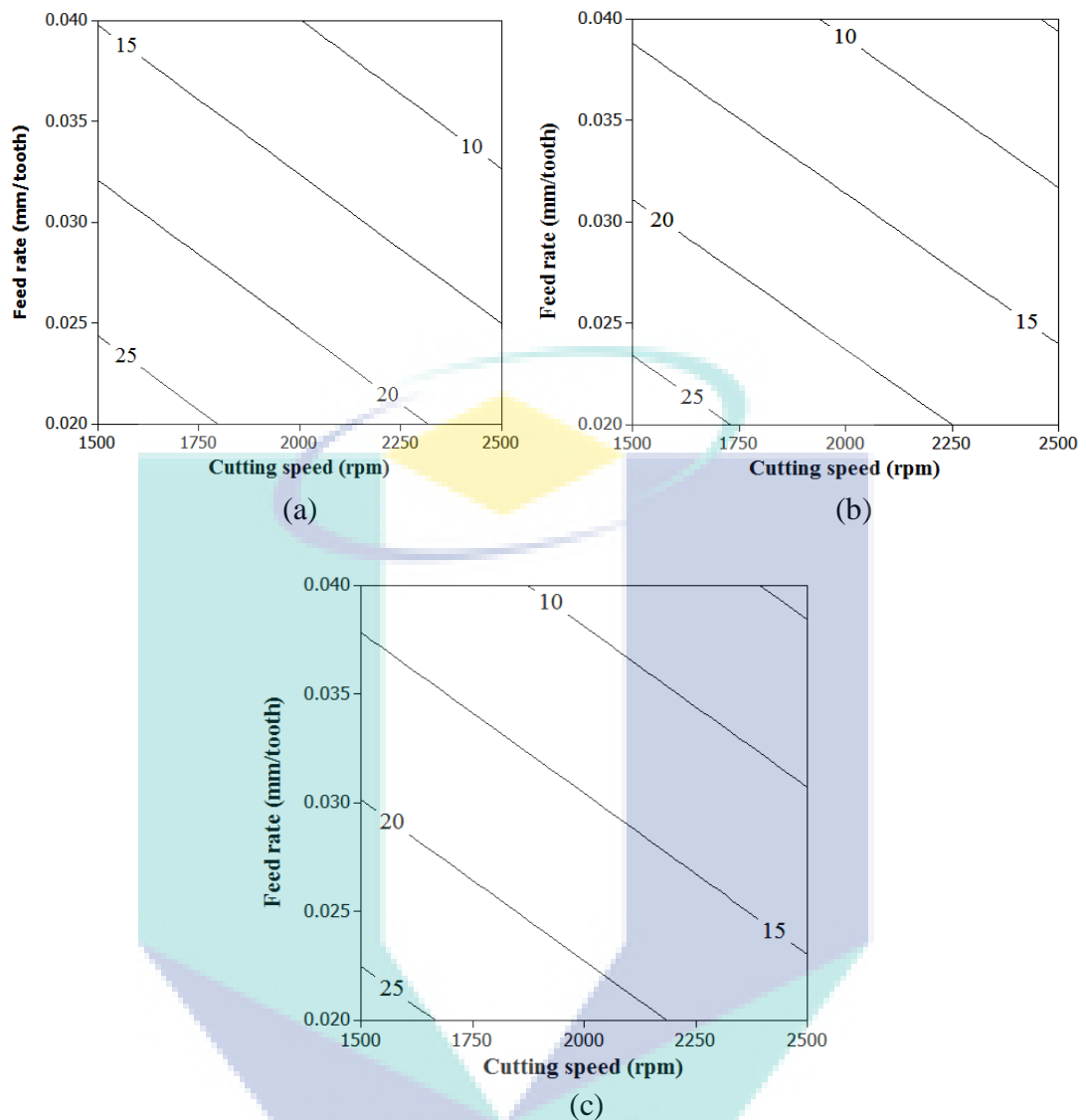
Figure 4.16: Tool life contour in cutting speed-feed rate plane for axial depth (a) 0.1 mm, (b) 0.2 mm and (c) 0.3 mm with water soluble coolant
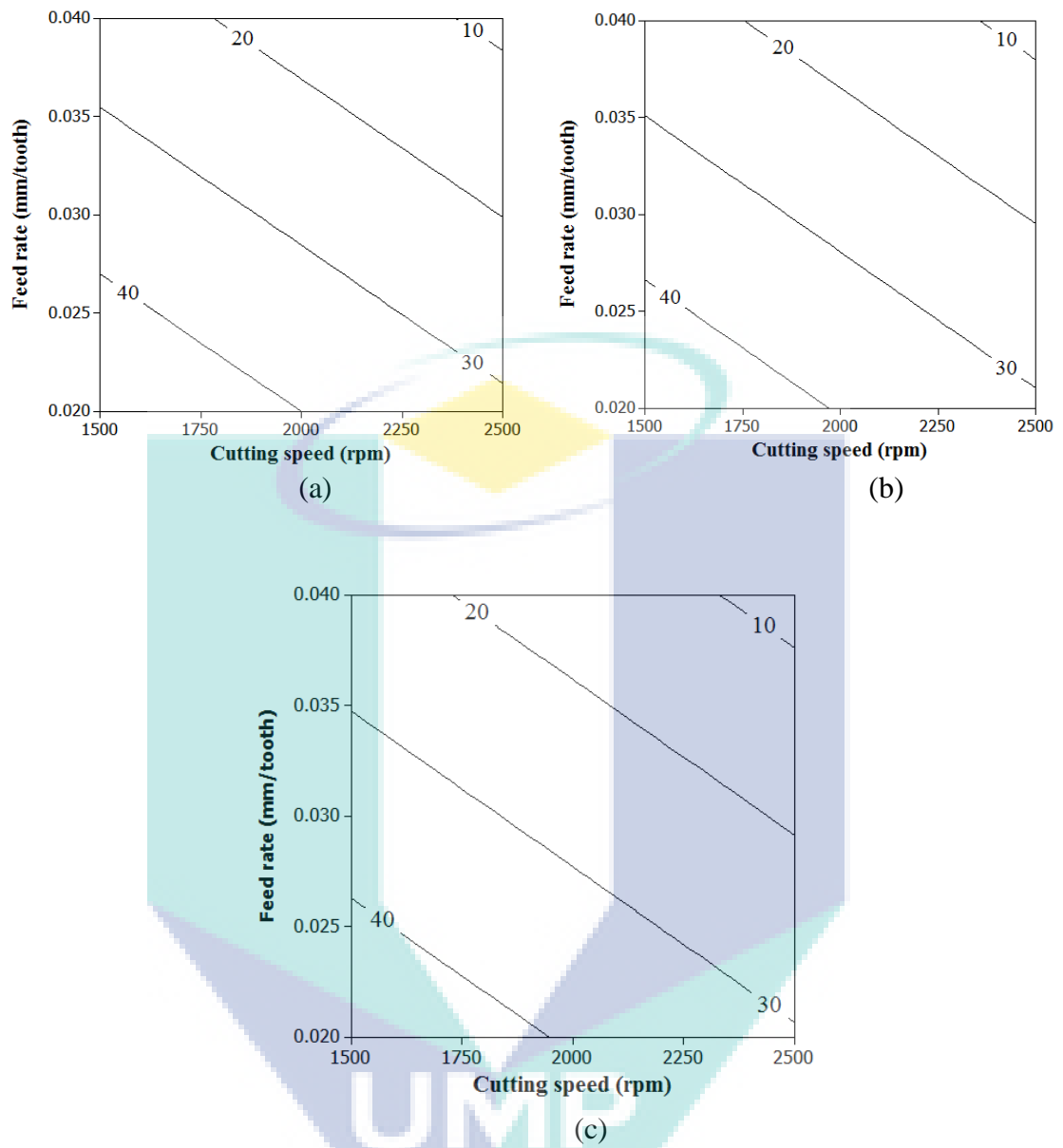
Figure 4.17: Tool life contour in cutting speed-feed rate plane for axial depth (a) 0.1 mm, (b) 0.2 mm and (c) 0.3 mm with nanofluid

4.7 ANALYSIS OF TOOL WEAR ON END-MILLING PERFORMANCE WITH WATER SOLUBLE COOLANT AND NANOFLUID.

Figure 4.18 and Figure 4.19 shows the variation in flank wear width with milling distance in end-mill AISI 304 stainless steel under water soluble coolant and nanofluid. From this figures, it can be noticed that the flank wear increases with an increases in milling distance. In a recent study carried out by Liew (2010) it was a similar pattern. The milling distance will be continued until the wear reached the ISO 8688-2-1989 (E) wear criterion, flank wear ≥ 0.3 mm. From Figure 4.18 it can be seen that Experiment 14 (cutting speed 2000 rpm, feed rate 0.04 mm/tooth and axial depth of cut 0.3 mm) having the highest flank wear rate compare to other experiment for water soluble coolant. The flank wear reach the failure criterion at milling distance around 740 mm for Experiment 14 meanwhile Experiment 10 (cutting speed 1500 rpm, feed rate 0.02 mm/tooth and axial depth of cut 0.2 mm) the flank wear reach the failure criterion around 980 mm of milling distance. This specifies that the influence of cutting speed and feed rate on the flank wear. The increases in cutting speed and feed rate the higher the flank wear. According to Thamizhmanii and Hasan (2007) the formation of flank wear is highly effected by the high heat generated on the flank area. The milling process at high cutting speed and feed rate will generate much higher heat on the tool-chip interface (Dearnley and Grearson, 1986). The retaining of heat on the tool tip will softens the tool tip and increases the wear. Therefore, the flank wear rate is much higher at high cutting speed and feed rate. The substitution of the water soluble coolant with ethylene glycol based TiO_2 nanofluid increased the milling distance for the similar cutting condition as shown in Figure 4.19. On the same milling condition, Experiment 14 and Experiment 10 having a great enhancement on milling distance to reach ISO 8688-2-1989 (E) wear criterion. The flank wear reach the failure criterion around 1296 mm and 1647 mm of milling distance for Experiment 14 and Experiment 10 respectively. Hence, nanofluid having great enchantment on flank wear rate for milling hard material such as AISI 305 stainless steel. The similar result were obtain by Khandekar et al. (2012) where the flank wear is minimum in the case of using nano-cutting fluid as cutting fluid. This is because of its improved conduction, convection and wettability compare to water soluble coolant. The superior properties of nanofluid in cooling and lubrication retain cutting tool the hardness for long period.

Figure 4.20-4.25 shows the transformation in the wear of the TiN coated in end-milling AISI 304 stainless steel with water soluble coolant and nanofluid respectively. In the early cutting distance of 180 mm, the coating on the flank face was removed and exposing the carbide structure for water soluble coolant milling as shown in Figure 4.20. The parallel outcome has been reported by Liew and Ding (2007) where stated that the coating layer of cutting insert will pilled of at cutting distance of 200 mm under high speed milling of stainless steel. On the other hand, the milling with nanofluid produces an impermanent layer on the flank face of the tool at the cutting distance of 180 mm as shown in Figure 4.23. This solid Ti nanoparticle layer has been embedded into the tiny holes on the cutting edge and act as additional layer to shield the cutting tool. Electron dispersive X-ray (EDX) analysis on the edge of the cutting insert was conducted to determine the composition of the layer found on the cutting edge. The spectral information shows that the layer formed by Ti particle deposit on the surface of the cutting insert. As shown in Figure 4.23 the composition of Ti particle is 63.92 by weight %. This layer is found to be the interfacial layer which is formed by the solid Ti nanoparticle which acts as a thermal bridge during the milling process. (Leong et al, 2006) (Junemoo and Clement, 2004).

Increasing the cutting distance from 180 mm to 720 mm caused much more coating and carbide layer to be removed. These cause the large damage on flank face and rake face. The damaged surface of the cutting tool shows evidence of chipping on the rake face as shown in Figure 4.21. However, milling with nanofluid show little damage on the edge of the cutting tool with large coating layer has been removed. But the interfacial layer still appeared on the edge of the cutting tool. EDX analysis shows that the Ti particles still occur on the edge of the cutting insert after 720 mm of cutting as shown in Figure 4.24. But, the composition was reduced to 55.37 weight %. The decrease in the composition Ti particles is due to the reduction in interfacial layer formed. Thus, the layer formed on the cutting edge is an impermanent layer which protects the cutting insert early stage of cutting process.

Increasing the cutting distance from 720 mm to 1100 mm led to the formation of cracks for milling under water soluble coolant. The crack was formed at the region where the coating has been removed as shown in Figure 4.22. It is also found that the crack appear

on the flank face were parallel to the cutting edge. The similar results as been reported by Liew and Ding (2007) where stated that cracks appear on the flank face at milling distance below than 1m when end-mill stainless steel. It has been reported earlier, the mechanical impact between the cutting tool and workpiece is the key reason for the cracks to form at the flank face. These cracks are referred as mechanical crack which spread to the rake face (Melo et al., 2006) (Gu et al., 1999). On the other hand, milling with nanofluid shows the cutting tool can withstand for longer distance. The failure on the flank face can be observed only after 1800 mm of cutting. The layer formed by the particle has been reduced. This can verified with the EDX analysis shows the Ti particle composition has been reduced to 46.5 weight %. This shows that the increasing in the cutting distance will reduced the nanoparticle layer formed on edge of the cutting tool. It can be noticed that chipping occur at cutting distance of 1800 mm for milling with nanofluid as shown in Figure 4.25. Meanwhile, the milling with water soluble coolant chipping occurs at cutting distance 720 mm. Therefore, it can be obviously seen that nanofluid function as an extraordinary coolant in preventing the cracking, fracture and catastrophic failure of the coated insert. This is because of the better thermal conductivity of nanofluid compare to water soluble coolant, reduce the heat generated on the cutting zone and tool wear was reduced extremely.

In addition, the spectral data obtained from EDX can be used to explain the type of the wear that occurs at the rake face of the cutting insert. Figure 4.26 shows the EDX spectrum and the SEM of rake face of worn insert subjected to milling for 180 mm of length with nanofluid at cutting speed of 1500 rpm, feed rate of 0.02 mm/tooth and axial depth of 0.1 mm. One can be noticed is the spectra shows an iron (Fe) peak obtained during the milling. This is an indication of an iron BUE occur during milling with nanofluid (Pinaki et al., 2008). Moreover, Hossein and Yahya (2005) stated that BUE can simply formed at low cutting speed during machining ductile material such as austenite stainless steel. Other visible elemental peaks that show is the spectra are chromium (Cr), manganese (Mn), sulfur (S), silicon (Si), nitrogen (N) and oxygen (O). Most of the element mention above are alloying element in AISI 304 stainless steel that used as milling workpiece. This is due to diffusion wear took place at the tool-chip interface and cause the element from the workpiece transfer to the insert rake face. According to Trent (1991) carbon and metal particles transfer into insert rake face in the

form of chips generated during the milling process. In same period, atoms of alloying element of the workpiece material diffuse into the rake face and react with insert coating to degrade further (Trent, 1991).

Figure 4.18: Progression of flank wear by distance for milling with water soluble coolant
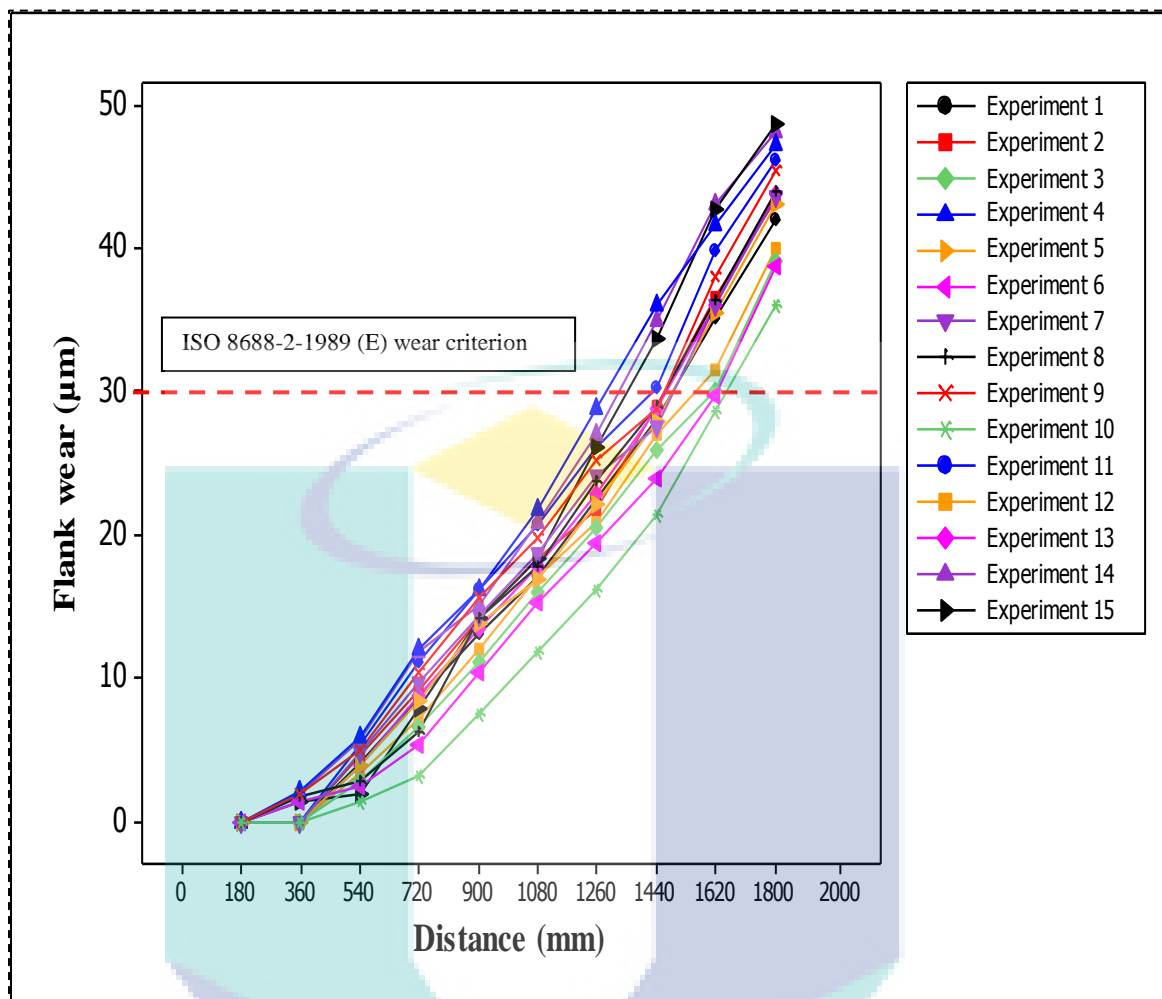
Figure 4.19: Progression of flank wear by distance for milling experiment with nanofluid
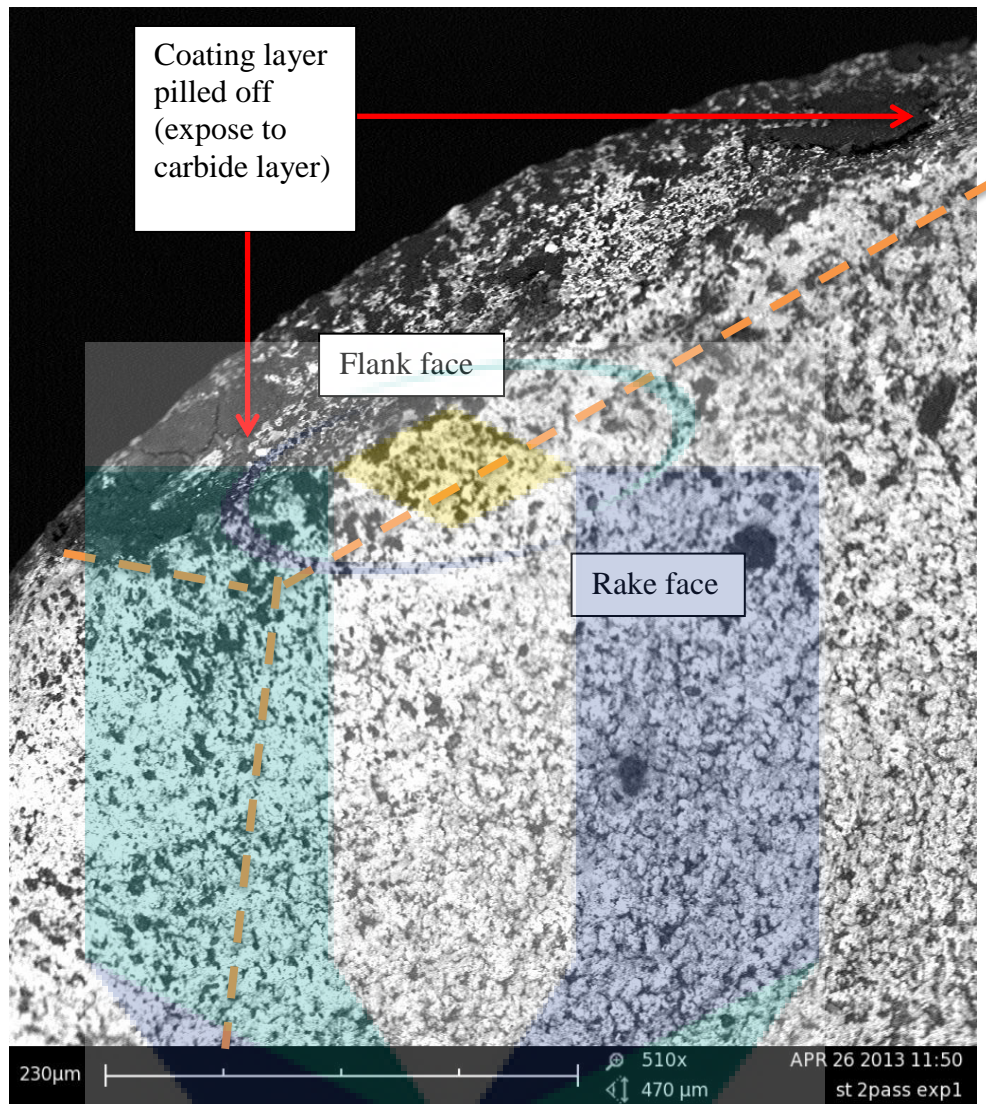
Figure 4.20: SEM of the cutting edge at cutting speed 2500 rpm, feed rate 0.04 mm/tooth, axial depth 0.2 mm under water soluble coolant at 180 mm
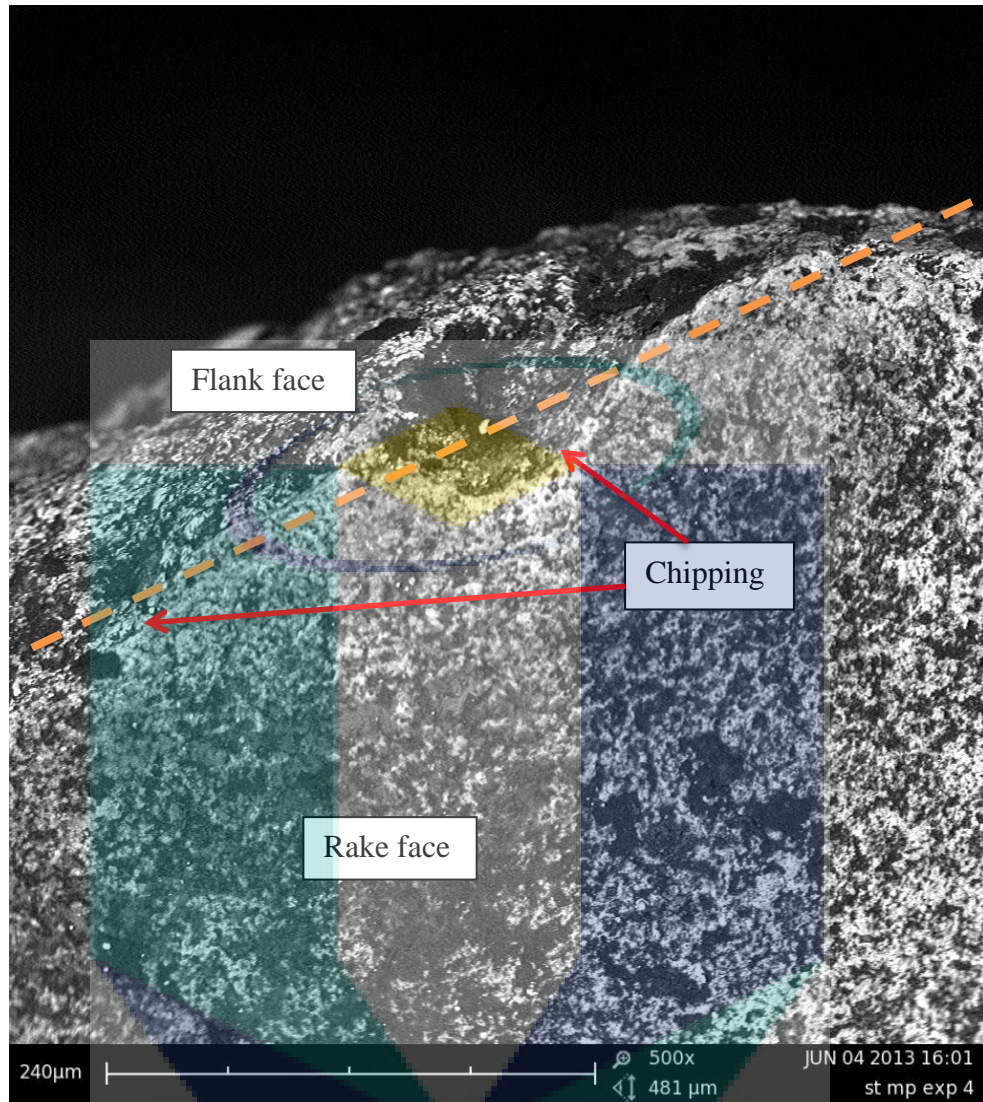
Figure 4.21: SEM of the cutting edge at cutting speed 2500 rpm, feed rate 0.04 mm/tooth, axial depth 0.2 mm under water soluble coolant at 720 mm
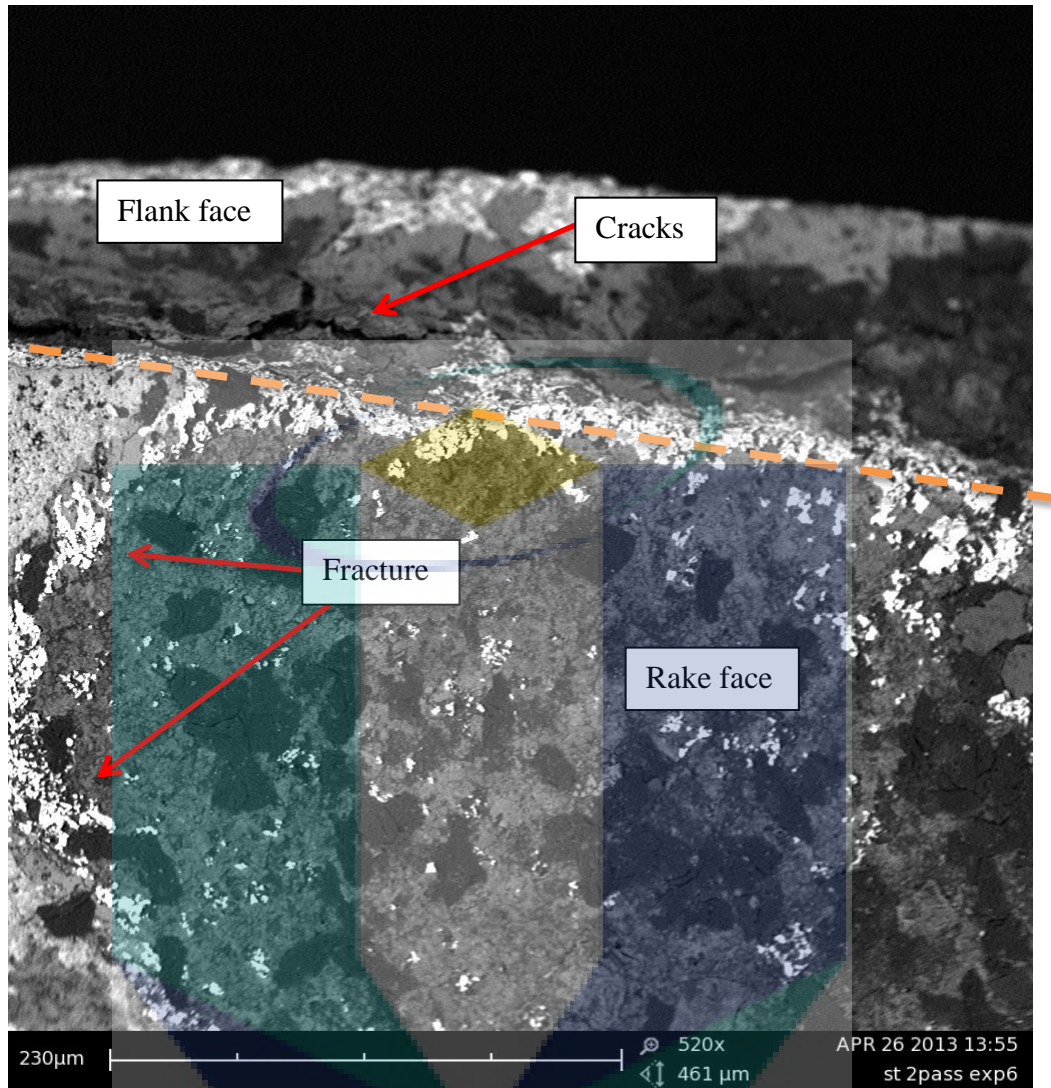
Figure 4.22: SEM of the cutting edge at cutting speed 2500 rpm, feed rate 0.04 mm/tooth, axial depth 0.2 mm under water soluble coolant at 1100 mm
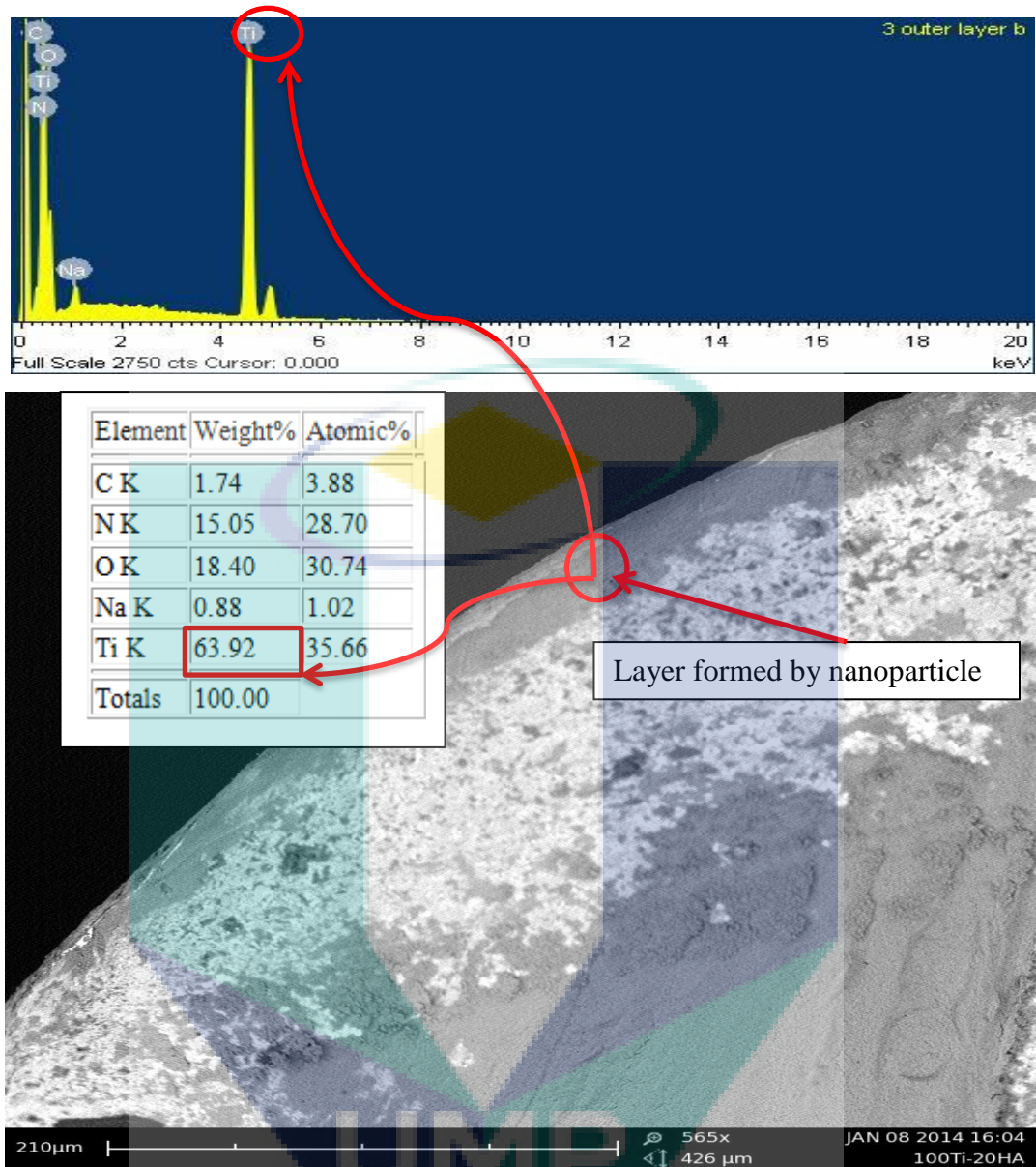
Figure 4.23: SEM and EDX of the cutting edge at cutting speed 2500 rpm, feed rate

0.04 mm/tooth, axial depth 0.2 mm under nanofluid at 180 mm
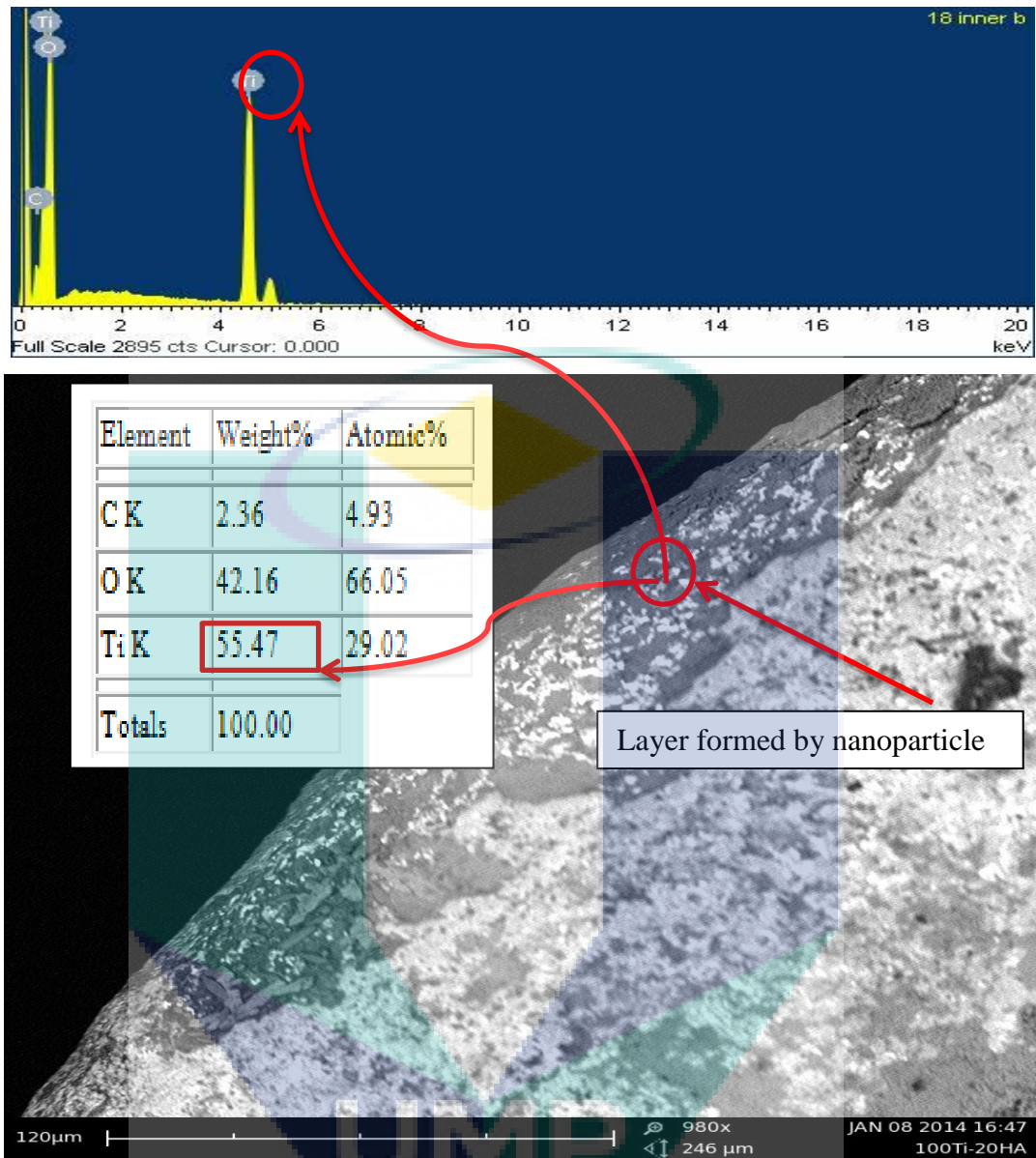
Figure 4.24: SEM and EDX of the cutting edge at cutting speed 2500 rpm, feed rate

0.04 mm/tooth, axial depth 0.2 mm under nanofluid at 720 mm

Figure 4.25: SEM and EDX of the cutting edge at cutting speed 2500 rpm, feed rate 0.04 mm/tooth, axial depth 0.2 mm under nanofluid at 1800 mm

Figure 4.26: SEM and EDX of cutting edge at cutting speed 1500 rpm, feed rate 0.02 mm/tooth, axial depth 0.1 mm under nanofluid at 180 mm of cutting distance.

4.8   Analysis of wear mechanism on end-milling performance with water soluble coolant and nano particle based coolant (TiO$_2$/EG).
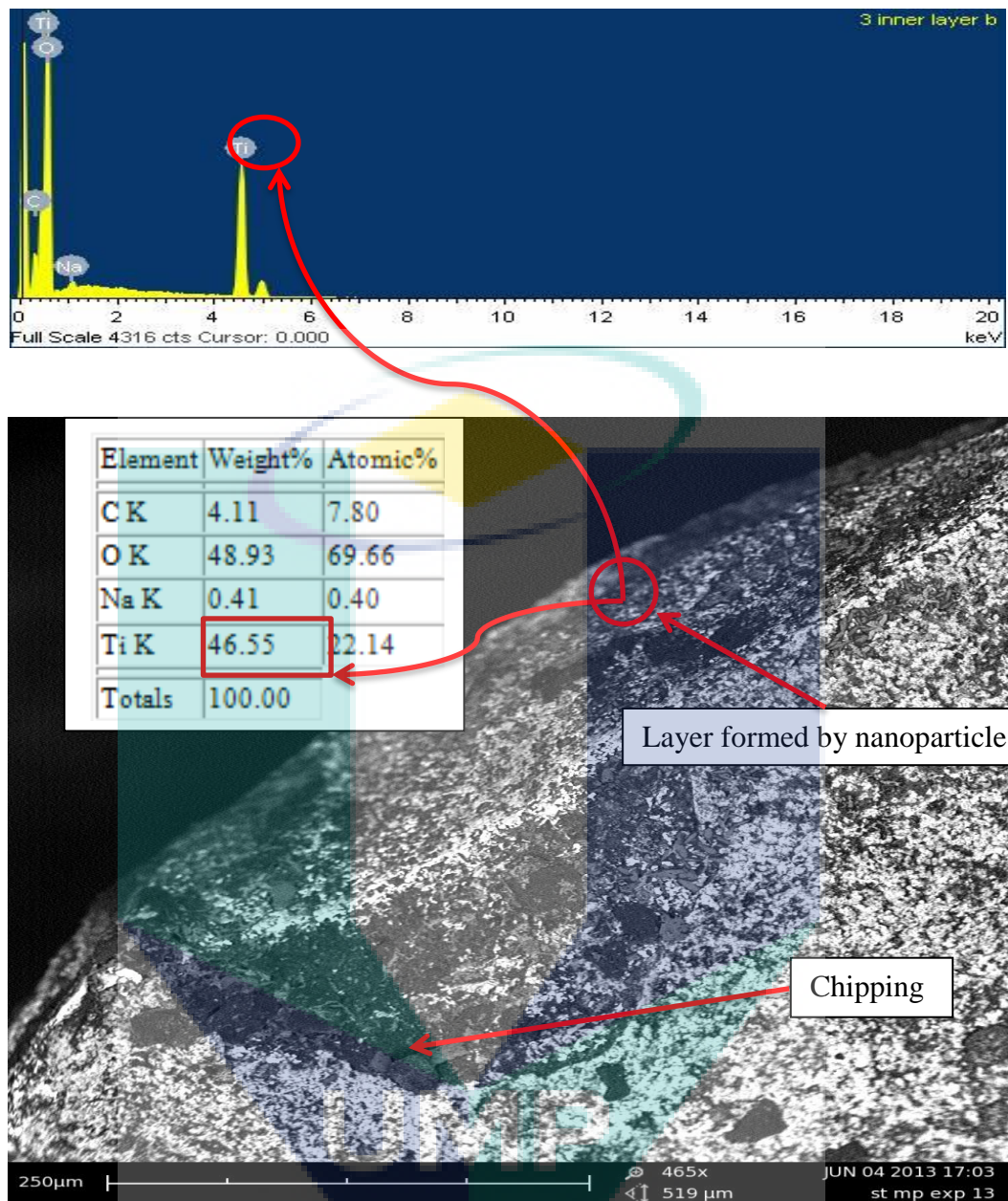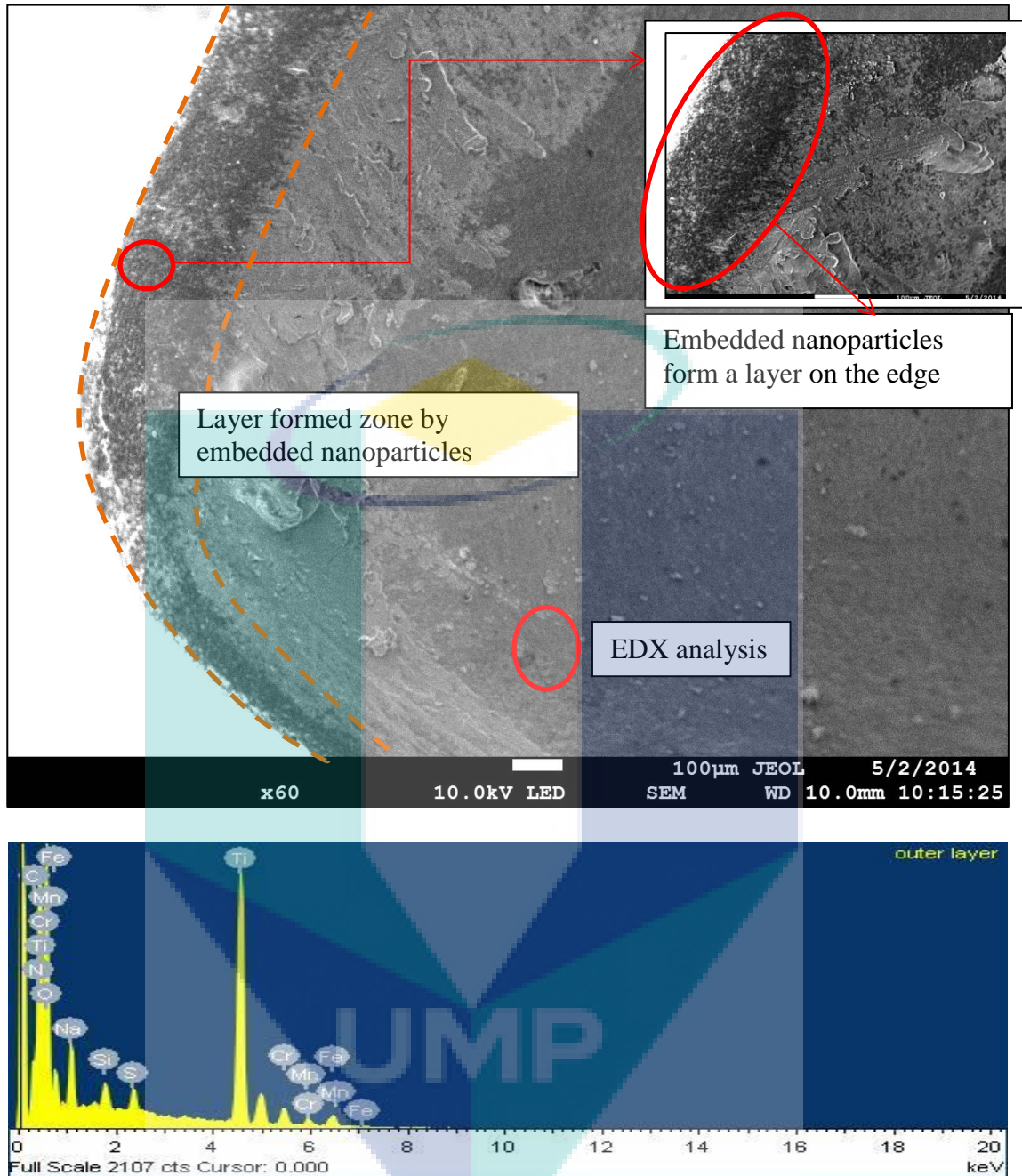
In addition, the spectral data obtained from EDX can be used to explain the type of the wear that occurs at the rake face of the cutting insert. Figure 4.27 shows the EDX spectrum and the SEM of rake face of worn insert subjected to milling for 180 mm of length with nanofluid at cutting speed of 1500 rpm, feed rate of 0.02 mm/tooth and axial depth of 0.1 mm. One can be noticed is the spectra shows an iron (Fe) peak obtained during the milling. This is an indication of an iron BUE occur during milling with nanofluid (Pinaki et al., 2008). Moreover, Hossein and Yahya (2005) stated that BUE can simply formed at low cutting speed during machining ductile material such as austenite stainless steel. Other visible elemental peaks that show is the spectra are chromium (Cr), manganese (Mn), sulfur (S), silicon (Si), nitrogen (N) and oxygen (O). Most of the element mention above are alloying element in AISI 304 stainless steel that used as milling workpiece. This is due to diffusion wear took place at the tool-chip interface and cause the element from the workpiece transfer to the insert rake face. According to Trent (1991) carbon and metal particles transfer into insert rake face in the form of chips generated during the milling process. In same period, atoms of alloying element of the workpiece material diffuse into the rake face and react with insert coating to degrade further (Trent, 1991). According to previous researcher by Jawaid et al. (2000), attrition wear is a removal of grains or agglomerates of tool material due to intermittent adhesion between the tool and the workpiece as a result of the irregular chip flow and the breaking of a partially stable BUE. Significant plucking of tool particles when milling steel material can be reasonably associated with attrition wear (Bhatia et al., 1979). The attrition behavior can be described as the cyclic adhesion and removal of workpiece and chip material from the tool, which also causes removal of tool particles (Diniz et al., 2010)(Trent, 1991).

On the other hand, the milling testing with nano particle base coolant (TiO$_2$/EG) the insert exhibits a micro-wear mechanism. Figure 4.28 shows the massive adhesion which contributes to BUE at milling distance of 720 mm. However, this BUE is not in stable state since many cutting insert exhibits this phenomenon (Karagoz and Fischmeister, 1999). It can be clearly seen in Figure 4.28, the adhesion of workpiece

material deposit on the rake face of milling insert. According to Konig et al. (1991), adhesion takes place after the coating has worm out. The adhesion of the workpiece material on the rake face of the milling insert can form a strong shield on the layer of the milling insert after the TiN coated layer has been removed. Besides that, the adhered Ti nanoparticle will also hit and squashed into the insert surface and deposit as a metal layer as shown in the Figure 2.25. This is proved when the EDX spectrum has a peak on Ti metal. The adhered layer will act as superfluous layer to shield the cutting insert since layer containing Ti nanoparticle. In most cases, the adhering metal was found mainly on the rake face rather than on the flank face after the tools had failed (Jawaid et al., 1999).

Although the cutting temperature has been reduced in the tool-workpiece interface during the milling process by using nano particle based coolant (TiO_2/EG) but oxidation still occurs during the milling process. Paul and Evans, 1996 said that the chemical significant step in oxidation wear when the O atoms are pulled from the water (H_2O) soluble coolant because they do not have unpaired d-electrons. Figure 4.29 shows the O peak on the EDX spectrum when machining with nano particle based coolant (TiO_2/EG). This proved that oxidation wear occur during milling with nano particle based coolant (TiO_2/EG). The small amount of oxygen get into the tool-workpiece interface during the milling process from the coolant (40% water, 60% EG). The oxidation layer were hard and it could not easily detached from the tool surface and it took parts of the tool material under severe impact of milling force, further protect the tool from micro cracking and chipping wear (Jinyang et al., 2013).
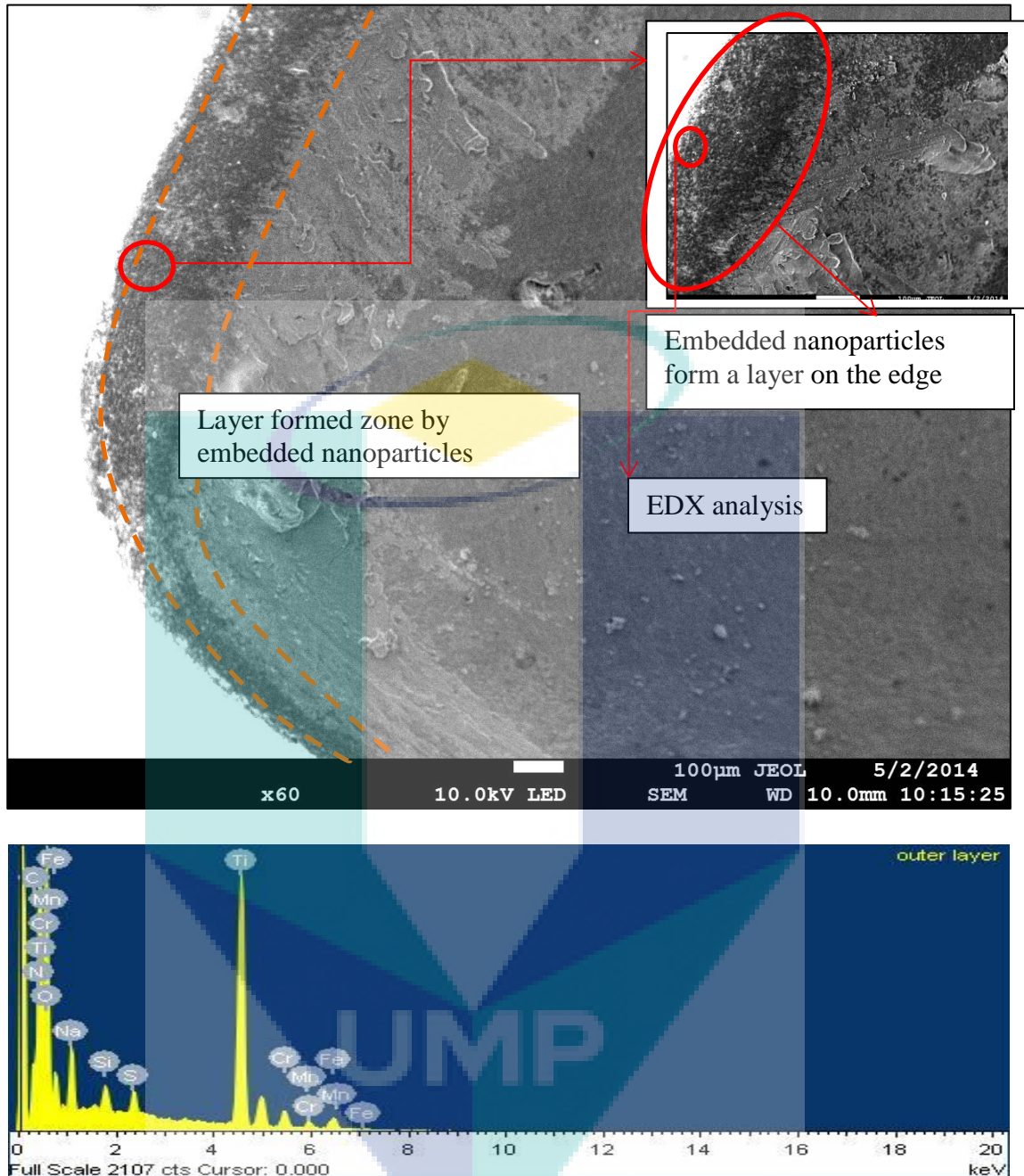
Figure 4.27: SEM and EDX of cutting edge at cutting speed 1500 rpm, feed rate 0.02 mm/tooth, axial depth 0.1 mm under nano particle based coolant at 180 mm of cutting distance (60 × magnification).
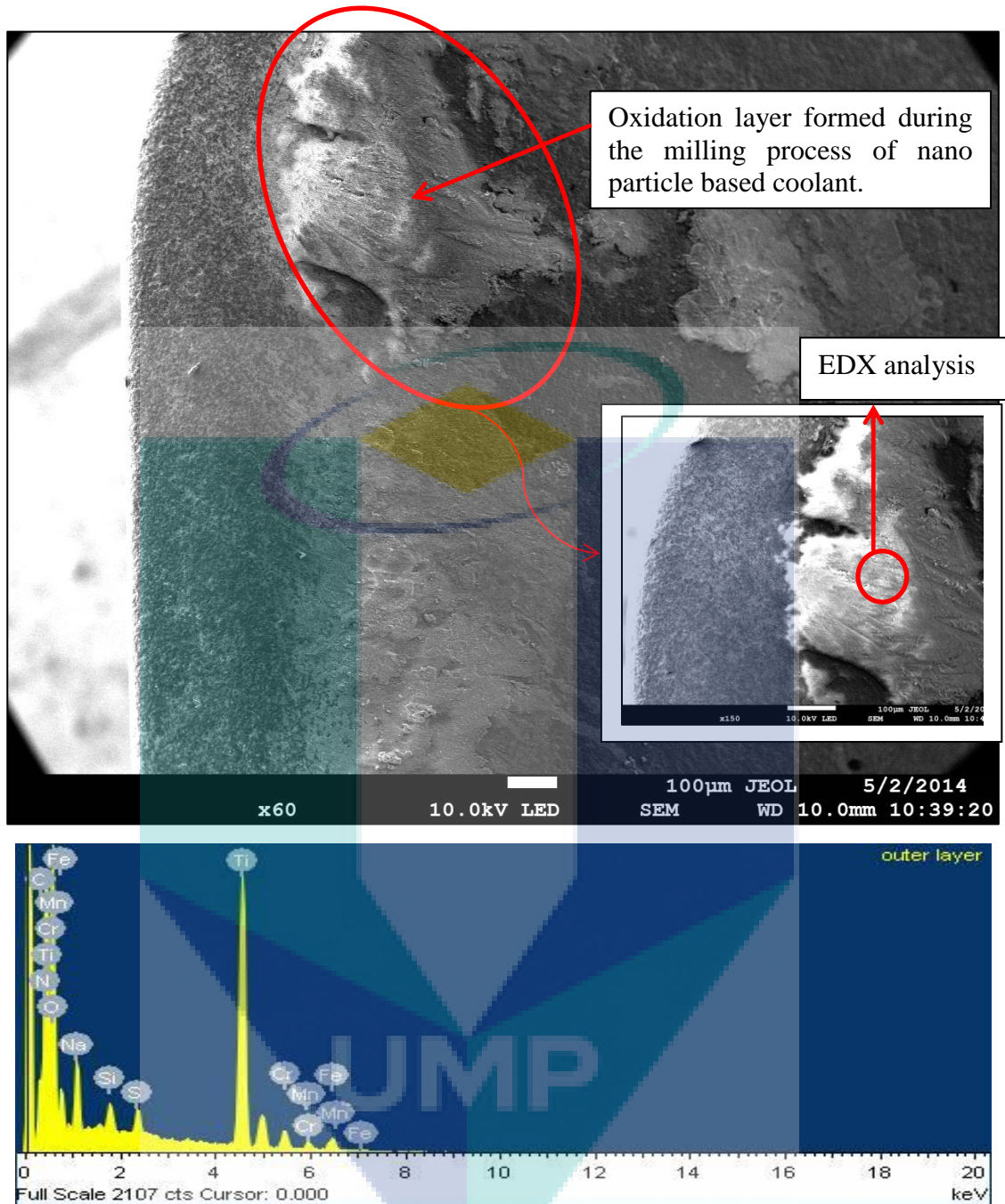
Figure 4.28: SEM and EDX of cutting edge at cutting speed 1500 rpm, feed rate 0.02 mm/tooth, axial depth 0.1 mm under nano particle based coolant at 180 mm of cutting distance ($60 \times$ magnification).
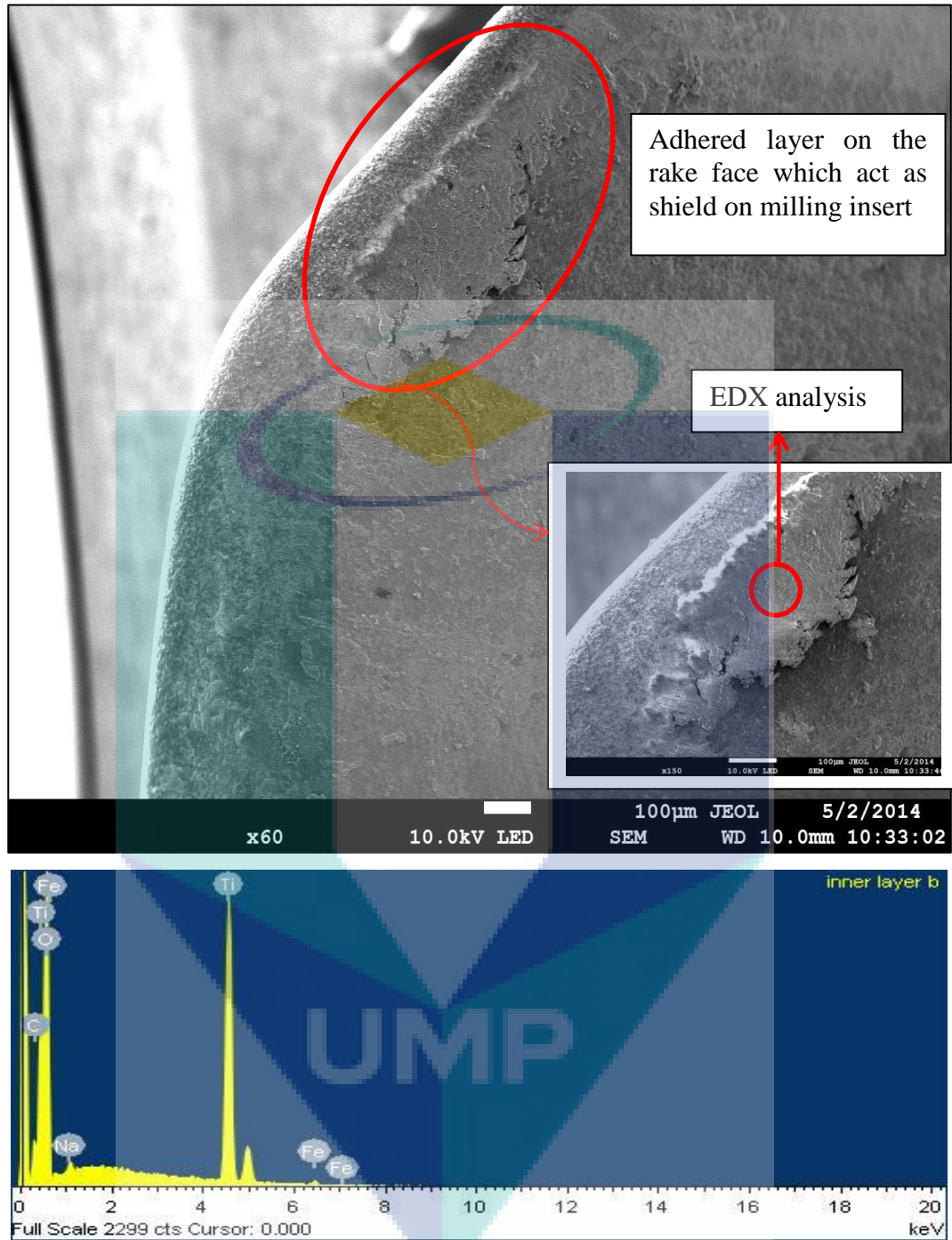
Figure 4.29: SEM and EDX of cutting edge at cutting speed 1500 rpm, feed rate 0.02 mm/tooth, axial depth 0.1 mm under nano particle based coolant at 180 mm of cutting distance (60 × magnification)

CHAPTER 5

CONCLUSION AND RECOMMENDATION

5.1   CONCLUSION

In the present study, linear mathematical model were developed to predict milling parameter for AISI 304 stainless steel using TiN coated carbide insert under two different milling environments which is using water soluble coolant and ethylene glycol based TiO_2 nanofluid as cutting fluid. The predicted linear model is used to find the optimum milling parameter for minimize the surface roughness and maximize the tool life based on RSM. The experimental results were compared with the predicted result. It can be summarized from the results and discussion as follows:

- Surface roughness is affected significantly by feed rate, followed by axial depth of cut and cutting speed for end milling process with water soluble coolant and ethylene glycol based TiO_2 nanofluid. The surface roughness increase with increasing of feed rate and axial depth of cut. Besides that, the surface roughness reduces when the cutting speed increases. The optimum milling condition for acquire finest surface roughness are; cutting speed 2500 rpm, feed rate 0.02 mm/tooth and axial depth of cut 0.1 mm.

- The tool life increases with decrease of cutting speed, feed rate and axial depth of cut. The feed rate has the most dominant effect on the tool life, followed by axial depth of cut and cutting speed for both end milling process with water soluble coolant and ethylene glycol base TiO_2 nanofluid.

- End milling process with ethylene glycol based TiO_2 nanofluid perform better than water soluble coolant in term of surface roughness and tool life. The minimum surface roughness produce by conducting the end-mill experiment with nanofluid is 0.135 μm meanwhile milling with water

soluble coolant is 0.191 μm. This showed that the using of nanofluid has reduced the surface roughness by 29.32 %. Besides that, the maximum tool life produced when end milling with nanofluid is 54.9 minutes but milling with water soluble coolant the tool life is just 32.67 minutes. This indicates that the using the ethylene glycol based TiO_2 nanofluid has increased the tool life by 40.55 %.

- Flank wear, chipping, cracking and fracture were the main tool failure modes when machining AISI 304 stainless steel with water soluble coolant.

- It has been found Ti nanoparticle layer has been formed on the edge of the insert during the milling process with ethylene glycol based TiO_2 nanofluid. The nanoparticle from the nanofluid embedded into and fills the holes in the insert and for a layer which act as a thermal bridge for the cutting insert.

- Attrition and Oxidation were the operating tool wear mechanism on the on coated carbide tool when machining AISI 304 stainless steel. On the other hand, BUE has been spotted by machining at low cutting speed.

5.2   RECOMMENDATION

This present work can be proposed for further work in following area:

- The related approach to be used to predict the other milling response such as cutting force, cutting temperature. Analysis of cutting tool temperature and workpiece temperature is important to predict the amount of heat has been dissipated in the cutting zone when milling with nanofluid. Therefore, infrared camera is suggested to be used to measure the temperature distribution on the workpiece and cutting tool. Besides that, the similar project can be proposed to predict the cutting parameter for other steel material.

- In addition, the machining process with nanofluid can recommend with turning and grinding. The identical approach is used to determine the effect of nanofluid in turning and grinding to reduce the difficulty that associate with heat.

- Furthermore, machining response can be studied for different type of nanoparticle used to prepare the nanofluid. There are several nanoparticles available in market which has high thermal conductivity such as SiC, Al_2O_3 and SiO. On the other hand, the study of cutting response also can be conducted by using different size of nanoparticle.

REFERENCE

Abou-El-Hossein, K. A., & Yahya, Z. (2005). High-speed end-milling of AISI 304 stainless steels using new geometrically developed carbide inserts. *Journal of materials processing technology*, *162*, 596-602.

Alauddin, M., El Baradie, M. A., & Hashmi, M. S. J. (1997). Prediction of tool life in end milling by response surface methodology. Journal of Materials Processing Technology, 71(3), 456-465.

Amor, R. B. (2003). *Thermomechanische Wirkmechanismen und Spanbildung bei der Hochgeschwindigkeitszerspanung*. PZH, Produktionstechn. Zentrum.

Astakhov, V. P. (1998). *Metal cutting mechanics*. CRC press.

Astakhov, V. P. (1999). A treatise on material characterization in the metal cutting process. Part 1: A novel approach and experimental verification. *Journal of Materials Processing Technology*, *96*(1), 22-33.

Astakhov, V. P. (2007). Effects of the cutting feed, depth of cut, and workpiece (bore) diameter on the tool wear rate. The International Journal of Advanced Manufacturing Technology, 34(7-8), 631-640.

Atkins, A. G. (2006). Toughness and oblique metalcutting. *Journal of manufacturing science and engineering*, *128*(3), 775-786.

Baik, M. C. (1988). *Beitrag zur Zerspanbarkeit von Kobalthartlegierungen mit polykristallinem kubischen Bornitrid (PKB) beim Drehen*. na.

Bandyopadhyay, B. P., & Teo, E. H. (1990). Application of factorial design of experiment in high speed turning. *Proc. Manuf. Int. Part*, *4*, 3-8.

Barshilia, H. C., Deepthi, B., Selvakumar, N., Jain, A., & Rajam, K. S. (2007). Nanolayered multilayer coatings of CrN/CrAlN prepared by reactive DC magnetron sputtering. *Applied Surface Science*, *253*(11), 5076-5083.

Behrens, B. A. (2010). *Handbuch Umformtechnik*. B. A. B. E. Doege (Ed.). Springer Berlin Heidelberg.

Bhatia, S. M., Pandey, P. C., & Shan, H. S. (1979). Failure of cemented carbide tools in intermittent cutting. Precision Engineering, 1(3), 148-152.

Birol, Y. (2013). Sliding wear of CrN, AlCrN and AlTiN coated AISI H13 hot work tool steels in aluminium extrusion. *Tribology International*, *57*, 101-106.

Bjurka, E. (2012). Analyze of insert geometries, wear types and insert life in milling.

Boothroyd, G. (1988). *Fundamentals of metal machining and machine tools*(Vol. 28). CRC Press.

Brosheer, B. C. (1948). How Smooth is Smooth? Part-I, Specification and Evaluation of Machined Finishes. *American Machinist, McGrow-Hill Publishing Company*, 97-112.

Buda, J., Vasilko, K., & Stranava, J. (1968). Neue Methode der Spanwurzelgewinnung zur Untersuchung des Schneidvorganges. *Industrie Anzeiger*, *90*(5).

Cakir, M. C., Ensarioglu, C., & Demirayak, I. (2009). Mathematical modeling of surface roughness for evaluating the effects of cutting parameters and coating material. Journal of materials processing technology, 209(1), 102-109.

Chakraborty, P., Asfour, S., Cho, S., Onar, A., & Lynn, M. (2008). Modeling tool wear progression by using mixed effects modeling technique when end-milling AISI 4340 steel. *Journal of materials processing technology*, *205*(1), 190-202.

Che-Haron, C. H. (2001). Tool life and surface integrity in turning titanium alloy. Journal of Materials Processing Technology, 118(1), 231-237.

Choi, C., Yoo, H. S., & Oh, J. M. (2008). Preparation and heat transfer properties of nanoparticle-in-transformer oil dispersions as advanced energy-efficient coolants. *Current Applied Physics*, *8*(6), 710-712.

Choudhury, I. A., & El-Baradie, M. A. (1999). Machinability assessment of inconel 718 by factorial design of experiment coupled with response surface methodology. Journal of Materials Processing Technology, 95(1), 30-39.

Choudhury, I. A., & El-Baradie, M. A. (1999). Machinability assessment of inconel 718 by factorial design of experiment coupled with response surface methodology. Journal of Materials Processing Technology, 95(1), 30-39.

D'Addona, D., Segreto, T., Simeone, A., & Teti, R. (2011). ANN tool wear modelling in the machining of nickel superalloy industrial products. *CIRP Journal of Manufacturing Science and Technology*, *4*(1), 33-37.

Das, S. K., Putra, N., & Roetzel, W. (2003). Pool boiling of nano-fluids on horizontal narrow tubes. *International Journal of Multiphase Flow*, *29*(8), 1237-1247.

de Melo, A. C., Milan, J. C. G., Silva, M. B. D., & Machado, Á. R. (2006). Some observations on wear and damages in cemented carbide tools. Journal of the Brazilian Society of Mechanical Sciences and Engineering, 28(3), 269-277.

Dearnley, P. A., & Grearson, A. N. (1986). Evaluation of principal wear mechanisms of cemented carbides and ceramics used for machining titanium alloy IMI 318. *Materials Science and Technology*, *2*(1), 47-58.

Duangthongsuk, W., & Wongwises, S. (2010). An experimental study on the heat transfer performance and pressure drop of TiO< sub> 2</sub>-water nanofluids flowing under a turbulent flow regime. International Journal of Heat and Mass Transfer, 53(1), 334-344.

El Baradie, M. A. (1993). Surface roughness model for turning grey cast iron (154 BHN). *Proceedings of the Institution of Mechanical Engineers, Part B: Journal of Engineering Manufacture*, *207*(1), 43-54.

Eriksson, L. (Ed.). (2008). Design of experiments: principles and applications. MKS Umetrics AB.

Gharagozloo, P. E., & Goodson, K. E. (2010). Aggregate fractal dimensions and thermal conduction in nanofluids. Journal of Applied Physics, 108(7), 074309.

Gorlenko, O. A. (1981). Assessment of surface roughness parameters and their interdependence. *Precision Engineering*, *3*(2), 105-108.

Gu, J., Barber, G., Tung, S., & Gu, R. J. (1999). Tool life and wear mechanism of uncoated and coated milling inserts. Wear, 225, 273-284.

Hill, R. (1954). The mechanics of machining: a new approach. Journal of the Mechanics and Physics of Solids, 3(1), 47-53.

Hoffmeister, H. W., & Wessels, T. (2005). Thermomechanische Wirkmechanismen bei der Hochgeschwindigkeitszerspanung von Titan-und Nickelbasislegierungen. *Hochgeschwindigkeitsspanen metallischer Werkstoffe*, 470-491.

Hoppe, S. (2003). Experimental and numerical analysis of chip formation in metal cutting (Doctoral dissertation, Universitätsbibliothek).

Huddedar, S., Kulkarni, A. P., Joshi, G., & Sargade, V. (2012). Microstructure and mechanical properties of AlTiCrN, AlCrN coatings deposited by cathodic arc evaporation (PVD) technique. In *Proc. 21st Int. Conf. Process. Fab. Adv, Mater* (Vol. 1, pp. 514-520).

Juneja, B. L., & Seth, N. (2003). Fundamentals of metal cutting and machine tools. New Age International.

Kadirgama, K., & Abou-El-Hossein, K. A. (2005). Power prediction model for milling 618 stainless steel using response surface methodology. American Journal of Applied Sciences, 2(7), 1182.

Khandekar, S., Sankar, M. R., Agnihotri, V., & Ramkumar, J. (2012). Nano-cutting fluid for enhancement of metal cutting performance. Materials and Manufacturing Processes, 27(9), 963-967.

Klose, H. J. (1993). Einfluss der Werkstofftechnologie auf die Zerspanbarkeit niedriglegierter Gusseisen. *Dr.-Ing. Diss., Universität Hannover*.

Koo, J., & Kleinstreuer, C. (2004). A new thermal conductivity model for nanofluids. Journal of Nanoparticle Research, 6(6), 577-588.

Korkut, I., Kasap, M., Ciftci, I., & Seker, U. (2004). Determination of optimum cutting parameters during machining of AISI 304 austenitic stainless steel. *Materials & Design*, *25*(4), 303-305.

Koshy, P., Dewes, R. C., & Aspinwall, D. K. (2002). High speed end milling of hardened AISI D2 tool steel (~ 58 HRC). Journal of Materials Processing Technology, 127(2), 266-273.

Leong, K. C., Yang, C., & Murshed, S. M. S. (2006). A model for the thermal conductivity of nanofluids–the effect of interfacial layer. *Journal of Nanoparticle Research*, *8*(2), 245-254.

Liew, W. Y. H. (2010). Low-speed milling of stainless steel with TiAlN single-layer and TiAlN/AlCrN nano-multilayer coated carbide tools under different lubrication conditions. Wear, 269(7), 617-631.

Liew, W. Y. H., & Ding, X. (2008). Wear progression of carbide tool in low-speed end milling of stainless steel. Wear, 265(1), 155-166.

Longo, G. A., & Zilio, C. (2011). Experimental measurement of thermophysical properties of oxide–water nano-fluids down to ice-point. Experimental Thermal and Fluid Science, 35(7), 1313-1324.

Lou, M. S., Chen, J. C., & Li, C. M. (1998). Surface roughness prediction technique for CNC end-milling. *Journal of Industrial Technology*, *15*(1), 1-6.

Matsumoto, Y., Hashimoto, F., & Lahoti, G. (1999). Surface integrity generated by precision hard turning. *CIRP Annals-Manufacturing Technology*, *48*(1), 59-62.

Montgomery, D. C. (2008). *Design and analysis of experiments*. John Wiley & Sons.

Murshed, S. M. S., Leong, K. C., & Yang, C. (2005). Enhanced thermal conductivity of TiO< sub> 2</sub>—water based nanofluids. International Journal of Thermal Sciences, 44(4), 367-373.

Murshed, S. M. S., Leong, K. C., & Yang, C. (2008). Thermophysical and electrokinetic properties of nanofluids–a critical review. Applied Thermal Engineering, 28(17), 2109-2125.

Neugebauer, R., Bouzakis, K. D., Denkena, B., Klocke, F., Sterzing, A., Tekkaya, A. E., & Wertheim, R. (2011). Velocity effects in metal forming and machining processes. CIRP Annals-Manufacturing Technology, 60(2), 627-650.

Peckner, D., & Bernstein, I. M. (1977). *Handbook of stainless steels* (pp. 19-3). New York, NY: McGraw-Hill.

Philip Selvaraj, D., Chandramohan, P., & Mohanraj, M. (2014). Optimization of surface roughness, cutting force and tool wear of nitrogen alloyed duplex stainless steel in a dry turning process using Taguchi method. Measurement, 49, 205-215.

Sandvik Coromant (Firm). (1994). *Modern metal cutting: a practical handbook.* Sandvik Coromant.

Shao, H., Liu, L., & Qu, H. L. (2007). Machinability study on 3% Co–12% Cr stainless steel in milling. *Wear*, *263*(1), 736-744.

Singh, G. P., Alphonsa, J., Barhai, P. K., Rayjada, P. A., Raole, P. M., & Mukherjee, S. (2006). Effect of surface roughness on the properties of the layer formed on AISI 304 stainless steel after plasma nitriding. *Surface and Coatings Technology*, *200*(20), 5807-5811.

Sturesson, P. O., Håkansson, L., & Claesson, I. (1997). Identification of Statistical Properties of Cutting Tool Vibrations in a Continuous Turning Operation— correlation to Structural Properties. Mechanical systems and signal processing, 11(3), 459-489.

Tekıner, Z., & Yeşilyurt, S. (2004). Investigation of the cutting parameters depending on process sound during turning of AISI 304 austenitic stainless steel. *Materials & design*, *25*(6), 507-513.

Thakur, D. G., Ramamoorthy, B., & Vijayaraghavan, L. (2009). Study on the machinability characteristics of superalloy Inconel 718 during high speed turning. *Materials & Design*, *30*(5), 1718-1725.

Thomas, T. R. (1981). Characterization of surface roughness. *Precision Engineering*, *3*(2), 97-104.

Toenshoff, H. K., & Denkena, B. (2013). Basics of cutting and abrasive processes. Heidelberg/Berlin: Springer.

Ueda, T., Hosokawa, A., Oda, K., & Yamada, K. (2001). Temperature on flank face of cutting tool in high speed milling. CIRP Annals-Manufacturing Technology, 50(1), 37-40.

Ulutan, D., & Ozel, T. (2011). Machining induced surface integrity in titanium and nickel alloys: A review. *International Journal of Machine Tools and Manufacture*, *51*(3), 250-280.

Vajjha, R. S., Das, D. K., & Kulkarni, D. P. (2010). Development of new correlations for convective heat transfer and friction factor in turbulent regime for nanofluids. *International Journal of Heat and Mass Transfer*, *53*(21), 4607-4618.

Wiklund, U., Rubino, S., Kádas, K., Skorodumova, N. V., Eriksson, O., Hedberg, S., ... & Leifer, K. (2011). Experimental and theoretical studies on stainless steel transfer onto a TiN-coated cutting tool. *Acta Materialia*, *59*(1), 68-74.

Wojciechowski, S., & Twardowski, P. (2012). Tool life and process dynamics in high speed ball end milling of hardened steel. *Procedia CIRP*, *1*, 289-294.

Xavior, M. A., & Adithan, M. (2009). Determining the influence of cutting fluids on tool wear and surface roughness during turning of AISI 304 austenitic stainless steel. *Journal of Materials Processing Technology*, *209*(2), 900-909.

Yazid, M. Z. A., CheHaron, C. H., Ghani, J. A., Ibrahim, G. A., & Said, A. Y. M. (2011). Surface integrity of Inconel 718 when finish turning with PVD coated carbide tool under MQL. *Procedia Engineering*, *19*, 396-401.

Yu, W., Xie, H., Chen, L., & Li, Y. (2009). Investigation of thermal conductivity and viscosity of ethylene glycol based ZnO nanofluid. Thermochimica Acta, 491(1), 92-96.

Zhou, L. P., Wang, B. X., Peng, X. F., Du, X. Z., & Yang, Y. P. (2009). On the specific heat capacity of CuO nanofluid. Advances in mechanical engineering, 2010.

206. ISO 8688-2:1989 End mill testing.